RF BREAKDOWN STUDIES USING PRESSURIZED CAVITIES

Final Report for Project Period 06/30/2008 through 04/14/2013

Principal Investigator: Rolland Johnson

Muons, Inc.

Batavia, IL 60510

PREPARED FOR THE UNITED STATES

DEPARTMENT OF ENERGY

Work Performed Under grant DE-FG02-08ER86352

DISCLAIMER

ABSTRACT

Many present and future particle accelerators are limited by the maximum electric gradient and peak surface fields that can be realized in RF cavities. Despite considerable effort, a comprehensive theory of RF breakdown has not been achieved and mitigation techniques to improve practical maximum accelerating gradients have had only limited success. Part of the problem is that RF breakdown in an evacuated cavity involves a complex mixture of effects, which include the geometry, metallurgy, and surface preparation of the accelerating structures and the make-up and pressure of the residual gas in which plasmas form. Studies showed that high gradients can be achieved quickly in 805 MHz RF cavities pressurized with dense hydrogen gas, as needed for muon cooling channels [1], without the need for long conditioning times, even in the presence of strong external magnetic fields [2]. This positive result was expected because the dense gas can practically eliminate dark currents and multipacting. In this project we used this high pressure technique to suppress effects of residual vacuum and geometry that are found in evacuated cavities in order to isolate and study the role of the metallic surfaces in RF cavity breakdown as a function of magnetic field, frequency, and surface preparation. One of the interesting and useful outcomes of this project was the unanticipated collaborations with LANL and Fermilab that led to new insights as to the operation of evacuated normal-conducting RF cavities in high external magnetic fields. Other accomplishments included:

(1) RF breakdown experiments to test the effects of SF6 dopant in H2 and He gases with Sn, Al, and Cu electrodes were carried out in an 805 MHz cavity and compared to calculations and computer simulations. The heavy corrosion caused by the SF6 components led to the suggestion that a small admixture of oxygen, instead of SF6, to the hydrogen would allow the same advantages without the corrosion in a practical muon beam line.
(2) A 1.3 GHz RF test cell capable of operating both at high pressure and in vacuum with replaceable electrodes was designed, built, and power tested in preparation for testing the frequency and geometry effects of RF breakdown at Argonne National Lab. At the time of this report this cavity is still waiting for the 1.3 GHz klystron to be available at the Wakefield Test Facility.
(3) Under a contract with Los Alamos National Lab, an 805 MHz RF test cavity, known as the All-Seasons Cavity (ASC), was designed and built by Muons, Inc. to operate either at high pressure or under vacuum. The LANL project to use the (ASC) was cancelled and the testing of the cavity has been continued under the grant reported on here using the Fermilab Mucool Test Area (MTA). The ASC is a true pillbox cavity that has performed under vacuum in high external magnetic field better than any other and has demonstrated that the high required accelerating gradients for many muon cooling beam line designs are possible.
(4) Under ongoing support from the Muon Acceleration Program, microscopic surface analysis and computer simulations have been used to develop models of RF breakdown that apply to both pressurized and vacuum cavities.

The understanding of RF breakdown will lead to better designs of RF cavities for many applications. An increase in the operating accelerating gradient, improved reliability and shorter conditioning times can generate very significant cost savings in many accelerator projects.

Table of Contents

Project Summary

Project Overview

This grant was unusual in that although the Phase II proposal to use the new technology of High Pressure RF cavities to study RF breakdown was reviewed well and recommended for funding, there were insufficient funds to grant the Phase II award to immediately follow the Phase I effort. After a year hiatus the STTR Phase II effort was granted with LBNL as our research partner. However, things had changed to give us more opportunities to collaborate with ANL, LANL, and FNAL to study breakdown parameters and, most important, the limitations of vacuum cavities operating in strong external magnetic fields.

One of the goals of the Phase II project was to understand the breakdown limitations of pressurized RF cavities as a function of RF frequency. Our plan was to use an existing and available 402.5 MHz power source at LBNL to power a new pressurized cavity to compare with our previous results at 805 MHz. The question to be answered is whether the strong frequency dependence of maximum achievable RF gradients of vacuum cavities applies also to pressurized cavities. Unfortunately, the power source was unavailable one year later and we had to change our plans. The grant funds that were to support this effort at LBNL were later used to support Daniel Bowring, a postdoc at LBNL, to use the SLAC ACE3P codes to model vacuum RF cavities.

During the Phase I project, we built a 1.3 GHz test cell that is capable of vacuum or pressurized operation and made arrangements to test it using the 1.3 GHz klystron at the ANL Wakefield Test Accelerator. This effort is described below and in the conference proceedings that are attached in the appendices. The klystron has not been available up to now, and the measurements are still on hold.

A new opportunity arose when LANL gave Muons, Inc. a $245,000 (later reduced to $185,000) contract to design and build a prototype 805 MHz vacuum RF cavity for a muon beam project at Los Alamos. They (primarily Sergey Kurennoy) were also interested in the potential of pressurized cavities, even though their baseline design only called for vacuum cavities. Thus the true pillbox cavity that we designed, built, and tested was capable of pressurized or vacuum operation and had the ability to change the end walls of the cavity so that it could test breakdown characteristics of various metals. It was bolted together with aluminum gaskets so that it could be easily disassembled to allow the examination of the internal surfaces. This was the first cavity ever built with a true pillbox shape capable of pressurized operation at the high pressure needed for a muon cooling channel. All previous studies with pressurized cavities used “doorknob electrodes” to achieve the RF gradients of interest. With these new and versatile capabilities it was called a cavity for all seasons or All Seasons Cavity (ASC).

The LANL muon beam project was cancelled before we finished the testing of the ASC. We used the 805 MHz klystron at the Fermilab Mucool Test Area to demonstrate its vacuum operation in the LBNL 5 T Solenoid. Unlike previous vacuum cavity tests, the ASC operated well at gradients above 20 MV/m even at the highest magnetic fields available at the MTA, eventually almost reaching 5 T. The effort to understand why the ASC succeeded to achieve the required RF gradient in strong external magnetic fields while other designs did not is still under

investigation. The last appendix in this report, "Electrical Breakdown in the All Seasons Cavity," is a discussion of the status of this analysis.

The "existence proof" provided by the ASC, showing that high accelerating gradients in vacuum RF cavities in strong magnetic fields are possible, is one of the important results made possible by the funding provided by this DEFG02-08ER86352 grant.

Figure 1: Gene Flanagan and Grigory Kazakevitch of Muons, Inc. showing the removable endplate of the All Seasons Cavity. The pillbox cavity, constructed to operate under vacuum or with up to 100 Atm of hydrogen gas, has so far only been used for vacuum tests. These have led to new insights for RF cavities operating in strong external magnetic fields. As a true pillbox cavity, it could be the first to operate under high pressure with the geometry expected in muon beam cooling channels.

Summary of Results Reported in Conference Proceedings (in chronological order)

The following summaries describe the results of various stages of this grant's progress, which were described in conference proceedings. The articles themselves, where more detail can be found, are attached as appendices to this report.

(* indicates primary grant support – others had contributions from this grant)

EPAC08 - STUDIES OF BREAKDOWN IN A PRESSURIZED RF CAVITY

M. BastaniNejad, A. A. Elmustafa, ODU, Norfolk, VA, C. M. Ankenbrandt, A. Moretti, M. Popovic, K. Yonehara, Fermilab, Batavia, IL, D. M. Kaplan, IIT, Chicago, IL, M. Alsharo'a, P. M. Hanlet, R. P. Johnson, M. Kuchnir, D. Newsham, Muons Inc, Batavia, IL, D. V. Rose, C. Thoma, and D. R. Welch, Voss Scientific, LLC, Albuquerque, NM

Summary

Microscopic images of the surfaces of metallic electrodes used in high-pressure gas-filled 805 MHz RF cavity experiments have been used to investigate the mechanism of RF breakdown. The images show evidence for melting and boiling in small regions of ~10 micron diameter on tungsten, molybdenum, and beryllium electrode surfaces. In these experiments, the dense hydrogen gas in the cavity prevents electrons or ions from being accelerated to high enough energy to participate in the breakdown process so that the only important variables are the fields and the metallic surfaces. The distributions of breakdown remnants on the electrode surfaces are compared to the maximum surface gradient E predicted by an ANSYS model of the cavity. The local surface density of spark remnants, proportional to the probability of breakdown, shows a strong exponential dependence on the maximum gradient, which is reminiscent of Fowler-Nordheim behavior of electron emission from a cold cathode. New simulation results have shown good agreement with the breakdown behavior of the hydrogen gas in the Paschen region and have suggested improved behavior with the addition of trace dopants such as SF6. Present efforts are to extend the computer model to include electrode breakdown phenomena and to use scanning tunneling microscopy to search for work function differences between the conditioned and unconditioned parts of the electrodes.

PAC09 - RF BREAKDOWN OF METALLIC SURFACES IN HYDROGEN*

M. BastaniNejad, A. A. Elmustafa, ODU, Norfolk, VA, K. Yonehara, M. Chung, A. Jansson, M. Hu, A. Moretti, M. Popovic, FNAL**,** Batavia IL, M. Alsharo'a, M. Neubauer, R. Sah, R.P. Johnson, Muons, Inc., Batavia, IL

Abstract

In earlier reports, microscopic images of the surfaces of metallic electrodes used in high-pressure gas-filled 805 MHz RF cavity experiments were used to investigate the mechanism of RF breakdown of tungsten, molybdenum, and beryllium electrode surfaces. Plots of remnants were consistent with the breakdown events being due to field emission, due to the quantum mechanical tunnelling of electrons through a barrier as described by Fowler and Nordheim. In the work described here, these studies have been extended to include tin, aluminium, and copper. Contamination of the surfaces, discovered after the experiments concluded, have cast some doubt on the proper qualities to assign to the metallic surfaces. However, two significant results are noted. First, the maximum stable RF gradient of contaminated copper electrodes is higher than for a clean surface. Second, the addition of as little as 0.01% of SF6 to the hydrogen gas increased the maximum stable gradient, which implies that models of RF breakdown in hydrogen gas will be important to the study of metallic breakdown.

PAC09 - RF BREAKDOWN STUDIES USING A 1.3-GHZ TEST CELL*

R. Sah, R. P. Johnson, M. Neubauer, Muons, Inc., Batavia IL, M. Conde, W. Gai, ANL, Argonne, IL, A. Moretti, M. Popovic, K. Yonehara, Fermilab, Batavia, IL, J. Byrd, D. Li, LBNL, Berkeley, CA, M. BastaniNejad, A. A. Elmustafa, ODU, Norfolk,VA

Summary

A 1.3-GHz RF test cell with replaceable electrodes (e.g. Mo, Cu, Be, W, and Nb) and pressure barrier capable of operating both at high pressure and in vacuum has been designed and built, and preliminary testing has been completed. A series of detailed experiments is planned at the Argonne Wakefield Accelerator. At the same time, computer simulations of the RF Breakdown process will be carried out to help develop a consistent physics model of RF Breakdown. In order to study the effect of the radiofrequency on RF Breakdown, a second test cell will be designed, fabricated, and tested at a lower frequency, most likely 402.5 MHz.

IPAC10 - STUDY OF ELECTRON SWARM IN HP H_2-FILLED RF CAVITIES

K. Yonehara, M. Chung, A. Jansson, A. Moretti, M. Popovic, A. Tollestrup, Fermilab, Batavia, IL, M. Alsharo'a, R.P. Johnson, M. Notani, Muons, Inc., Batavia, IL, D. Huang, Illinois Institute of Technology, Chicago, IL, T. Oka, H. Wang, University of Chicago, Chicago, IL, D. V. Rose, Voss Scientific, Albuquerque, NM, Z. Insepov, Argonne National Lab, Argonne, IL

Summary

A high pressure hydrogen gas filled RF cavity has been proposed for use in the muon collection system for a muon collider. It allows for high electric field gradients in RF cavities located in strong magnetic fields, a condition frequently encountered in a muon cooling channel. In addition, an intense muon beam will generate an electron swarm via the ionization process in the cavity. A large amount of RF power will be consumed into the swarm. We show the results from our studies of the HV RF breakdown in a cavity without a beam and present some results on the resulting electron swarm dynamics. This is preliminary to actual beam tests which will take place late in 2010.

PAC11 - RF BREAKDOWN STUDIES USING PRESSURIZED CAVITIES*

R. Sah, A. Dudas, R. P. Johnson, M. Neubauer, Muons, Inc., Batavia IL, M. Conde, W. Gai, ANL, Argonne, IL, A. Moretti, M. Popovic, K. Yonehara, Fermilab, Batavia IL, J. Byrd, D. Li, LBNL, Berkeley, CA; D. Rose, Voss Scientific, Albuquerque NM, M. BastaniNejad, M. Elmustafa, ODU, VA

Summary

A 1.3-GHz RF test cell with replaceable electrodes (e.g. Mo, Cu, Be, W, and Nb) has been built, and a series of detailed experiments is planned at the Argonne Wakefield Accelerator. These experiments will be followed by additional experiments using a second test cell operating at 402.5 MHz.

PAC11 - MULTI-PURPOSE 805 MHZ PILLBOX RF CAVITY (All Seasons Cavity)*

Grigory Kazakevich, Gene Flanagan, Rolland Johnson, Mike Neubauer, Richard Sah, Muons, Inc., Batavia, IL, Alfred Moretti, Milorad Popovic, Katsuya Yonehara, Fermilab, Batavia, IL, Kwok-Chi D. Chan, Andrew J. Jason, Sergey S. Kurennoy, Haruo Miyadera, Peter J. Turchi, LANL, Los Alamos, NM, Yagmur Torun, IIT, Chicago, IL

Summary

An 805 MHz RF pillbox cavity has been designed and constructed to investigate potential muon beam acceleration and cooling techniques. The cavity can operate at vacuum or under pressure to 100 atmospheres, at room temperature or in a liquid nitrogen bath at 77 K. The cavity is designed for easy assembly and disassembly with bolted construction using aluminum seals. The surfaces

of the end walls of the cavity can be replaced with different materials such as copper, aluminum, beryllium, or molybdenum, and with different geometries such as shaped windows or grid structures. Different surface treatments such as electro-polished, high-pressure water cleaned, and atomic layer deposition are being considered for testing. The cavity has been designed to fit inside the 5-Tesla solenoid in the MuCool Test Area at Fermilab. Current status of the cavity prepared for initial conditioning and operation in the external magnetic field is discussed.

PAC11 - HIGH PRESSURE RF CAVITY TEST AT FERMILAB

B. Freemire , P.M. Hanlet, D.M. Kaplan, Y. Torun, IIT, Chicago, IL, M.R. Jana, A. Moretti, M. Popovic, A.V. Tollestrup, K. Yonehara, FNAL, Batavia, IL, G. Flanagan, R.P. Johnson, M. Notani, Muons, Inc., Batavia, IL

Summary

Operating a high gradient radio frequency cavity embedded in a strong magnetic field is an essential requirement for muon beam cooling. However, a magnetic field influences the maximum RF gradient due to focusing of dark current in the RF cavity. This problem is suppressed by filling the RF cavity with dense hydrogen gas. As the next step, we plan to explore the beam loading effect in the high pressure cavity by using a 400 MeV kinetic energy proton beam in the MuCool Test Area at Fermilab. We discuss the experimental setup and instrumentation.

IPAC12 - CONDITIONING AND PLANS FOR A MULTI-PURPOSE 805 MHZ CAVITY*

G. Kazakevich, G. Flanagan, R. P. Johnson, M. Neubauer, R. Sah, A. Dudas, F. Mahrhauser Muons, Inc., Batavia, IL, A. Moretti, M. Popovic, K. Yonehara, G. Romanov, Fermilab, Batavia, IL, Y. Torun, IIT, Chicago, IL, S. Kurennoy, LANL, Los Alamos, NM

Summary

An 805 MHz RF pillbox cavity (All Seasons Cavity) has been designed and constructed to investigate potential muon beam acceleration and cooling techniques for a Muon Collider or Neutrino Factory. The cavity can operate in vacuum or under pressure up to 100 atmospheres, at room temperature or in a liquid nitrogen bath at 77K. The cavity has been designed for easy assembly and disassembly utilizing a bolted construction with aluminum seals. To perform vacuum and high-pressure breakdown studies of materials and geometries most suitable for the collider or factory, the surfaces of the end walls of the cavity can be replaced with different materials such as copper, aluminum, beryllium, or molybdenum, and with different geometries such as shaped windows or grid structures. The cavity has been designed to fit inside the 5-Tesla solenoid in the MuCool Test Area (MTA) at Fermilab. In this paper we present the vacuum conditioning results with and without an external magnet field. Additionally, we discuss the future plans for the cavity.

IPAC12 - KINETIC MODELING OF RF BREAKDOWN IN H-P GAS-FILLED CAVITIES*

D. V. Rose, C. H. Thoma, Voss Scientific, Albuquerque, NM, A. V. Tollestrup, K. Yonehara, Fermilab, Batavia, IL, J. Byrd, D. Li, LBNL, Berkeley, R. P. Johnson, M. Neubauer, R. Sah, Muons Inc., Batavia, IL.

Summary
Studies have shown that high field gradients can be achieved quickly in high-pressure gas-filled cavities without the need for long conditioning times, because the dense gas can dramatically reduce dark currents and multipacting. In this project we use this high pressure technique to suppress effects of residual vacuum and geometry found in evacuated cavities to isolate and study the role of the metallic surfaces in RF cavity breakdown as a function of operating frequency and surface preparation. A series of experiments at 805 MHz using hydrogen fill pressures up to 0.01 g/cm3 of H2 have demonstrated high electric field gradients and scaling with the DC Paschen law limit, up to about 30 MV/m, depending on the choice of electrode material. At higher pressures, the breakdown characteristics deviate from the Paschen law scaling. Fully-kinetic 0D collisional particle-in-cell (PIC) simulations give breakdown characteristics in H2 and H2/SF6 mixtures in good agreement with the 805 MHz experimental results below this field stress threshold. At higher pressures the formation of streamers at operating parameters below the Paschen limit are examined using 2D simulations.

IPAC12 - INFLUENCE OF INTENSE BEAM IN H-P H_2 GAS FILLED RF CAVITIES

K. Yonehara, M. Chung, M.G. Collura, M.R. Jana, M. Leonova, A. Moretti, M. Popovic, T. Schwarz, A. Tollestrup, Fermilab, Batavia, IL, R.P. Johnson, G. Flanagan, M. Notani, Muons, Inc., Batavia, IL, B. Freemire, Y. Torun, P. Hanlet, Illinois Institute of Technology, Chicago, IL

Summary
The influence of an intense beam in a high-pressure gas filled RF cavity has been measured by using a 400 MeV proton beam in the Mucool Test Area at Fermilab. The ionization process generates dense plasma in the cavity and the resultant power loss to the plasma is determined by measuring the cavity voltage on a sampling oscilloscope. The energy loss has been observed with various peak RF field gradients (*E*), gas pressures (*p*), and beam intensities in nitrogen and hydrogen gases. Observed RF energy dissipation in single electron (*dw*) in N2 and H2 gases was 2 10-17 and 3 10-17 Joules/RF cycle at *E/p* = 8 V/cm/Torr, respectively. More detailed *dw* measurement have been done in H2 gas at three different gas pressures. There is a clear discrepancy between the observed *dw* and analytical one. The discrepancy may be due to the gas density effect that has already been observed in various experiments.

PAC13 - SUMMARY OF DENSE H_2 GAS FILLED RF CAVITY TESTS

K. Yonehara, M. Chung, M.R. Jana, M. Leonova, A. Moretti, A. Tollestrup, Fermilab, Batavia, IL, R.P. Johnson, Muons, Inc., Batavia, IL, B. Freemire, Y. Torun, P. Hanlet, Illinois Institute of Technology, Chicago, IL

Summary
We show the recent analysis of a dense gas-filled RF cavity test by using a 400 MeV proton beam from Fermilab Linac. A large amount of RF power loading was observed in a gas-filled RF test cell when protons pass through the test cell. It can be explained that an ionized electron-ion plasma consumes RF power and transfers its kinetic energy to neutral gas molecules via the Coulomb interaction. We used several correction factors based on certain assumptions to evaluate the RF power consumption. The validity of these corrections and assumptions is discussed in this report.

PAC13 - H-P GAS-FILLED RF CAVITIES FOR USE IN A MUON COOLING CHANNEL

B. Freemire, P.M. Hanlet, Y. Torun, IIT, Chicago, IL, M. Chung, M.R. Jana, M. Leonova, A. Moretti, T. Schwarz, A.V. Tollestrup, K. Yonehara, FNAL, Batavia, IL, R.P. Johnson, Muons, Inc., Batavia, IL, M.G. Collura, Politecnico di Torino, Torino, Italy

Summary

A high pressure hydrogen gas-filled RF (HPRF) cavity can operate in the multi-Tesla magnetic fields required for a muon accelerator cooling channel. A beam test was performed at the Fermilab MuCool Test Area by sending a 400 MeV proton beam through an 805 MHz cavity and quantifying the effects of the resulting plasma within the cavity. The resulting energy loss per electron-ion pair produced has been measured at 10^-18 to 10^-16 J every RF cycle. Doping the hydrogen gas with oxygen greatly decreases the lifetime of an electron, thereby improving the performance of the HPRF cavity. Electron lifetimes as short as 1 ns have been measured, and electron-ion recombination rates are on the order of 10^-6 cm3/s. The recombination rate of positive and negative ions in the cavity has been measured on the order of 10^-8 cm3/s. Extrapolation in both gas pressure and beam intensity are required to obtain Muon Collider parameters, however the results indicate HPRF cavities can be used in a muon accelerator cooling channel. (Note, the use of SF6 dopant to attach electrons was used earlier in tests of RF breakdown. The suggestion to use oxygen to attach electrons to reduce plasma loading for beam tests was made by Johnson while supported by this grant DE-FG02-08ER86352.

IPAC14 - RF CAVITY DESIGNS FOR A HELICAL MUON BEAM COOLING CHANNEL

F Marhauser, G Flanangan, R. P. Johnson, S. A. Kahn, Muons, Inc. IL, K. Yonehara, Fermilab, Batavia, IL

Summary

A Helical Cooling Channel (HCC) promises efficient six-dimensional ionization cooling of muon beams by utilizing high-pressurized gas as a continuous absorber within a magnetic channel embedding RF cavities. The progress on cavity design, tailored for such a cooling channel, is discussed.

IPAC14 - PLASMA CHEMISTRY IN A H-P GAS FILLED RF TEST CELL

B. Freemire, Y. Torun, Illinois Institute of Technology, Chicago, IL, M. Chung, M.R. Jana, M. Leonova, A. Moretti, T. Schwarz, A.V. Tollestrup, K. Yonehara FNAL, Batavia, IL, R.P. Johnson, Muons, Inc., Batavia, IL

Summary

Current muon collider schemes call for significant six dimensional (6D) cooling of the muon beam before it is accelerated [1]. One cooling scheme, the Helical Cooling Channel (HCC), employs RF cavities filled with high pressure hydrogen gas [2]. The gas acts both as an energy loss mechanism to allow for ionization cooling [3, 4], and as a buffer in order to prevent RF breakdown [5]. When a beam of particles passes through a HPRF cavity, it will ionize the gas. The amount of plasma generated is dependent on the beam energy, the stopping power of the gas, and the density of the gas. The resulting plasma will gain energy from the RF electric field and transfer it through collisions to the gas. This effect is called plasma loading. An experiment

performed at the MuCool Test Area at Fermilab studied the formation of plasma created by a proton beam and its evolution over the course of many 805 MHz RF cycles [6].

Technical Note – Electrical Breakdown in the All Seasons Cavity
K. Yonehara FNAL, Batavia, IL, et al.
Summary
The All Seasons Cavity (ASC) was tested at the MTA in December 2013. The maximum RF surface gradient was measured as a function of solenoid magnetic field.

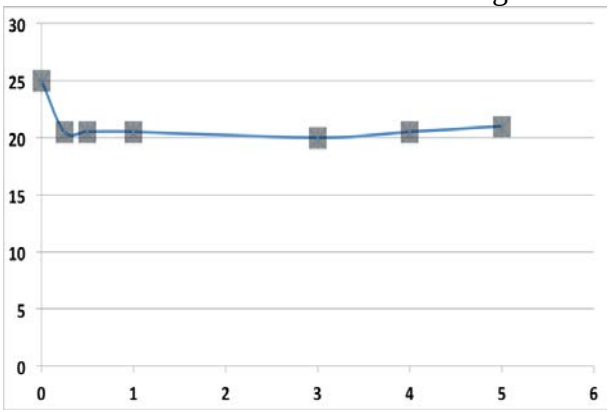

Figure 3: The observed maximum RF surface gradient (MV/m) in the ASC as a function of external solenoid magnetic field (Tesla).

The ASC interior was inspected after the test, where many pits were found on the surface of the RF windows (called end plates in this note). The pit pattern on both plates seems to be mirror symmetric. It suggests that a pit pair is simultaneously generated by an electric discharge or spark due to electric breakdown. Interestingly, the pits are distributed uniformly on the plate, even though the field enhancement on the iris is higher than that on the cavity center. Probably, the cavity was conditioned well. In this note, the electron dynamics in the ASC is described first to show how the uniform pit distribution seems to be unexpected. We also show that the pit pattern has two specific orientations.

References

[1] R.P. Johnson, R.E. Hartline (Muons, Inc.), C. Ankenbrandt, M. Kuchnir, A. Moretti, M. Popovic (FNAL), M. Alsharo'a, E. Black, D.M. Kaplan (Illinois Institute of Technology, Gaseous Hydrogen for Muon Beam Cooling, PAC03, Portland, OR.
[2] P. Hanlet, M. Alsharo'a, R. E. Hartline, R. P. Johnson, M. Kuchnir, K. Paul, Muons Inc, Batavia, IL
C. M. Ankenbrandt, A. Moretti, M. Popovic, FNAL, Batavia, IL, D. M. Kaplan, K. Yonehara, IIT, Chicago, IL
HIGH PRESSURE RF CAVITIES IN MAGNETIC FIELDS, EPAC08, Edinburgh , Scotland.

STUDIES OF BREAKDOWN IN A PRESSURIZED RF CAVITY*

M. BastaniNejad, A. A. Elmustafa, ODU, Norfolk, VA
C. M. Ankenbrandt, A. Moretti, M. Popovic, K. Yonehara, Fermilab, Batavia, IL
D. M. Kaplan, IIT, Chicago, IL,
M. Alsharo'a, P. M. Hanlet, R. P. Johnson, M. Kuchnir, D. Newsham, Muons Inc, Batavia, IL
D. V. Rose, C. Thoma, and D. R. Welch, Voss Scientific, LLC, Albuquerque, NM

Abstract

Microscopic images of the surfaces of metallic electrodes used in high-pressure gas-filled 805 MHz RF cavity experiments [1] have been used to investigate the mechanism of RF breakdown [2]. The images show evidence for melting and boiling in small regions of ~10 micron diameter on tungsten, molybdenum, and beryllium electrode surfaces. In these experiments, the dense hydrogen gas in the cavity prevents electrons or ions from being accelerated to high enough energy to participate in the breakdown process so that the only important variables are the fields and the metallic surfaces. The distributions of breakdown remnants on the electrode surfaces are compared to the maximum surface gradient E predicted by an ANSYS model of the cavity. The local surface density of spark remnants, proportional to the probability of breakdown, shows a strong exponential dependence on the maximum gradient, which is reminiscent of Fowler-Nordheim behavior of electron emission from a cold cathode. New simulation results have shown good agreement with the breakdown behaviour of the hydrogen gas in the Paschen region and have suggested improved behaviour with the addition of trace dopants such as SF_6 [3]. Present efforts are to extend the computer model to include electrode breakdown phenomena and to use scanning tunnelling microscopy to search for work function differences between the conditioned and unconditioned parts of the electrodes.

INTRODUCTION

RF cavities pressurized with hydrogen gas are being developed to produce low emittance, high intensity muon beams for muon colliders, neutrino factories, and other applications. The high-pressure gas suppresses dark currents, multipacting, and other effects that are complicating factors in the study of breakdown in usual RF cavities that operate in vacuum.

In the studies reported here, various metals were tested in a pressurized cavity where RF breakdown is expected to be due only to the interaction of the metallic surfaces with the electromagnetic fields. After exposure to the RF fields, metallic Be, Mo, Cu, and W samples were examined using a Hirox microscope and a scanning electron microscope (SEM) to measure the distribution of breakdown events on the electrode surfaces.

Apparatus

A schematic of the 805 MHz Test Cell (TC) geometry is shown in Figure 1. The TC is a cylindrical stainless steel pressure vessel. RF power is fed into the chamber via a coaxial line. A solenoid magnet (not shown in the figure) provides an axial magnetic field of up to 3 T, which is used in some of the data sets. Replaceable hemispherical electrodes of various materials (Cu, Mo, Be, W) are separated by a 2 cm gap.

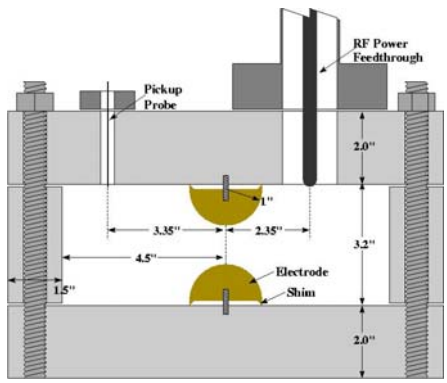

Fig. 1: Cross section of the test cell showing the replaceable one inch radius Cu, Mo, W, or Be hemispherical electrodes. The top and bottom plates and the cylinder are copper-plated stainless steel (the gas input/exhaust port is not shown in the figure).

EXPERIMENTAL RESULTS

RF breakdown

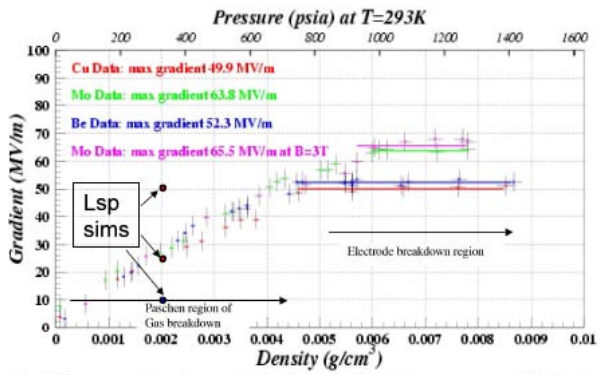

Fig. 2: Maximum stable TC gradient as a function of hydrogen gas density or pressure for Cu, Be, and Mo with no external magnetic field and Mo with 3 T. The three points labelled Lsp sims correspond to simulation results discussed below.

Increasing gas density reduces the mean free collision path for ions giving them less chance to accelerate to energies sufficient to initiate showers and avalanches. As shown in Figure 2, it is found that Cu and Be electrodes

operated stably with surface gradients near 50 MV/m, Mo near 65 MV/m, while W achieved values near 75 MV/m.

Electrode Analysis

After the exposure of the electrodes to acquire the data shown in figure 2, each electrode was examined using secondary and Hirox microscopes. The local surface density of breakdown remnants was recorded as a function of the zenith angle (zero angle corresponds to the axis of the TC). On Be, the breakdown remnants mostly look like boiled melted areas in a tadpole shape with head and tail (figure 3).

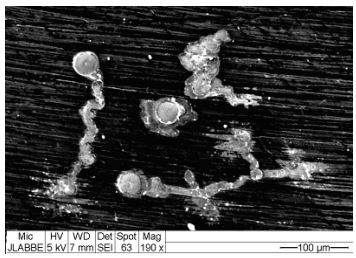

Fig. 3: Beryllium breakdown remnants.

For Mo the breakdown remnants look like overlapped circular melted regions and some splashed areas. Small holes in the melted region may be vents of metallic vapor due to boiling (Figures 4, 5).

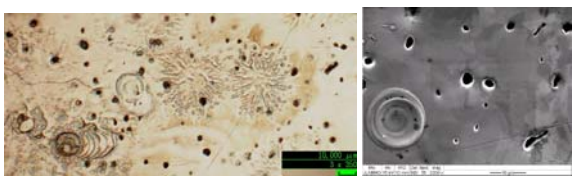

Figs. 4, 5: Molybdenum remnants.

Tungsten breakdown remnants are furrow-shaped melted areas extended on the surface ending in a series of overlapped circles (Figures 6, 7, 8). Cracks that are seen on the breakdown areas are assumed to have occurred subsequent to breakdowns because they are seen on the last ending circle of the set of repeated circles.

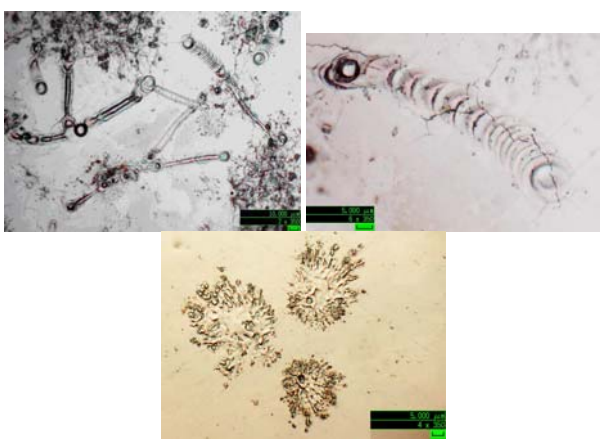

Figs. 6, 7, 8: Tungsten Breakdown.

EXPERIMENTAL DATA ANALYSIS

To investigate the correlation of breakdown and the electric field, the local surface density of breakdown remnants was compared with the maximum expected electric field using an ANSYS model. Least squares fits of the data to a power of the predicted maximum electric gradient at the surfaces of the electrodes show good agreement for high values of the exponent. Figure 9 shows the predicted maximum surface gradient (dashed), the data (black with error bars) as described above, and the best least squares fit (red) to the data $y=0.34E^7$ versus zenith angle for Be. Figures 10 and 11 show the experimental data, the ANSYS model data, and best fits for Mo and W respectively.

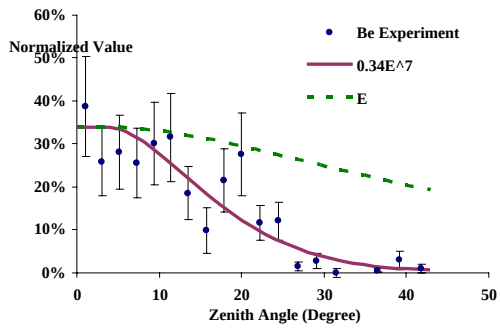

Fig. 9: Be breakdown area fraction vs. zenith angle.

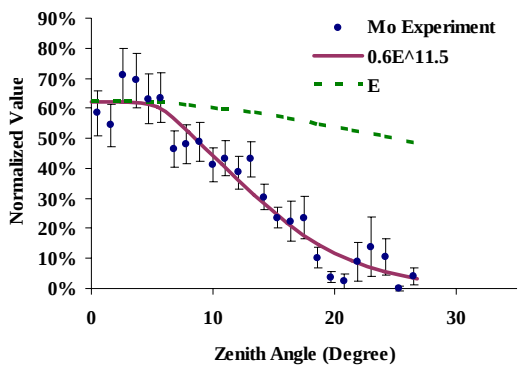

Fig. 10: Mo breakdown area fraction vs. zenith angle.

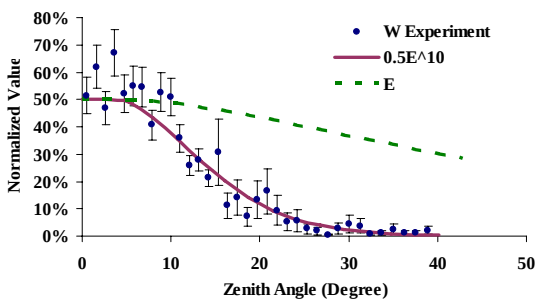

Fig. 11: W breakdown area fraction vs. zenith angle.

The plots also show that the breakdown data correlates with a high power of electric field: 7 for Be, 11.5 for Mo and 10 for W. This suggests that the breakdown is a

quantum mechanical effect described by the Fowler-Nordheim theory of field emission by tunnelling of electrons through a barrier in the presence of a high electric field.

FIRST COMPUTER SIMULATIONS

Computer calculations to simulate the behaviour of breakdown in helium-filled spark-gap switches [4] have been extended to use hydrogen in the Muons, Inc. Test Cell [5]. Three values of electric field were used for the calculations in the conditions of figure 2 at a density of .002 g/cm^3 as indicated by the three red and blue dots.

Figure 12 shows the simulation results for the three electric filed strengths, where the electron density is stable below the Paschen curve (10 MV/m), slightly unstable at the curve (25 MV/m), and very unstable for values above the curve (50 MV/m).

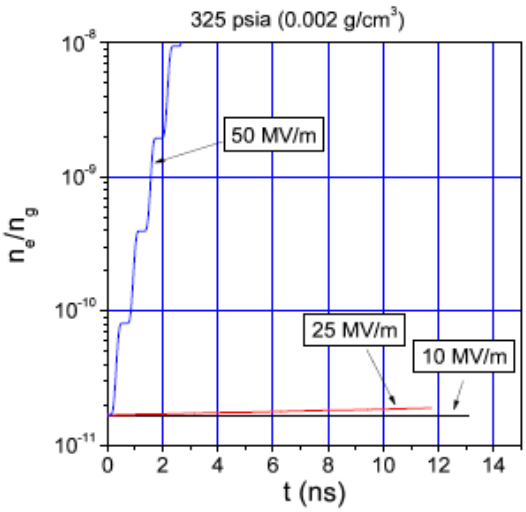

Fig. 12: Electron density as a function of time at 805 MHz and gas density 0.002 g/cm^{-3}.

The temporal evolution of these curves is consistent with the results of the experiment; for E_0 = 10 MV/m, the electron population does not grow because the field is too low to induce ionization of the neutral H_2. At 25 MV/m, the electron density is slowly growing, consistent with this value of E_0 being at the edge of the Paschen law breakdown limit in Figure 2. At 50 MV/m, the electric field drives electrons in the tail of the distribution to high enough energies to efficiently ionize the gas. It is interesting that the 805 MHz period is seen in the growth of the electron density.

One proposed method to increase the effective breakdown threshold for the gas at a given pressure is to introduce a low concentration of electro-negative gas to the H_2. A very low ratio mixture of SF_6 is used to examine this effect. Three additional particle species of neutral SF_6, SF_6^+, and SF_6^- are added to the calculation. The results of a calculation at E_0 = 25 MV/m are shown in figure 13, which plots the electron and negative ion density as a function of time. The initial electron population rapidly decreases, as the negative ion density increases. This demonstrates the desired effect of increasing the Paschen limit for breakdown in pure H_2.

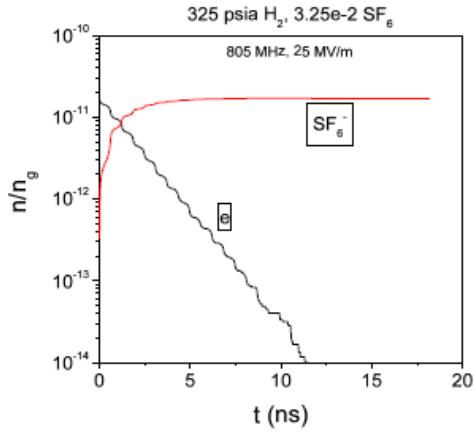

Fig. 13: Electron density depletion and SF_6 ion density growth as a function of time at H_2 density 6×10^{20} cm−3 and SF_6 density 6×10^{16} cm−3.

CONCLUSIONS

The breakdown data shown in figures 9, 10 and 11 show good agreement with high powers of electric field. This strong electric field dependence of the breakdown in pressurized gas is so similar to the dark current dependence predicted by Fowler and Nordheim that breakdown of a metal in a strong electromagnetic field is very likely also a quantum mechanical effect. The fact that the conditioned surfaces of the electrodes are rougher than the unconditioned areas implies the surface enhancement factor in the Fowler-Nordheim expression is not the dominant effect. Thus the work function is a likely factor in the ultimate breakdown limit of metallic structures. This has inspired the study of the distributions of work functions in the electrodes using scanning tunnelling microscopy. On another front, computer simulations of the Paschen region of the breakdown data of the Test Cell show good agreement. The next steps to extend the model to include the metallic electrodes may give more insight to the mechanism of RF breakdown.

REFERENCES

[1] P. Hanlet, M. Alsharo'a, R. E. Hartle, R. P. Johnson, M. Kuchnir, K. Paul, C. M. Ankenbrandt, A. Moretti, M. Popovic, D. M. Kaplan, et al., in Proceedings of EPAC06, Edinburgh, Scotland (2006), p. 1364.

[2] M. BastaniNejad et al., in Proceedings of PAC07, Albuquerque, New Mexico (2007), p. 2499.

[3] Lsp is a software product developed by ATK Mission Research, Albuquerque, NM 87110.

[4] C. Thoma, et al. IEEE Trans. Plasma Sci. 34, 910 (2006)].

[5] D. V. Rose, C. Thoma, D. R. Welch, and R. E. Clark, Low Emittance Muon Collider Workshop, Fermilab, 2008, http://www.muonsinc.com/lemc2008/presentations/ROSE_LEMC2008.ppt

RF BREAKDOWN OF METALLIC SURFACES IN HYDROGEN*

M. BastaniNejad#, A. A. Elmustafa, ODU, Norfolk, VA USA
K. Yonehara, M. Chung, A. Jansson, M. Hu, A. Moretti, M. Popovic, FNAL, Batavia IL USA
M. Alsharo'a, M. Neubauer, R. Sah, R.P. Johnson, Muons, Inc., Batavia, IL USA

Abstract

In earlier reports, microscopic images of the surfaces of metallic electrodes used in high-pressure gas-filled 805 MHz RF cavity experiments were used to investigate the mechanism of RF breakdown of tungsten, molybdenum, and beryllium electrode surfaces. Plots of remnants were consistent with the breakdown events being due to field emission, due to the quantum mechanical tunnelling of electrons through a barrier as described by Fowler and Nordheim. In the work described here, these studies have been extended to include tin, aluminium, and copper. Contamination of the surfaces, discovered after the experiments concluded, have cast some doubt on the proper qualities to assign to the metallic surfaces. However, two significant results are noted. First, the maximum stable RF gradient of contaminated copper electrodes is higher than for a clean surface. Second, the addition of as little as 0.01% of SF_6 to the hydrogen gas increased the maximum stable gradient, which implies that models of RF breakdown in hydrogen gas will be important to the study of metallic breakdown.

INTRODUCTION

RF cavities pressurized with hydrogen gas are being developed to produce low emittance, high intensity muon beams for muon colliders, neutrino factories, and many other applications. The high-pressure gas suppresses dark currents, multipacting, and other effects that are complicating factors in the study of breakdown in usual RF cavities that operate in vacuum. Measurements using the test cell described below in strong magnetic fields have shown that pressurized gas allows higher gradients than can be achieved in vacuum cavities with similar parameters [1,2]. In the studies reported here, various metals are tested in a pressurized cavity where RF breakdown is expected to be due primarily to the interaction of the metallic surfaces with the electromagnetic fields.

APPARATUS

A schematic of the 805 MHz Test Cell (TC) geometry is shown in Figure 1. The TC is a cylindrical copper-plated stainless steel pressure vessel. RF power is fed into the chamber via a coaxial line Replaceable hemispherical electrodes of various materials (Sn, Al, Cu, Mo, Be, W) are separated by a 2 cm gap. The characteristics of the cavity and the MTA experimental conditions have been described previously [1]. The data described here were taken at the same time as data reported in another paper at this conference [3].

After exposure to the RF fields, the metallic Al, Cu and Sn samples were examined using a High-Scope Advanced Microscope (Hirox†) and scanning electron microscope (SEM) to determine if breakdown events are associated with characteristics of the material surfaces.

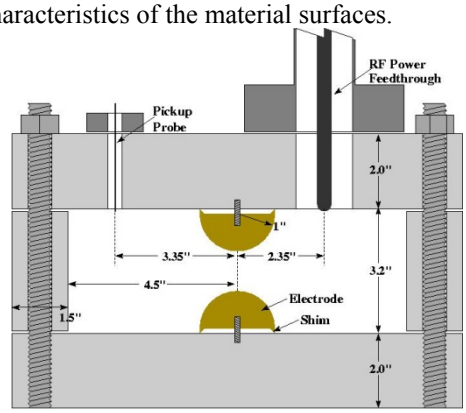

Figure 1: Cross-section of the Muons, Inc. Test Cell.

EXPERIMENTAL RESULTS

The experimental results of maximum stable RF gradient as a function of hydrogen pressure for Al, Cu and Sn are shown in Figure 2. The usual model for this is that increased gas density reduces the mean free collision path for ions giving them less chance to accelerate to energies sufficient to initiate showers and avalanches.

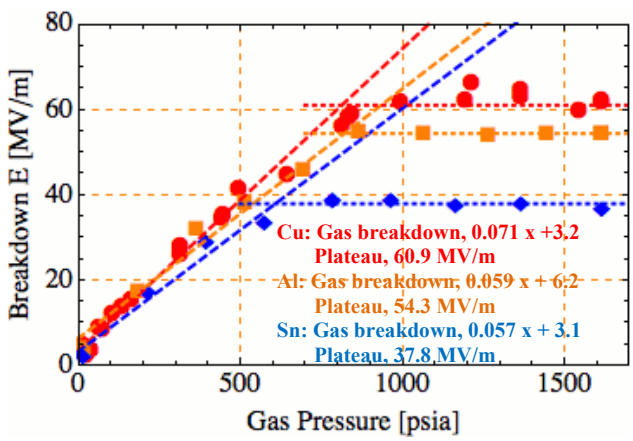

Figure 2: Maximum stable TC gradient as a function of hydrogen gas pressure for Al, Cu and Sn.

This model applies to the linearly rising gradient as the pressure is increased. At some point, the gradient

* Supported in part by DOE STTR grant DE-FG02-05ER86252 and FRA DOE contract number DE-AC02-07CH11359
# Mahzad@jlab.org
† Thanks to College of William & Mary use of the Hirox.

becomes high enough to cause the metallic surface to break down and the maximum gradient does not increase as the pressure is increased further. As shown in Figure 2, it is found that Cu electrodes operated stably with surface gradients near 60 MV/m, Al near 54 MV/m, while Sn achieved values near 38 MV/m. The three electrode materials were run at their maximum voltages for several hours.

Melting point and breakdown voltage

The Maximum gradient for all materials, Al, Cu and Sn, from the data set reported here is shown in blue on figure 3 along with Cu, Be, Mo, and W in red from previous measurements in terms of melting point.

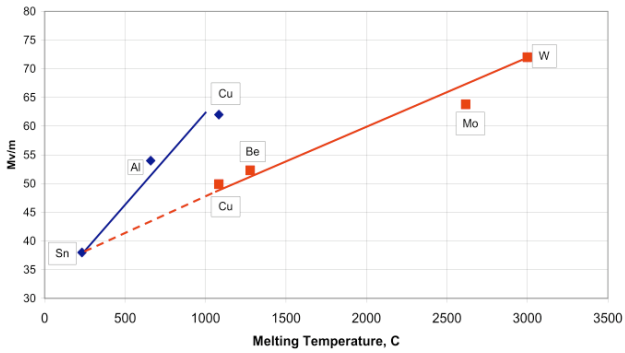

Figure 3: Breakdown voltage vs melting point of various electrode materials. Red squares are older data, blue diamonds are the data reported here.

It should be noted that the melting point is unlikely to be the actual independent variable, since a straightforward calculation indicates the energy deposited in a breakdown event should lead to a different dependence [4]. However, the melting point should scale with the bond strength. And the bond strength should be related to other relevant parameters like fatigue limits, as suggested by recent work by Dolgashev and Tantawi [5].

An unexpected result was that a new set of copper electrodes which were meant to be an experimental control had a higher breakdown gradient than had been seen in previous experiments with a different set of copper electrodes. Surface analysis after the experiments ended indicated that the new copper electrodes were a different grade of copper with surface contaminants of machine oil and sulfur, the latter presumably deposited during the SF_6 doping measurements described below.

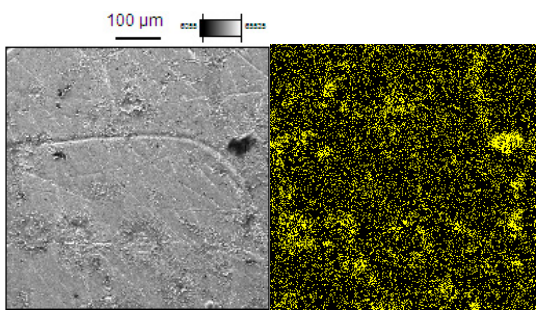

Figure 4: The carbon mapping of the copper surface.

Figures 4, 5, and 6 show the SEM map of Carbon and Oxygen on the copper and aluminium electrode surfaces after the test, respectively. Table 1 shows the Energy Dispersive X-ray (EDX) analysis of the materials on the copper surface. The carbon and oxygen may be from machine oil.

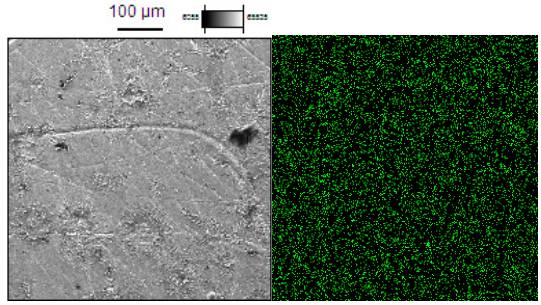

Figure 5: The oxygen mapping of the copper surface SEM

Table 1: Amount of different elements on the Cu surface.

Element	Weight %	Weight % Error	Norm. Wt.%	Atom %	Atom % Error
C	22.67	+/- 0.66	22.67	58.78	+/- 1.72
O	1.64	+/- 0.24	1.64	3.20	+/- 0.47
S	1.93	+/- 0.06	1.93	1.87	+/- 0.06
S	---	---	---	---	---
Cu	73.76	+/- 0.89	73.76	36.14	+/- 0.43
Cu	---	---	---	---	---
Total	100.00		100.00	100.00	

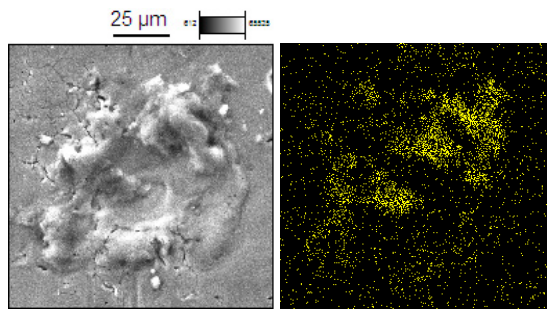

Figure 6: The C mapping of the Al surface

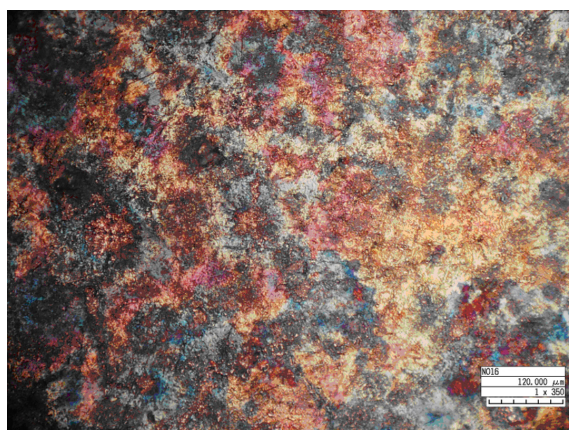

Figure 7: Picture of copper electrode surface after the breakdown experiments. Blue and red discolorations are copper oxides and the white areas correspond to sulphur. The total width of the picture is about 1 mm.

EFFECTS OF SF_6 DOPING

A companion paper reported at this conference studied the results of the same experiment from the standpoint of the RF breakdown at lower pressures, where the gas properties determine the maximum stable RF gradient.

The measurements shown in figure 2 were done with undoped hydrogen gas. One of the reasons that the surfaces may have been contaminated as described above, was that studies carried out in parallel and reported elsewhere at this meeting were testing the use of SF_6 as a means to improve the ability of hydrogen-filled RF cavities to work in the presence of intense beams of ionizing radiation. The breakdown of the SF_6 during these experiments probably accounts for the trace amounts of sulphur shown in table 1.

However, the results of the maximum stable gradient versus pressure studies with the dopant have clearly shown that one of the hypotheses that has inspired the use of pressurized cavities as a means to study RF breakdown is not correct. Namely, it was believed that the pressurized gas would absorb dark currents and thereby allow the study of breakdown of metal surfaces to be simplified such that the major variables would only be the metallic surface and the electromagnetic fields.

The unexpected result can be seen in figure 8, which shows the usual plot of electric gradient versus pressure for the case of the aluminum electrodes. The red points correspond to the case of pure hydrogen gas and the green points to the case of 0.01% SF_6 doped hydrogen. As shown in the companion paper, the rising slope at low pressure, the Paschen region, is improved by an amount that is predicted by a simulation model of gas breakdown with SF_6 doping.

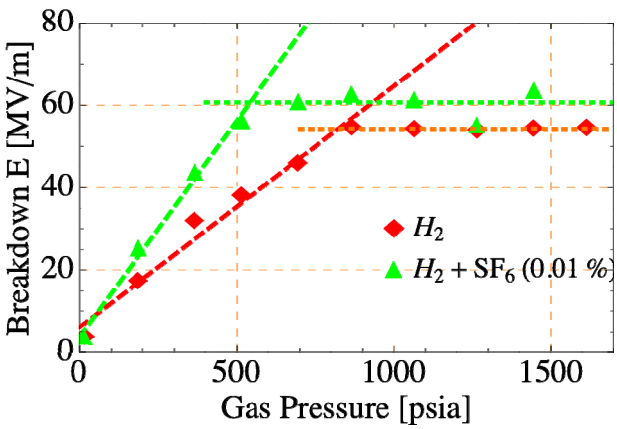

Figure 8: Observed breakdown as a function of gas pressure and dopant in aluminum electrodes.

The higher pressure regions of the figure, where the breakdown gradient does not change with pressure, show that the maximum stable gradient is significantly affected by the SF_6 dopant. This effect is also seen in the studies of the copper and tin electrodes.

Earlier studies of the plateau region of various electrode materials did not show any obvious differences between hydrogen or nitrogen gas and that led credence to the idea that the gas has little effect on the metallic breakdown phenomena. These SF_6 doping studies have demonstrated that not to be the case, and models of metallic breakdown in pressurized cavities will have to include the gas. As shown in the companion paper [3], gas models can be developed and tested in the Paschen region and already have some satisfying agreement with experimental data. A new 1.3 GHz test cell has been constructed that will allow breakdown studies under pressurized and vacuum conditions [6]. This will allow the experimental investigation of theories of RF breakdown over a wide range of parameters [7].

CONCLUSIONS

Systematic studies of breakdown in pressurized cavities are continuing to investigate the role of bond strength, as described by melting or boiling point, in determining the maximum stable RF gradient. The latest studies were inconclusive because of contamination of the electrode surfaces. Unexpectedly, the contaminated copper surface allowed a higher maximum gradient that was earlier achieved with a clean surface,

New measurements of the effects of SF_6 doping imply that gas composition can have a significant effect on the maximum stable gradient in the plateau region of the gradient versus pressure curves. Breakdown models in pressurized cavities will have to include the details of the gas interaction.

REFERENCES

[1] M. BastaniNejad et al., EPAC08
[2] P. M. Hanlet et al., EPAC06
[3] K. Yonehara et al., this conference
[4] A.Tollestrup, http://beamdocs.fnal.gov/AD-public/DocDB/ShowDocument?docid=3345
[5] S. G. Tantawi, Progress in High Gradient Accelerator Structure Research for Future Linear Colliders, PAC09
[6] R. Sah et al., this conference.
[7] J. Norem, et al, "Dark current, breakdown and magnetic field effects in a multicell, 805 MHz cavity," Phys. Rev, 6, 2003.

RF BREAKDOWN STUDIES USING A 1.3-GHZ TEST CELL*

R. Sah†, R. P. Johnson, M. Neubauer, Muons, Inc., Batavia IL
M. Conde, W. Gai, ANL, Argonne, IL
A. Moretti, M. Popovic, K. Yonehara, Fermilab, Batavia, IL
J. Byrd, D. Li, LBNL, Berkeley, CA
M. BastaniNejad, A. A. Elmustafa, ODU, Norfolk,VA

Abstract

Many present and future particle accelerators are limited by the maximum electric gradient and peak surface fields that can be realized in RF cavities. Despite considerable effort, a comprehensive theory of RF breakdown has not been achieved and mitigation techniques to improve practical maximum accelerating gradients have had only limited success. Recent studies have shown that high gradients can be achieved quickly in 805 MHz RF cavities pressurized with dense hydrogen gas without the need for long conditioning times, because the dense gas can dramatically reduce dark currents and multipacting. In this project we use this high pressure technique to suppress effects of residual vacuum and geometry found in evacuated cavities to isolate and study the role of the metallic surfaces in RF cavity breakdown as a function of magnetic field, frequency, and surface preparation. A 1.3-GHz RF test cell with replaceable electrodes (e.g. Mo, Cu, Be, W, and Nb) and pressure barrier capable of operating both at high pressure and in vacuum has been designed and built, and preliminary testing has been completed. A series of detailed experiments is planned at the Argonne Wakefield Accelerator. At the same time, computer simulations of the RF Breakdown process will be carried out to help develop a consistent physics model of RF Breakdown. In order to study the effect of the radiofrequency on RF Breakdown, a second test cell will be designed, fabricated, and tested at a lower frequency, most likely 402.5 MHz.

INTRODUCTION (805-MHZ STUDIES)

RF cavities pressurized with hydrogen gas are being developed to produce low emittance, high intensity muon beams for muon colliders, neutrino factories, and other applications. The high-pressure gas suppresses dark currents, multipacting, and other effects that are complicating factors in the study of breakdown in usual RF cavities that operate in vacuum.

In the earlier 805-MHz studies, various metals were tested in a pressurized cavity where RF breakdown is expected to be due to the interaction of the metallic surfaces with the electromagnetic fields. After exposure to the RF fields, metallic Be, Mo, Cu, and W samples were examined using a Hirox microscope and a scanning electron microscope (SEM) to measure the distribution of breakdown events on the electrode surfaces [1].

*Work supported in part by USDOE STTR Grant DE-FG02-08ER86352 and FRA DOE Contract DE-AC02-07CH11359
†richard@muonsinc.com

Experimental Results: RF breakdown

Unlike in the case of vacuum RF breakdown, high-pressure RF breakdown exhibits different behavior in two distinct regimes: (1) a gas breakdown region where the maximum gradient follows the Paschen curve, and (2) a surface breakdown region where increasing the gas pressure does not change the maximum gradient. See Figure 1.

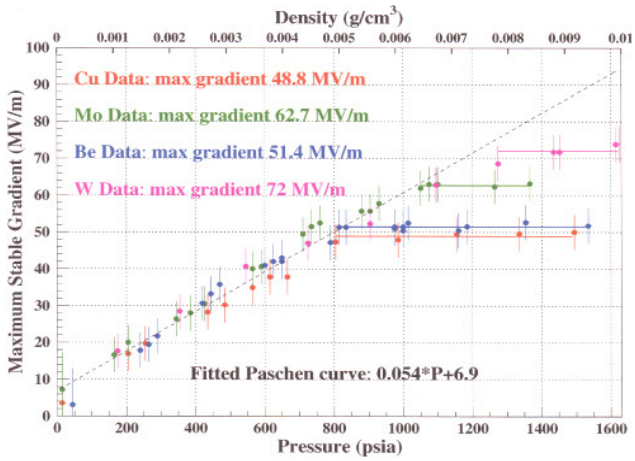

Figure 1: Maximum stable TC gradient as a function of hydrogen gas density or pressure for Cu, Be, Mo, and W with no external magnetic field.

Increasing gas density reduces the mean free collision path for ions giving them less chance to accelerate to energies sufficient to initiate showers and avalanches. It was found that Cu and Be electrodes operated stably with surface gradients near 50 MV/m, Mo near 63 MV/m, while W achieved values near 72 MV/m [2].

To investigate the correlation of breakdown and the electric field, the local surface density of breakdown remnants was compared with the maximum expected electric field using an ANSYS model. Least squares fits of the data to a power of the predicted maximum electric gradient at the surfaces of the electrodes showed good agreement for high values of the exponent. These results showed that the breakdown data correlated with a high power of electric field (7 for Be, 11.5 for Mo, and 10 for W) and suggest that the breakdown is a quantum mechanical effect described by the Fowler-Nordheim theory of field emission [3] by tunneling of electrons through a barrier in the presence of a high electric field.

Recent Experimental Results

The experiments at Fermilab were recently extended to include electrodes made of tin, aluminum, and copper. The maximum stable RF gradient in the surface breakdown region increased linearly with the melting point of the metallic electrodes. Since the melting point should scale with the bond strength, it is possible that the important parameter might be bond strength or fatigue limits, as has been suggested by recent work by Dolgashev and Tantawi [4].

Also, the experiments at Fermilab included the use of N_2 gas and the use of SF_6 as an electronegative dopant to capture free electrons.

NEW TEST CELLS

1.3 GHz Test Cell

A 1.3 GHz test cell was designed by scaling the 805 MHz cell internal dimensions. See Figure 2. The input power is through a 1-5/8" coax with an epoxy window designed for high pressure from the 805 MHz cavity test assembly. The pickup probe is a 0.141" coax antenna with an OSM connector. The vacuum seal for the probe is a mini-conflat flange and the seal for the threaded vacuum port is a viton o-ring seal. All other seals are 0.008" aluminum shims. The 1-5/8" coax seal was torqued to 40 ft-lbs and the cavity seals torqued to 90 ft-lbs. The cavity is designed to withstand 1600 psi pressure, and is made from copper-plated 316 stainless steel. The top and bottom "lids" are 2 in. thick and the cylindrical walls are 1.6 in. thick. The electrodes are OFHC copper.

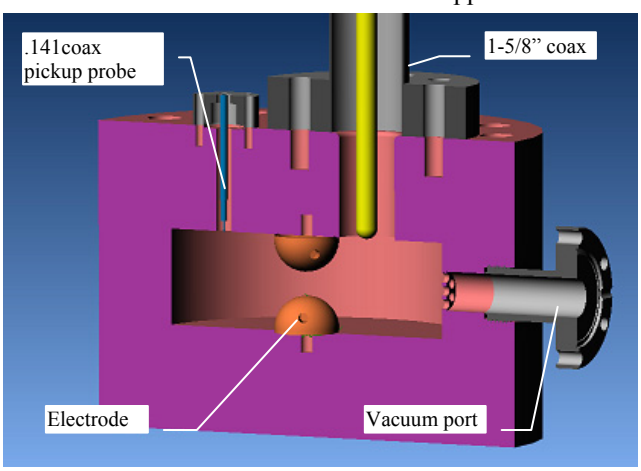

Figure 2: Cutaway view of the 1.3 GHz Cavity

The 1.3-GHz test cell was assembled at Fermilab and mounted on a pump stand, as shown in Figure 3. After cold testing was completed, the test cell was vacuum tested at Fermilab and found to hold a vacuum of about 5 10^{-6} Torr, measured at the ion pump. This vacuum was good enough to proceed with operation with RF power, so the test cell along with its pump stand was transported to the Argonne Wakefield Accelerator (AWA). Although our primary interest is to study the operation of this test cell under high-pressure conditions, it was decided to initiate high-power tests of this test cell under vacuum conditions, because it was much quicker to acquire safety approvals to operate under vacuum conditions.

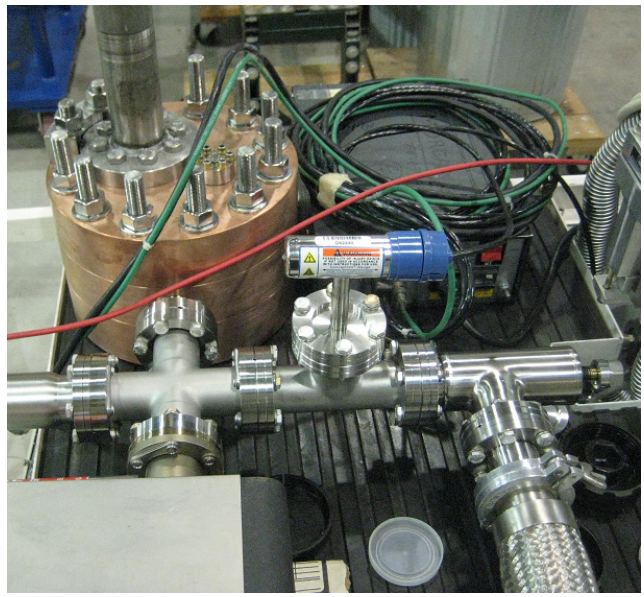

Figure 3: 1.3-GHz Cavity and vacuum System

The test cell's coax feed line was connected to the output waveguide of the AWA 1.3-GHz test stand, via a transition element, and operation with RF power commenced. At the beginning, of course, there was considerable multipacting, and the gas pressure increased quickly. A process of RF conditioning was undertaken, in which the RF power was slowly increased, while keeping the gas pressure below 1 10^{-5} Torr. After 2.5 days of effort, the conditioning of the 1.3-GHz test cell was completed. At that point, the gas pressure was typically in the low 10^{-6} range at a 5-Hz pulse rate, and the pulse shape seen at the pickup electrode was clean, without any evidence of multipacting nor of RF breakdown.

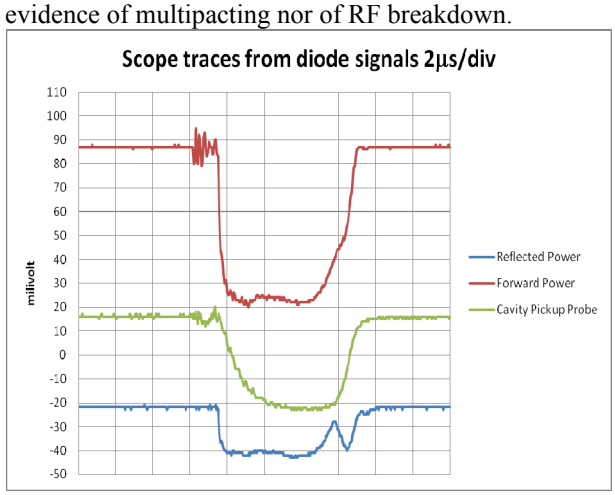

Figure 4: Scope traces of the signals from the 1.3-GHz test cell

Figure 4 shows the scope traces of the forward power, cavity pickup, and reflected power. Measurements of the

RF parameters were analyzed, and the power in the test cell was found to be 221 kW, corresponding to a gradient of 71 MV/m.

The process of requesting ANL safety approval for high-pressure operation of this test cell has already begun. After this approval is granted, we plan to conduct a detailed series of experiments using this 1.3-GHz test cell. Among the many experimental variables we hope to study are different electrode metals, different surface preparation, different gases, and different magnetic fields.

402.5 MHz Test Cell

In order to study the effect of the radiofrequency on RF Breakdown in gas-filled cavities, we plan to conduct a follow-up series of experiments at a lower frequency. Because of the availability of a 402.5-MHz test stand at LBNL, it is likely that we shall choose this frequency. The plan is to bring this test stand to operational condition, design and build a 402.5-MHz test cell, and to conduct a similarly-detailed series of experiments at this lower frequency. Earlier, a 500-MHz test cell had already been designed as shown in figure 5, so we anticipate that a modification of the existing design will be used for the 402.5-MHz test cell.

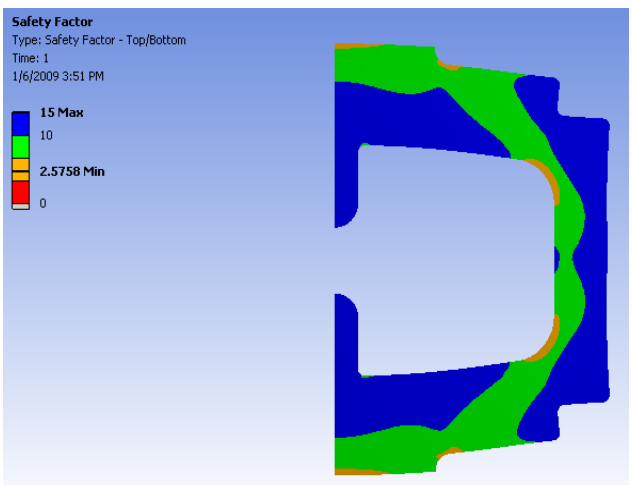

Figure 5: Axi-symmetric ANSYS calculations for the 500 MHz cavity with safety factor calculations at 1600 psi

COMPUTER SIMULATIONS

Separate computer simulations are being carried out for the gas breakdown region and the surface breakdown region.

Gas Discharge Simulations

Muons, Inc. is presently working with Dr. Dave Rose of Voss Scientific on physical models of RF breakdown in hydrogen gas as part of our program to develop RF cavities for muon cooling [5]. This effort is directed toward understanding and mitigating breakdown in the conditions of a muon cooling channel, where there are large magnetic and radiation fields. This modeling effort is focused on the breakdown of the pressurized gas itself, but we now know that the nature of the gas also plays a role in the breakdown of the metallic surfaces of the cavity, even in the surface-breakdown region.

Metal Surface Simulations

ANSYS modeling will be used to study the heating of small areas of the metal surface. We shall examine the effects of current flow at asperities and at low-work-function areas, in order to understand the characteristic behaviors of different physical models. We expect these simple simulations to give us useful insights into the physics at the metal surface.

REFERENCES

[1] M. BastaniNejad et al., EPAC08, Genoa Italy
[2] P.M. Hanlet et al., "High pressure RF cavities in magnetic fields," EPAC06, Edinburgh, Scotland.
[3] R.H. Fowler and L. Nordheim, "Electron emission in intense electric fields," in Proc. Roy. Soc. (London), A119, pp. 173-181, 1928
[4] S.G. Tantawi, "Progress in High Gradient Accelerator Structure Research for Future Linear Accelerators," PAC09
[5] D.V. Rose *et al.,* Proc. 16th International Pulsed Power Conference, Albuquerque, NM, 2007

STUDY OF ELECTRON SWARM IN HIGH PRESSURE HYDROGEN GAS FILLED RF CAVITIES*

K. Yonehara#, M. Chung, A. Jansson, A. Moretti, M. Popovic, A. Tollestrup, Fermilab, Batavia, IL 60510, U.S.A.
M. Alsharo'a, R.P. Johnson, M. Notani, Muons, Inc., Batavia, IL 60510, U.S.A.
D. Huang, Illinois Institute of Technology, Chicago, IL 60616, U.S.A.
T. Oka, H. Wang, University of Chicago, Chicago, IL 60637, U.S.A.
D. V. Rose, Voss Scientific, Albuquerque, NM 87108, U.S.A.
Z. Insepov, Argonne National Lab, Argonne, IL 60439, U.S.A.

Abstract

A high pressure hydrogen gas filled RF cavity has been proposed for use in the muon collection system for a muon collider. It allows for high electric field gradients in RF cavities located in strong magnetic fields, a condition frequently encountered in a muon cooling channel. In addition, an intense muon beam will generate an electron swarm via the ionization process in the cavity. A large amount of RF power will be consumed into the swarm. We show the results from our studies of the HV RF breakdown in a cavity without a beam and present some results on the resulting electron swarm dynamics. This is preliminary to actual beam tests which will take place late in 2010.

INTRODUCTION

The operation of High Pressure hydrogen gas filled RF (HPRF) cavity has been successfully tested under various conditions [1, 2]. A description of the physics processes in a HPRF cavity with beam is described at length in [3]. Beam tests are necessary to verify the theory and are planned in the near future.

A high intensity beam passing through dense hydrogen gas forms a beam-induced electron swarm via the ionization process. These electrons are shaken by the RF field, and thus their inelastic collisions with the hydrogen molecules will consume a large amount of RF power from the cavity. Consequently, the cavity Q value is degraded as a function of the amount of beam passing through the cavity. The degradation will be an issue since the beam in the later part of bunch train will see less electric acceleration amplitude than that in the earlier part of bunch train. In case of muon collider, 10^{11} muons per bunch at kinetic energy 100 ~ 400 MeV may pass through a 200 atm HPRF cavity during 60 ns and generate up to 10^{14} cm^{-3} electron swarm in the cavity [3]. In the worst case, a half of RF acceleration field will be dissipated into this amount of electrons if all ionized electrons survive in 60 ns. However, the recombination rate in such a dense hydrogen gas has never been investigated.

A HPRF cavity beam test is scheduled to investigate beam-induced electron swarm [4]. A 400 MeV H^- beam line has been built from the Linac to the MTA (Mucool Test Area) experimental hall at Fermilab. Up to 10^{13} protons per 20 μs bunch train will be sent to the MTA hall. The density of built-up beam-induced electron swarm can be large enough to perturb the RF resonance field. Therefore, the recombination rate can be observed precisely by measuring the time domain amplitude of RF field with a well-known intensity beam [5]. The first beam test will be carried out in summer of 2010.

Meanwhile, we have studied the electron swarm which was generated in an RF breakdown without beam. In this analysis, we used a RF field pickup and the optical spectroscopic signals. The experimental result and analysis are discussed in this document.

EXPERIMENT

Breakdown probability

The RF breakdown probability in the HPRF cavity was measured systematically. Fig. 1 shows the observed external electric field with Cu electrodes as a function of the hydrogen gas pressure. The color codes correspond to the probability of breakdown. The lowest probability reproduces the breakdown curve in the past measurements. The maximum electric field was 50 MV/m with the breakdown probability less than 10^{-4} at higher gas pressure than 1000 psi.

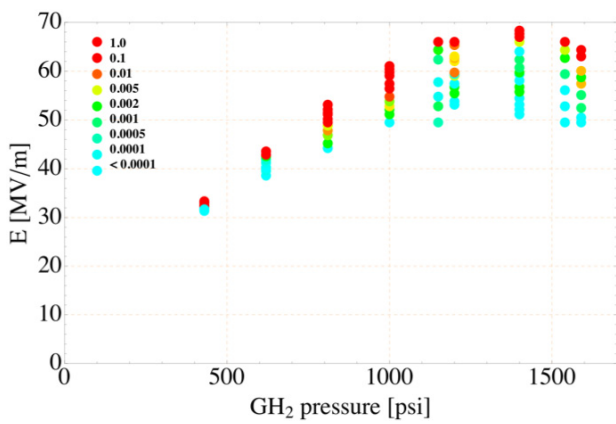

Fig. 1: The breakdown probability plot in the HPRF cavity.

A clear Paschen curve was observed at GH2 pressure below 1000 psi. In this pressure region, the derivative of

*Work supported by DOE STTR grant DE-FG02-08ER86350 & FRA under DOE contract DE-AC02-07CH11359
#yonehara@fnal.gov

breakdown probability with respect to the electric field strength was very steep, and the reproducibility was quite good, i.e. the maximum electric field strength was reproduced immediately after many breakdowns. On the other hand, we observed large fluctuations in the breakdown probability at gas pressure range above 1000 psi. The RF cavity conditioning was needed during a long time (although it was ~30 mins. with 15 Hz RF rep rate) to recover the maximum RF amplitude after many breakdowns. This is likely due to heavy surface damage by multiple breakdown.

Analysis of electron swarm by resonance frequency measurement

The RF cavity electrically forms the high-Q LC resonance circuit. Therefore, the RF resonance field is very sensitive to the electron swarm. Such a destructive process of resonance field was measured by the RF pickup probe. An electrical model of the cavity has been used to extract information about the discharge channel. Initially, field emission starts a streamer propagating across the cavity which changes into an arc upon reaching across the cavity. Initially the current grows exponentially, but when it reaches a current of several hundred amps a pinch occurs and the current can increase to more than 1000 amps near the end of the discharge. The period before the pinch has been analyzed by the reduction of the cavity voltage versus time. The using the known mobility of the electrons in the gas allows an estimation to be made of the total number of electrons participating in the initial stages of the discharge. A plot of the growth of the number of electrons per half cycle is shown in Figure 2.

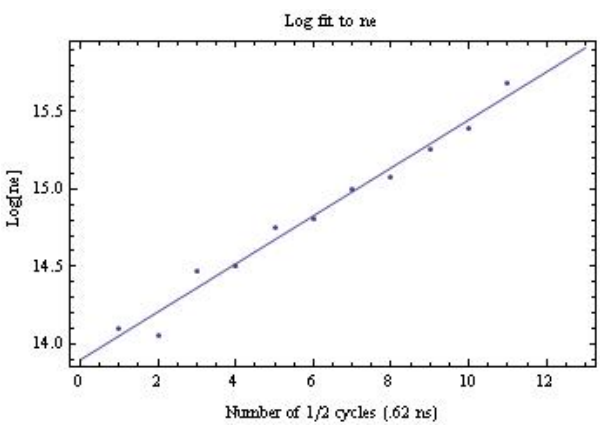

Fig. 2: Growth of electron swarm as a function of a half of RF cycles.

Electron swarm in spectroscopic measurement

A spectroscopic measurement with various hydrogen gas pressures (540, 740, 930, 1120, and 1310 psi) was done. Strong light was observed during the RF breakdown. The spectrometer system consists of a pressure tight 1-mm diameter optical feed-through that is connected to an optical spectrometer (Horiba iHR320 + Hamamatsu H5783-20). The resolution of the spectrometer was set to ± 2.5 nm. In order to obtain a clear light signal, the light was accumulated over 100 RF breakdowns. The applied electric field strength was carefully adjusted to make the breakdown probability of less than 1 % to avoid sequential breakdowns. To obtain a stable trigger signal, an additional PMT (Hammamatsu H5783) and an optical fiber was connected to another optical port. The trigger level was high enough to remove any background signal, e.g. cosmic ray. Figure 2 shows the observed non-corrected 503 and 656 nm time domain spectroscopic lights from 740 psi HPRF cavity. The "zero" timing is at the peak of spectroscopic light signal. Since only one PMT was assembled on the spectrometer only one wavelength light was taken for one data acquisition.

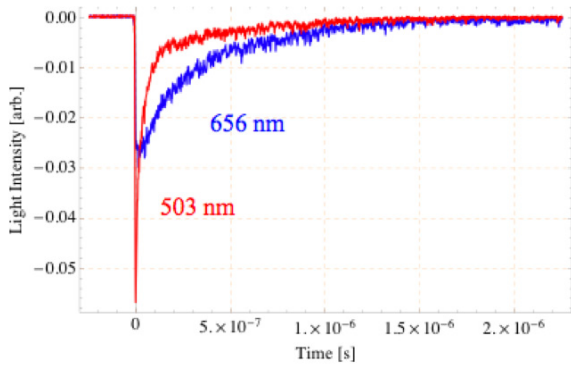

Fig. 3: 503 and 656 nm spectroscopic lights from 740 psi HPRF cavity. The signal was accumulated over 100 RF breakdowns.

The spectroscopic light intensity (integrated within Δt = 1 ns) was corrected by the sensitivity of PMT and the transmission efficiency of optical system as a function of wavelength and was normalized by the integrated intensity of trigger PMT signal. We observed a very broad spectrum and an Hα resonance peak (Fig. 3). The broad spectrum is well fitted with a blackbody radiation formula. In the blackbody radiation analysis, the non-resonant data points are chosen (red point). The obtained plasma temperature is 15,000 K at t = 0 ns. This value is quite independent from pressure of gaseous hydrogen.

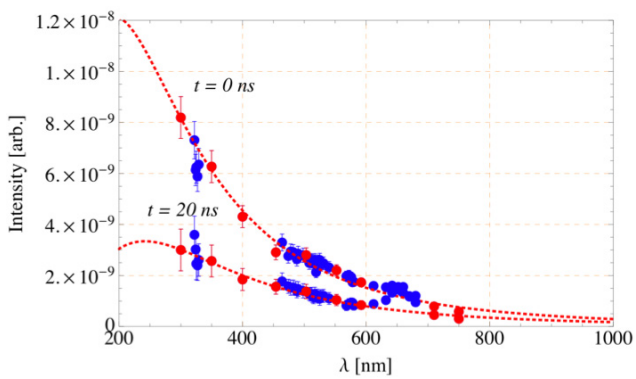

Fig. 4: Spectra from 740 psi HPRF cavity with various timing. Red points are chosen for the blackbody radiation analysis.

The Hα line shape is extracted by fitting a Lorentz distribution curve. Figure 4 shows the enlarged spectra from Figure 3 and the fitted Lorenz curve on Hα resonance. First, we noticed that the intensity of Hα resonance at t = 0 ns was much smaller than the Hα at t = 20 ns. In this time duration, the plasma temperature goes down from 15,000 to 12,000 K. The time delay can be due to the pumping and spontaneous emission rates of hydrogen molecule/atom.

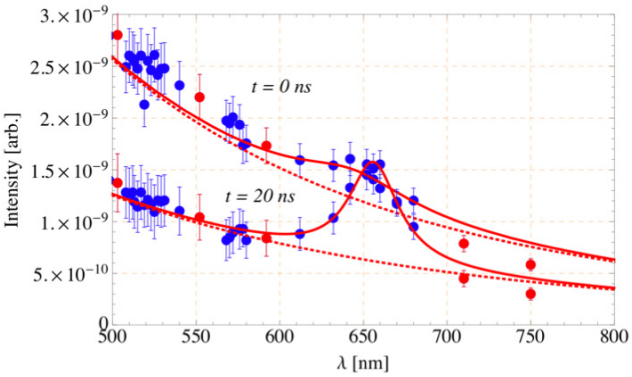

Fig. 5: Enlargement around Hα resonance from Figure 3. The dotted line is the blackbody curve and the solid line includes the Lorentz curve.

Fig. 5 shows the width of Hα line as a function of time. A similar broadening of resonant light in dense hydrogen plasma conditions has been reported by several groups. They proved that the Stark effect can well explain the broadening [7, 8] where the hydrogen energy level is perturbed by a local electric field. Therefore, the line width strongly depends on the plasma density and the plasma temperature. We are working on further analysis.

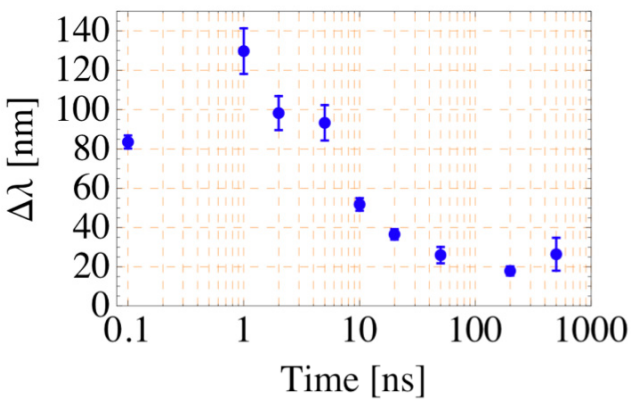

Fig. 6: Full Width Half Maximum of Hα line as a function of time where t = 0.1 ns corresponds to t = 0 ns

HPRF BEAM TEST

Polyatomic hydrogen

Ionized hydrogen ions quickly form polyatomic hydrogen cluster ions which recombine with ionized electrons faster than H_2^+ and H^+. This process has been well known in molecular physics in dilute hydrogen gas conditions, i.e. in stellar hydrogen, for a long time. Polyatomic hydrogen is produced in a chain process in a very short time. The molecular hydrogen ion H_2^+ forms H_3^+ via the reaction $H_2^+ + H_2 \rightarrow H_3^+ + H$ which forms cluster ions very quickly via chain of reaction. Additional three body interaction is taken place and generates larger hydrogen cluster ions, i.e., $H_3^+ + 2H_2 \rightarrow H_5^+ + H_2$, $H_5^+ + 2H_2 \rightarrow H_7^+ + H_2$ etc [3, 6]. Two crucial questions remain to be answered by actual beam tests. The first is how quickly the electrons are neutralized and thus their loading effect on the cavity reduced to tolerable values. And second how long it takes the plasma in the cavity to dissipate so it doesn't induce a break down on subsequent RF pulses.

Electronegative dopant gas

Adding an electronegative dopant gas in hydrogen plasmas is another important topics in the beam test if the beam induced RF Q reduction is significant. SF_6 and c-C_4F_8, which are candidate gasses, have a different attachment cross-section as a function of electron kinetic energy (Fig. 6). The ionized electron kinetic energy is widely distributed. Thus, c-C_4F_8 may be more effective for electron density reduction than SF_6 if the electron kinetic energy is high.

Admixtures of SF_6 in H_2 have been studied in the HPRF cavity without beam [1]. The maximum RF amplitude (in the Paschen limit) is increased ~20 % with 0.2% levels of SF_6. However, SF_6 may be dissociated during RF breakdown, forming F^- and HF. These elements are very active and interact with metals. In fact, cavity surface damage was observed after the tests. Non-fluorine dopant gasses exists will be more useful from practical point view although their attachment cross-sections are orders of magnitude lower than SF_6 and c-C_4F_8.

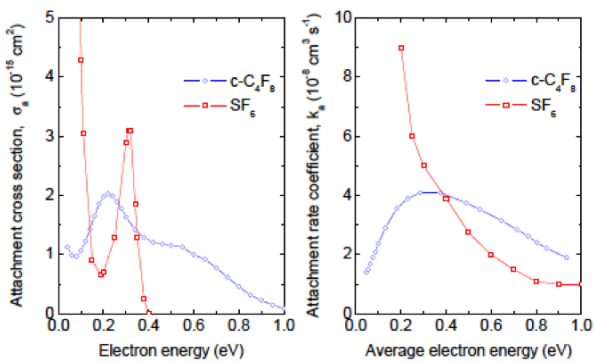

Fig. 7: (Left) Attachment cross-sections and (Right) attachment coefficients of SF_6 and c-C_4F_8

REFERENCES

[1] K. Yonehara et al., PAC09, TU5PFP020.
[2] P. Hanlet et al., EPAC06, TUPCH147.
[3] A. Tollestrup et al., FERMILAB-TM-2430-APC.
[4] M. Chung et al., IPAC'10, WEPE066.
[5] M. Chung et al., NFMCC-doc-532-v2.
[6] K. Hiraoka, J. Chem. Phys. **87**, 4048-4055 (1987).
[7] St. Boddeker et al., Phys. Rev. **E47**, 2785 (1993).
[8] H.R. Griem, Phys. Rev. **A28**, 1596 (1983).

RF BREAKDOWN STUDIES USING PRESSURIZED CAVITIES*

R. Sah, A. Dudas, R. P. Johnson, M. Neubauer, Muons, Inc., Batavia IL
M. Conde, W. Gai, ANL, Argonne, IL
A. Moretti, M. Popovic, K. Yonehara, Fermilab, Batavia IL
J. Byrd, D. Li, LBNL, Berkeley, CA; D. Rose, Voss Scientific, Albuquerque NM
M. BastaniNejad, M. Elmustafa, ODU, VA

Abstract

Many present and future particle accelerators are limited by the maximum electric gradient and peak surface fields that can be realized in RF cavities. Despite considerable effort, a comprehensive theory of RF breakdown has not been achieved, and mitigation techniques to improve practical maximum accelerating gradients have had only limited success. Recent studies have shown that high gradients can be achieved quickly in 805 MHz RF cavities pressurized with dense hydrogen gas without the need for long conditioning times, because the dense gas can dramatically reduce dark currents and multipacting. In this project we use this high pressure technique to suppress effects of residual gas and geometry found in evacuated cavities to isolate and study the role of the metallic surfaces in RF cavity breakdown as a function of radiofrequency and surface preparation. A 1.3-GHz RF test cell with replaceable electrodes (e.g. Mo, Cu, Be, W, and Nb) has been built, and a series of detailed experiments is planned at the Argonne Wakefield Accelerator. These experiments will be followed by additional experiments using a second test cell operating at 402.5 MHz.

INTRODUCTION (EARLIER 805-MHZ STUDIES)

RF cavities pressurized with hydrogen gas are being developed to produce low emittance, high intensity muon beams for muon colliders, neutrino factories, and other applications. The high-pressure gas suppresses dark currents, multipacting, and other effects that are complicating factors in the study of breakdown in usual RF cavities that operate in vacuum.

In the earlier 805-MHz studies, various metals were tested in a pressurized cavity where RF breakdown is expected to be due only to the interaction of the metallic surfaces with the electromagnetic fields. After exposure to the RF fields, metallic Be, Mo, Cu, and W samples were examined using a Hirox microscope and a scanning electron microscope (SEM) to measure the distribution of breakdown events on the electrode surfaces [1].

Apparatus

A schematic of the 805 MHz Test Cell (TC) geometry is shown in Figure 1. The TC is a cylindrical stainless steel pressure vessel. RF power is fed into the chamber via a coaxial line. A solenoid magnet (not shown in the figure) provides an axial magnetic field of up to 3 T, which is used in some of the data sets. Replaceable hemispherical electrodes of various materials (Cu, Mo, Be, W) are separated by a 2 cm gap.

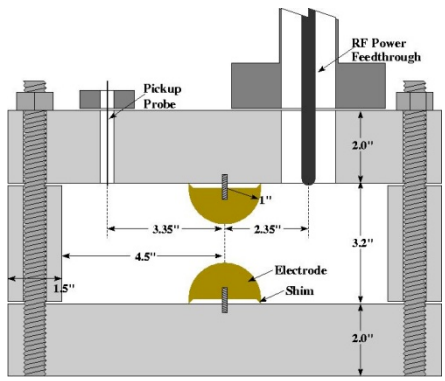

Figure 1: Cross section of the 805-MHz test cell showing the replaceable one inch radius Cu, Mo, W, or Be hemispherical electrodes. The top and bottom plates and the cylinder are copper-plated stainless steel (the gas input/exhaust port is not shown in the figure).

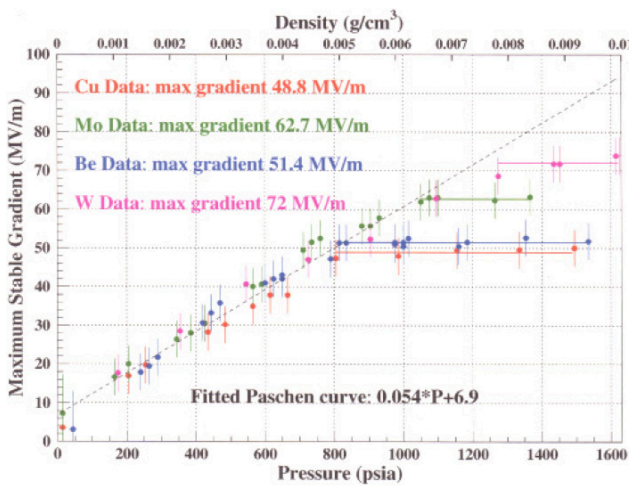

Figure 2: Maximum stable TC gradient as a function of hydrogen gas density or pressure for Cu, Be, Mo, and W with no external magnetic field.

Experimental Results: RF breakdown

Increasing gas density reduces the mean free collision path for ions giving them less chance to accelerate to

*work supported in part by USDOE STTR Grant DE-FG02-08ER86352 and FRA DOE Contract DE-AC02-07CH11359

energies sufficient to initiate showers and avalanches. As shown in Figure 2, it is found that Cu and Be electrodes operated stably with surface gradients near 50 MV/m, Mo near 63 MV/m, while W achieved values near 72 MV/m [2].

NEW TEST CELLS

1.3 GHz Test Cell

A 1.3 GHz test cell was designed by scaling the 805 MHz cell internal dimensions. The input power is through a 1-5/8 coax with an epoxy window designed for high pressure from the 805 MHz cavity test assembly. The pickup probe is a .141 coax antenna with an OSM connector as shown in Figure 5.

The cavity is designed to withstand 1600 psi pressure, and is made from copper plated 316 stainless steel. The top and bottom "lids" are 2 in. thick and the cylindrical walls are 1.6 in. thick. The electrodes are OFHC copper, but other interchangeable electrodes can be used.

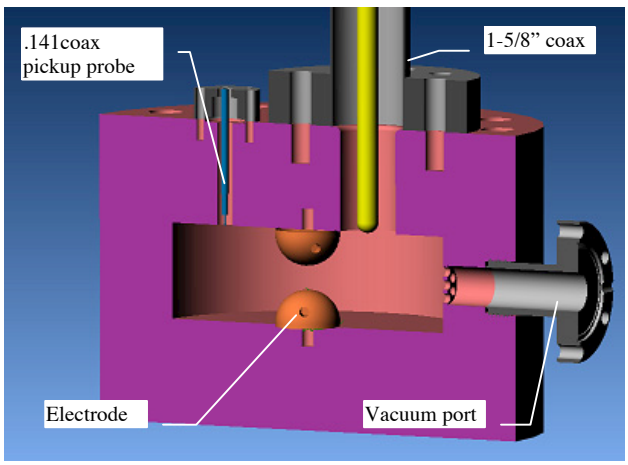

Figure 3: Cutaway view of the 1.3 GHz Cavity.

After assembly and vacuum testing at Fermilab, the test cell along with its pump stand was transported to the Argonne Wakefield Accelerator (AWA). Although our primary interest is to study the operation of this test cell under high-pressure conditions, it was decided to initiate high-power tests of this test cell under vacuum conditions, because it was much quicker to acquire safety approvals to operate under vacuum conditions.

A process of RF conditioning was undertaken, in which the RF power was slowly increased, while keeping the gas pressure below 1 10^{-5} Torr. After 2.5 days of effort, the conditioning of the 1.3-GHz test cell was completed. At that point, the gas pressure was typically in the low 10^{-6} range at a 5-Hz pulse rate, and the pulse shape seen at the pickup electrode was clean, without any evidence of multipacting nor of RF breakdown. Measurements of the RF parameters were analyzed, and the power in the test cell was found to be 221 kW, corresponding to a gradient of 71 MV/m.

The process of requesting ANL safety approval for high-pressure operation of this test cell has already begun. After this approval is granted, we plan to conduct a detailed series of experiments using this 1.3-GHz test cell. Among the many experimental variables we hope to study are electrodes made of different metals, surface preparation, and different gases.

Frequency Tuning

High-pressure testing of the 1.3-GHz test cell will involve pressures of 0 to 1500 psi. For a fixed test-cell geometry, the resonant frequency will vary as the pressure of the hydrogen gas, according to Figure 4 below.

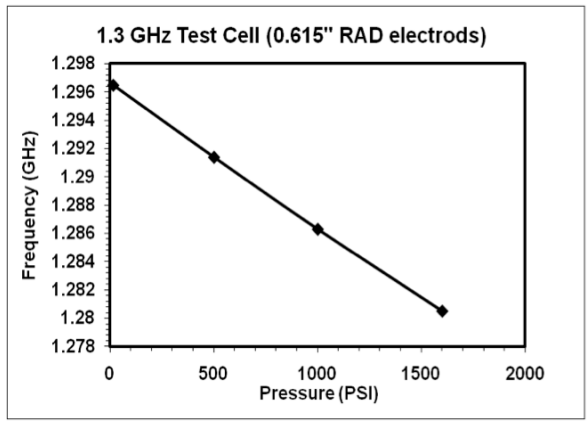

Figure 4: Resonant Frequency Varies with Pressure

Since the AWA test stand cannot provide frequency adjustments over the required range, it will be important to provide frequency adjustment in the design of the test cell itself. That is, when the gas pressure is varied, the frequency shift should be compensated, so that the test-cell resonant frequency remains at 1.3 GHz.

An adjustable electrode has been designed to perform this function without opening the cavity. The electrode will be built into a new cavity end plate, and will be pressure sealed using a Static O-Ring Seal. With proper design these seals are good for sealing up to 103.5 bar (~1500 psi). Our design will incorporate two such O-rings in series, backing rings, and close tolerances. Any "leakage" past the O-rings will be slight. The electrode will electrically contact the end-wall of the cavity using a finger stock ring within the end wall just below the inner surface of the cavity. Superfish and Comsol simulations show that a single electrode movement of ~30 mils will be sufficient to vary cavity frequency over the range necessary to accommodate the change due to the 1500 psi pressure change. When using a 3/32 – 32 threaded rod to move the electrode, approximately one complete turn of the rod will move the electrode by 31 mils. Assuming a test point is taken roughly every 200 psi of pressure, the rod will need to move ~4 mils, or ~45° between test points.

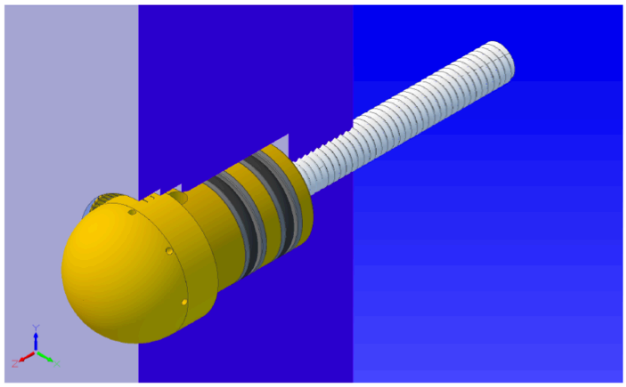

Figure 5: Cut-away view of moveable electrode design.

402.5 MHz Test Cell

In order to study the effect of the radiofrequency on RF Breakdown in gas-filled cavities, we plan to work with our LBNL colleagues to conduct a follow-up series of experiments at a lower frequency, most likely 402.5 MHz.

COMPUTER SIMULATIONS

The data in Figure 2 shows that there are two distinct regimes for the observed RF breakdown: a low-pressure region where the effects of the gas and the gas pressure dominate, and a high-pressure region where the characteristics of the metal surface dominate.

Gas Discharge Simulations

Fully kinetic, collisional particle simulations using the LSP code [3] have been carried out to study breakdown field threshold as a function of pressure for H_2 with small admixtures of electronegative gases. The initial phase of the modeling effort included inter-species elastic and inelastic processes such as electron-neutral and Coulomb scattering, ionization, and attachment. Starting from a low-density seed plasma population, the growth and decay of the plasma density over many RF cycles was used to estimate field gradient breakdown curves for different gas mixtures [4]. This modeling correctly predicted the increased breakdown strength at relatively low gas pressures that could be obtained through the inclusion of small admixtures of an electronegative gas such as SF_6 to H_2-filled RF accelerating cavities [5]. At higher pressures, the field gradient strongly deviates from the Paschen curve. The point at which the measurements begin to deviate from the Paschen curve and the behavior of this deviation at higher pressures is dependent somewhat on the choice of electrode material, gas mixture, the amplitude of an applied transverse magnetic field.

The next phase of the analysis is to examine the dynamic breakdown of high-pressure RF cavities through detailed numerical simulations. Measurements of the formative time associated with breakdown of the RF cavity, including light emission and the change in reflected RF input power, suggest relatively fast streamer-leader propagation times. Recently, a photon transport/ionization capability has been implemented in LSP for treatment of UV and soft x-ray radiation generation, transport and absorption. Preliminary simulations of streamer propagation in H_2 and SF_6 under DC fields are in good agreement with measured streamer propagation speeds [6]. Application of the simulation model to gas-filled RF cavities is planned to assist in the analysis of the measured breakdown characteristics. These models are also applicable to high-vacuum, high-gradient accelerator cavities.

REFERENCES

[1] M. BastaniNejad *et al.*, "Studies of Breakdown in a Pressurized RF Cavity," in EPAC08, Genoa, Italy, June 23–27, 2008, p.736.
[2] P.M. Hanlet et al., "High pressure RF cavities in magnetic fields," EPAC06, Edinburgh, Scotland.
[3] D. R. Welch, D. V. Rose, M. E. Cuneo, *et al.*, Phys. Plasmas **13**, 063105 (2006).
[4] D. V. Rose, C. Thoma, D. R. Welch, *et al.*, Voss Sci. Rep. VSL-0909 (2009).
[5] K. Yonehara, M. Chung, A. Jansson, *et al.*, Proc. IPAC'10, Kyoto, Japan, 2010, p. 3503.
[6] D. V. Rose, D. R. Welch, C. Thoma, *et al.*, manuscript in preparation (2011).

MULTI-PURPOSE 805 MHZ PILLBOX RF CAVITY FOR MUON ACCELERATION STUDIES*

Grigory Kazakevich#, Gene Flanagan, Rolland Johnson, Mike Neubauer, Richard Sah, Muons, Inc., Batavia, IL 60510
Alfred Moretti, Milorad Popovic, Katsuya Yonehara, Fermilab, Batavia, IL 60510
Kwok-Chi D. Chan, Andrew J. Jason, Sergey S. Kurennoy, Haruo Miyadera, Peter J. Turchi, LANL, Los Alamos, NM 87545
Yagmur Torun, IIT, Chicago, IL 60616

Abstract

An 805 MHz RF pillbox cavity has been designed and constructed to investigate potential muon beam acceleration and cooling techniques. The cavity can operate at vacuum or under pressure to 100 atmospheres, at room temperature or in a liquid nitrogen bath at 77 K. The cavity is designed for easy assembly and disassembly with bolted construction using aluminum seals. The surfaces of the end walls of the cavity can be replaced with different materials such as copper, aluminum, beryllium, or molybdenum, and with different geometries such as shaped windows or grid structures. Different surface treatments such as electro polished, high-pressure water cleaned, and atomic layer deposition are being considered for testing. The cavity has been designed to fit inside the 5-Tesla solenoid in the MuCool Test Area at Fermilab. Current status of the cavity prepared for initial conditioning and operation in the external magnetic field is discussed.

INTRODUCTION

Ionization cooling, where all momentum components are degraded by an energy absorbing material and only the longitudinal momentum is restored by RF cavities, provides a means to quickly reduce transverse beam sizes. However, the beam energy spread cannot be reduced by this method unless the longitudinal emittance can be transformed or exchanged into the transverse emittance. One scheme to achieve emittance exchange is to pass a beam through a bending magnet to introduce dispersion, the beam can then be made incident to a wedge shaped absorber. The higher momentum particles pass through more of the absorber material than the low momentum particles and thus suffer larger ionization energy losses. Much work has been done on a second cooling scheme, one in which a continuous absorber such as gaseous H_2 is used in a Helical Cooling Channel (HCC). In the HCC higher momentum corresponds to a longer path length. The path length dependence means high momentum particles must pass through more absorber and therefore experience a larger ionization energy loss compared low momentum particles. The theory of this helical channel has been described elsewhere [1]. The use of high pressure gas not only serves as an ideal absorber, it helps in the suppression of RF breakdown, and if one can design the appropriate thermal barrier between the RF cavity and magnet it will also function as part of the cavity cooling system.

A HCC consisting of a pressurized gas absorber imbedded in a magnetic channel that provides solenoid, helical dipole and helical quadrupole fields has shown considerable promise in providing six-dimensional cooling for muon beams. The energy lost by muons traversing the gas absorber needs to be replaced by inserting RF cavities into the lattice. Replacing the substantial muon energy losses using RF cavities with reasonable gradients will require a significant fraction of the channel length be devoted to RF. However, to provide the maximum phase space cooling and minimal muon losses, the helical channel should have a short period and length.

Demonstrating the technology of such a cooling channel would represent enormous progress toward the next energy frontier machine. The multipurpose 805 MHz cavity described here will facilitate the understanding of how to build a cooling channel. Additionally it is conceptually compatible with another Muons, Inc. proposal that aims to design and build a 10 T, 805 MHz segment of a helical cooling channel which builds on previous work by Muons, Inc. [2].

The cavity also can serve as a test resonator for large-acceptance high-gradient linac for acceleration of low energy muons and pions in a strong solenoidal magnetic field, [3]. Such a linac was proposed at LANL for homeland defense and industrial applications. The acceleration starts immediately after collection of pions from a target by solenoidal magnets and brings muons to a kinetic energy of about 200 MeV over a distance of the order of 10 m. At this energy, both an ionization cooling of the muon beam and its further acceleration in a superconducting linac become feasible. The required large longitudinal and transverse acceptances can be achieved in a normal-conducting linac consisting of independently fed TM_{010} mode RF cavities with wide apertures closed with thin metal windows or grids. The guiding magnetic field is provided by external superconducting solenoids. Due to the low energy of the initial pions and muons, vacuum cavities are preferred, at least in the beginning of

*Work is supported by DOE grant DE-FG-08ER86352.
Corresponding author. Current affiliation: Muons, Inc., Batavia, IL 60510, U.S.A.
E-mail: grigory@muonsinc.com (G.M. Kazakevich)

the normal-conducting linac to minimize particle energy losses.

FEATURES OF THE CAVITY INTENDED FOR COOLING OF MUONS

The work reflects an attempt to create a universal design of an accelerating cavity model allowing to work with 100 atm. compressed hydrogen or with vacuum. To simplify technology and design the cavity model was made from thick elements of stainless steel SS-316 clamped with bolts, Fig. 1. The sealing is provided by flat pure aluminum sealing rings demonstrated good ability to work with pressurized gas.

The developed pillbox cavity intended to operate with TM_{010} mode of RF field consists of the elements including two covers, cylindrical body and two test plate holders which allow using test plates as insets to check various materials for operation with a high-gradient RF field. All the elements are plated with 25-37 μm thick copper. For sealing the cavity for vacuum using flat aluminum sealing rings we have developed technology for manufacturing of the rings and machining the respective sealing surfaces of the cavity parts.

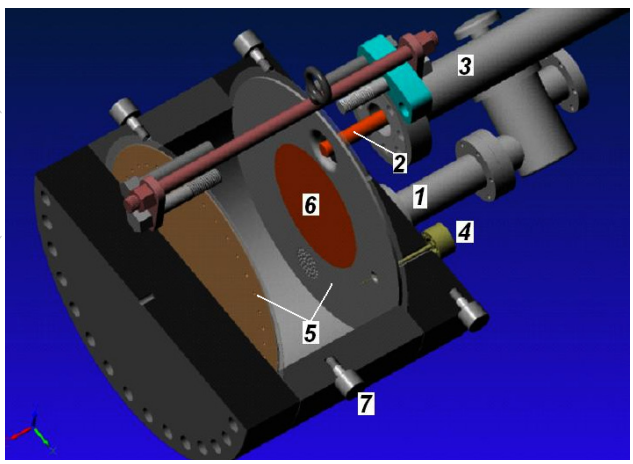

Figure 1: The model of the cavity for cooling of muons. 1-vacuum port, 2- antenna, 3- RF coax feeder, 4- probe, 5- test plate holder, 6- test plate to study materials at high gradients of RF field, 7- roller.

Cleaning of the cavity elements after machining with oil containing coolants was done with a detergent (Palm Olive soap) dissolved in hot (45 C^0) deionized water followed by two rinses in hot deionized water. The developed technology allowed us to reach vacuum of $3x10^{-8}$ Torr after baking at 106° C for a few days. The pumping was provided by a type TMH 071 P turbo pump and the V20 ion pump. The ion pump was turned on after the cavity had cooled down. The cavity temperature and vacuum measured at the cavity evacuation are shown in the vacuum log, Fig. 2.

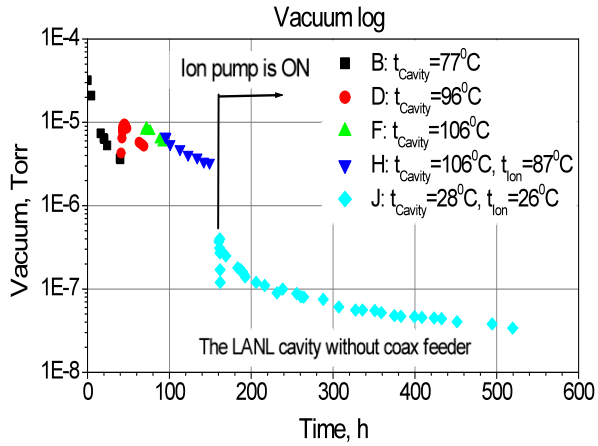

Figure 2: Vacuum log of the 805 MHz pillbox RF cavity.

Installation of the RF coax feeder, which utilizes an epoxy window does not drop noticeably the vacuum value. The epoxy window of the RF coax feeder is designed to work up to 100 atm.

CALCULATED AND MEASURED PARAMETERS OF THE PILLBOX CAVITY

The parameters of the cavity with the coax input were calculated analytically and numerically using 3-D programs (Microwave Studio, Comsol). By choosing the appropriate thickness for the test plates, which are inserted in the test plate holders, one can fit the cavity frequency. Fig. 3 shows the frequency shift vs. the test plate thickness.

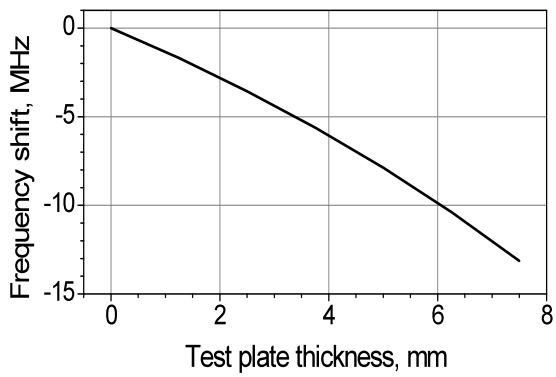

Figure 3: Computed the cavity frequency shift vs. the test plate thickness.

Without the test plates the cavity was machined for resonance frequency of 809.5 MHz, the measured (under vacuum) value is 810.16 MHz. Computed value of the wall-loss Q-factor is: $Q_0=2.882x10^4$, the measured value is $3x10^4$±5%.

Computed parameters of the cavity vs. the required gradient of the RF field value are shown in Table 1.

Table 1: Parameters of the Cavity vs. the Gradient of the RF Field

Gradient, MV/m	Stored energy, J	Wall loss power, MW	Feeder voltage, kV	Average wall loss power, W
20	4.715	0.754	8.68	226.2
25	7.367	1.178	10.85	353.5
30	10.61	1.697	13.03	509
35	14.44	2.309	15.2	692.8
40	18.86	3.016	17.37	904.8

The last column of the table shows the expected average power lost in the cavity walls for standard operation of the RF source during conditioning (assuming a repetition rate of 15 Hz and the RF pulse duration of 20 μs).

As follows from the last column of the table, the standard conditioning parameters will lead to noticeable heating of the cavity. Without additional cooling the cavity temperature will rise linearly and after ~8 hr's it will have increased by ≈120°C. This temperature is unacceptable, especially when working with pressurized hydrogen. Moreover, a drift of the cavity temperature causes a drift in the cavity resonance frequency, approximately 13 kHz/C^0. Simple cooling systems can help to solve the problem of heating.

The cavity coupling system utilizes an antenna matched to the coax feeder impedance to provide critical coupling to the cavity. This helps avoid overvoltage in the coax feeder during high power transmission from the RF source, Table 1. Since overvoltage in the antenna neighborhood is undesirable, optimized sizes, design, and positioning of the antenna were chosen based on the 3-D simulations (HFSS and CST Microwave Studio codes). Fig. 4 shows measured the cavity coupling coefficient, β, vs. the immersion depth, δ, of the optimized antenna into the cavity.

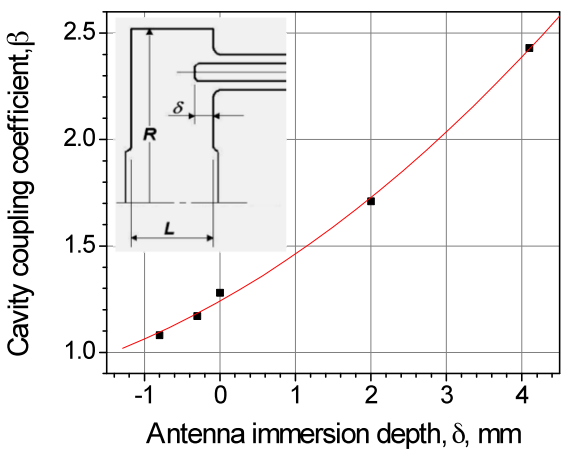

Figure 4: Measured the cavity coupling coefficient vs. the antenna immersion depth.

Tuning of the cavity coupling was done by varying the immersion depth of the antenna, this is facilitated by a sliding collar contact made in the central wire of the coax feeder.

The RF field distribution in the cavity was computed with Comsol for a RF power of 1 MW, this provides an accelerating gradient of 23.4 MV/m is shown in Fig. 5.

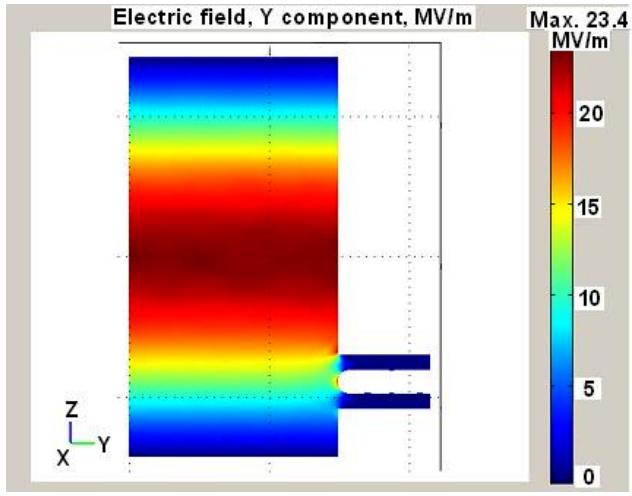

Figure 5: Computed the RF electric field distribution in the pillbox cavity at 1 MW RF power and critical coupling of the cavity.

The cavity has been prepared for conditioning at the FNAL MuCool Test Area [4]. The cavity was mounted in the movable compact vacuum bench including dry scroll pump, turbo pump and ion pump.

SUMMARY

A prototype of a universal TM_{010} mode pillbox accelerating cavity intended for operation with 100 atm. hydrogen or vacuum and the required manufacturing technologies have been developed. The prototype pillbox cavity will be used to study RF operation at high-gradient electric field in the presence of an external magnetic field, a configuration that will most likely be required for muon cooling. Preparation of the cavity conditioning without and with the magnetic field is in progress.

REFERENCES

[1] Y. Derbenev and R.P. Johnson, PRSTAB 8, 041002 (2005)
[2] S.A. Kahn et al., "Incorporating RF into a Muon Helical Cooling Channel.", Proceedings of EPAC08, Genoa, Italy.
[3] S.S. Kurennoy, A.J. Jason, H. Miyadera, Proceed. of IPAC10, Kyoto, Japan, 2010, p. 3518.
[4] http://apc.fnal.gov/MUONRD/MTA_Mucool_Mice/

HIGH PRESSURE RF CAVITY TEST AT FERMILAB*

B. Freemire†, P.M. Hanlet, D.M. Kaplan, Y. Torun, IIT, Chicago, IL 60616, USA
M.R. Jana, A. Moretti, M. Popovic, A.V. Tollestrup, K. Yonehara, FNAL, Batavia, IL 60510, USA
G. Flanagan, R.P. Johnson, M. Notani, Muons, Inc., Batavia, IL 60510, USA

Abstract

Operating a high gradient radio frequency cavity embedded in a strong magnetic field is an essential requirement for muon beam cooling. However, a magnetic field influences the maximum RF gradient due to focusing of dark current in the RF cavity. This problem is suppressed by filling the RF cavity with dense hydrogen gas. As the next step, we plan to explore the beam loading effect in the high pressure cavity by using a 400 MeV kinetic energy proton beam in the MuCool Test Area at Fermilab. We discuss the experimental setup and instrumentation.

INTRODUCTION

The concept of using muons in colliders or neutrino factories has been around for many years [1, 2]. Ionization cooling allows rapid emittance reduction, with energy restored through radio frequency (RF) cavities. The problem with this scheme is that high gradient RF cavities must be placed in strong magnetic fields (on the order of a few Tesla) [3, 4]. These magnetic fields can focus field emission electrons onto the wall of the cavity, greatly reducing the maximum stable RF gradient [5]. A number of ideas have been proposed to fix this problem, and the MuCool Test Area (MTA) was created partially as an R&D facility for this purpose.

It has been demonstrated that filling an 805 MHz RF cavity with a high pressure gas suppresses breakdown [6]. Tests carried out with a hydrogen gas filled cavity show stable operating gradients on the order of 65 MV/m. Electrodes made of copper, molybdenum, and beryllium were tested without an external magnetic field, and an external field of 3 T was applied with the molybdenum electrodes. Fig. 1 shows the results obtained in these tests. The cavity reached a higher gradient with Molybdenum electrodes. Note there was virtually no difference in maximum gradient attained using the molybdenum electrodes in a 3 T field.

Tests have been performed using different gas species as well. Fig. 2 shows the data taken using a copper electrode with nitrogen, hydrogen, hydrogen with a SF_6 dopant. As can been seen in both Fig. 1 and Fig. 2, there is a region at lower pressures in which the gradient depends linearly on pressure, and a region at higher pressures in which the gradient plateaus and no longer depends on pressure. These are called the Paschen region and metallic region, respectively [7].

A high pressure RF (HPRF) cavity has never been operated with beam before. The effect of beam loading must be investigated. It is thought that ionization electrons will recombine with hydrogen before they can form a dense plasma and degrade the cavity Q. If this is not the case, a dopant electronegative gas will be tested. Nitrogen is a candidate, as it forms ammonia (NH_3) with hydrogen when dissociated. Sulfur hexafluoride (SF_6) is another candidate.

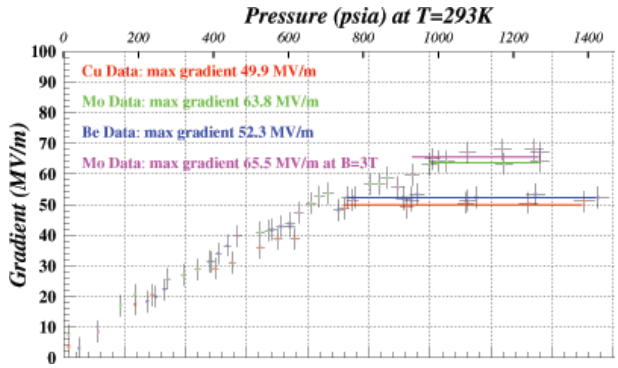

Figure 1: Breakdown gradient with different electrode materials without beam. Copper electrode data is in red, beryllium in blue, molybdenum in green, and molybdenum in a 3 T external magnetic field is in pink [6].

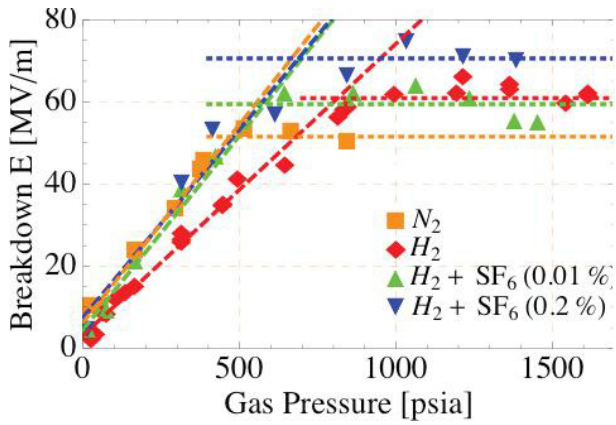

Figure 2: Breakdown gradient for different gas species without beam. Nitrogen is orange, hydrogen blue, hydrogen + SF_6(0.01%) green, and hydrogen + SF_6(0.2%) is blue [8].

MTA EXPERIMENTAL HALL

The MTA experimental hall has been built to accommodate various test programs: RF power is provided at 201 and 805 MHz, high pressure gases including hydrogen up to 1600 psi are available, a 5 T solenoid magnet provides a strong magnetic field, and a proton beamline has been commissioned. Safety issues with regard to the use of pres-

* Work supported in part by grants from the National Science Foundation and the US Department of Energy.

† freeben@iit.edu

surized hydrogen have been addressed, and there is a 15 ft radius around the cavities in which no electrical equipment may be placed.

Beamline

The MTA utilizes the 400 MeV kinetic energy proton beam provided by the Fermilab linac. The allotted 60 pulses per hour deliver 10^{12} to 10^{13} protons per pulse. The final beam intensity is tuned by a collimator placed just upstream of the cavity. The layout of the experimental hall is shown in Fig. 3.

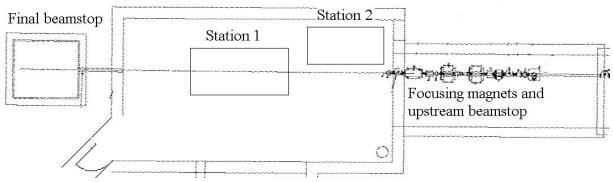

Figure 3: MTA Experimental Hall. RF Station 1 is located inside the solenoid magnet. RF Station 2 is located on a stand upstream and outside of the magnet.

Experimental Apparatus

There are two stations that support RF cavity operation. Station 1 is located in a 5 T, 1.088 m long, 44 cm bore diameter solenoid magnet. The solenoid is on the beamline axis and an extension beampipe ends 1 m from its face. Station 2 is located upstream of the magnet and off the beamline axis. An RF switch has been installed to supply 805 MHz to either station. In order to test the cavity with beam or external magnetic field, the cavity must be located in RF Station 1. RF Station 2 is used for conditioning the cavity and calibrating instrumentation.

The side view schematic for Station 1 operation can be seen in Fig. 4. The beampipe extension is on the left, with a CCD camera (PL-B955U camera) and a Chromox luminescent screen for beam tuning. The two piece stainless steel collimator provides the final beam intensity control, with full or 10% intensity. Two toroids, one before the collimator and one between the collimator and cavity, are used to measure the number of particles incident on the cavity. RF power is fed to the cavity via a waveguide on the downstream side. A beam counter telescope triggers on elastically scattered protons (∼360 MeV KE) from the vacuum window at the end of the beampipe. Additionally there are 10 scintillation counters placed in the vacinity of the cavity.

SIGNALS AND INSTRUMENTATION

Each station in the hall is equipped with cabling for electrical and magnetic pickup, forward and reflected power, and optical signals. The cables consist of $\frac{1}{2}$ inch and $\frac{1}{4}$ inch heliax and green RG58. Table 1 shows the type and number of signals provided by each station.

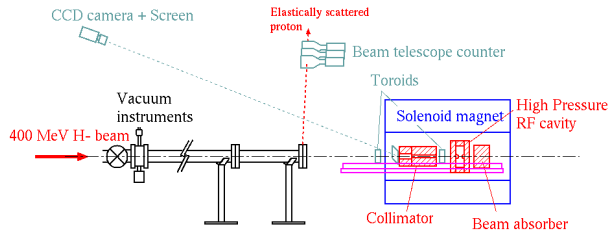

Figure 4: Side view of Station 1 setup. The proton beam comes from the left and passes through the collimator, cavity and beam absorber placed inside the solenoid magnet.

Table 1: Signals per Station

Station	Cable Type	Number of Cables
1	E/M Pickup	2
	For/Ref Power	2
	Optical	3
2	E/M Pickup	2
	For/Ref Power	2
	Optical	6
1 or 2	Spare	9

Calibration

As determining when breakdown occurs during the RF cycle is very important, picosecond timing resolution is necessary. A preliminary timing calibration has been done excluding the cavity, and a more detailed calibration will take place involving the cavity. A laser (PiLas PIL063 laser head and EIG 1000D controller) was used to send light to a Hamamatsu H5783 PMT as a trigger. A signal was also sent through the other instrumentation cables and a Horiba MicroHR Motorized Spectrometer (with a Hamamatsu H5783-20 PMT). The relative delays were measured. Fig. 5 shows the setup and Fig. 6 shows a typical signal delay screenshot. Table 2 lists these cable delays.

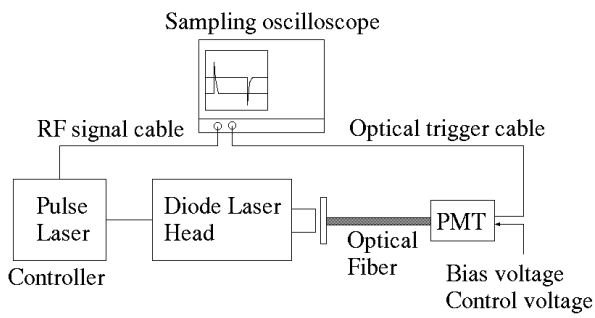

Figure 5: Timing calibration setup. A picosecond laser sends a signal directly to the oscilloscope and through the cables to the scope.

Two ferrite core toroids will be placed on the upstream face of the collimator and between the collimator and cavity. An output signal calibration has been done using a handmade current pulse generator that is based on a fast switching transistor (2N2369A). The current was

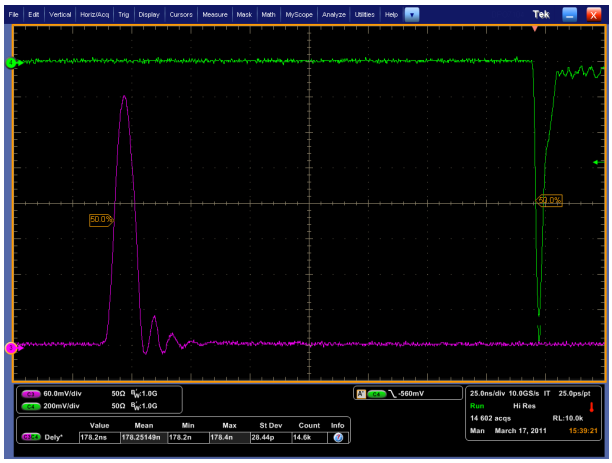

Figure 6: Timing calibration screenshot. The optical signal is in green, and the electrical pickup from Station 1 is in magenta.

Table 2: Cable Delays Relative to PMT Trigger

Station	Cable	Delay
1	1	152.7 +/− 0.3 ns
	2	158.7 +/− 0.2 ns
	3	150.9 +/− 0.2 ns
	4	151.4 +/− 0.4 ns
2	1	182.1 +/− 0.4 ns
	2	182.3 +/− 0.2 ns
	3	181.1 +/− 0.2 ns
	4	181.1 +/− 0.3 ns
Spectrometer		6.9 +/− 0.2 ns

sent through the toroids and the output signal was measured on an oscilloscope. Fig. 7 shows the calibration, 21.26 mV/mA was measured.

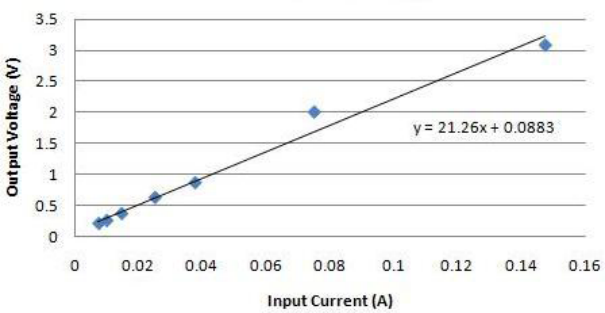

Figure 7: Toroid output voltage versus input current.

DATA ACQUISITION

The data acquisition system consists of two PCs that control the power supplied to the RF cavity and record the various signals. One PC runs a CAMAC and NIM based system. It reads the electrical and magnetic pickup signals, produces an RF envelope and uses the counters to create a trigger. The other PC runs a LabVIEW based system. During conditioning the RF power level is increased every so often until a spark occurs, at which point it decreased and begins to increment again. It uses an external trigger to record resonant frequency, RF envelope, and oscilloscope traces after a specified number of RF cycles. The fast signals (e.g. RF pickups and optical) are fed directly into the oscilloscopes. The slow signals (e.g. RF envelope) are fed into the PCs, which record waveforms from the scopes when a breakdown occurs.

OUTLOOK

Data will soon be taken using the HPRF cavity with and without an external magnetic field, and with and without beam. The results should indicate whether high pressure gases allow RF cavities to be operated in strong magnetic fields with beam.

REFERENCES

[1] D. Neuffer, "Principles and Applications of Muon Cooling," Part. Accel. 14 (1983) 75, http://lss.fnal.gov/archive/test-fn/0000/fermilab-fn-0378.shtml.

[2] S. Geer, "Neutrino Beams From Muon Storage Rings: Characteristics and Physics Potential," Phys. Rev. D57 (1998) 6989, http://prd.aps.org/abstract/PRD/v57/i11/p6989_1.

[3] J. Gallardo et al., "$\mu^+\mu^-$ Collider: A Feasibility Study," DPF/DPB Summer Study on New Directions for High Energy Physics, Snow-mass, Colorado, 25 Jun - 12 Jul 1996, BNL-52503, Fermilab-Conf-96-092, LBNL-38946, http://www.cap.bnl.gov/mumu/pubs/snowmass96.html.

[4] S. Geer, "Muon Colliders and Neutrino Factories," Ann. Rev. Nucl. Part. Sci. 59 (2009) 347, http://dx.doi.org/10.1146/annurev.nucl.010909.083736.

[5] J. Norem, V. Wu, A. Moretti, M. Popovic, Z. Qian, L. Ducas, Y. Torun and N. Solomey, "Dark Current, Breakdown, and Magnetic Field Effects in a Multicell, 805 MHz Cavity," Phys. Rev. ST Accel. Beams 6 (2003) 072001, http://prst-ab.aps.org/abstract/PRSTAB/v6/i7/e072001.

[6] P. Hanlet et al, "High Pressure RF Cavities in Magnetic Fields," EPAC'06, Edinburgh, June 2006, TUPCH147, p. 1364, http://jacow.org/e06/PAPERS/TUPCH147.PDF.

[7] M. BastaniNejad et al, "RF Breakdown of Metallic Surfaces in Hydrogen," PAC'09, Vancouver, BC, Canada, May 2009, WE5PFP008, p. 2000, http://jacow.org/PAC2009/papers/we5pfp008.pdf.

[8] K. Yonehara et al, "Doped H_2-Filled RF Cavities for Muon Beam Cooling," PAC'09, Vancouver, BC, Canada, May 2009, TU5PFP020, p. 855, http://jacow.org/PAC2009/papers/tu5pfp020.pdf.

[9] M. R. Jana, "Refurbished Pill Box Data," MAP Winter Meeting, Jefferson Lab, March 2011, http://conferences.jlab.org/muon2011/index.html.

CONDITIONING AND FUTURE PLANS FOR A MULTI-PURPOSE 805 MHZ PILLBOX CAVITY FOR MUON ACCELERATION*

G. Kazakevich#, G. Flanagan, R. P. Johnson, M. Neubauer, R. Sah, A. Dudas, F. Mahrhauser
Muons, Inc., Batavia, IL 60510
A. Moretti, M. Popovic, K. Yonehara, G. Romanov, Fermilab, Batavia, IL 60510
Y. Torun, IIT, Chicago, IL 60616
S. Kurennoy, LANL, Los Alamos, NM 87545

Abstract

An 805 MHz RF pillbox cavity has been designed and constructed to investigate potential muon beam acceleration and cooling techniques for a Muon Collider or Neutrino Factory. The cavity can operate in vacuum or under pressure up to 100 atmospheres, at room temperature or in a liquid nitrogen bath at 77K. The cavity has been designed for easy assembly and disassembly utilizing a bolted construction with aluminium seals. To perform vacuum and high-pressure breakdown studies of materials and geometries most suitable for the collider or factory, the surfaces of the end walls of the cavity can be replaced with different materials such as copper, aluminium, beryllium, or molybdenum, and with different geometries such as shaped windows or grid structures. The cavity has been designed to fit inside the 5-Tesla solenoid in the MuCool Test Area (MTA) at Fermilab. In this paper we present the vacuum conditioning results with and without an external magnet field. Additionally, we discuss the future plans for the cavity.

INTRODUCTION

Ionization cooling, where all momentum components are degraded by an energy absorbing material and only the longitudinal momentum is restored by RF cavities, provides a means to quickly reduce transverse beam sizes. However, the beam energy spread cannot be reduced by this method unless the longitudinal emittance can be transformed or exchanged into the transverse emittance. One scheme to achieve emittance exchange is to pass a beam through a bending magnet to introduce dispersion; the beam can then be made incident to a wedge shaped absorber. The higher momentum particles pass through more of the absorber material than the low momentum particles and thus suffer larger ionization energy losses. Much work has been done on a second cooling scheme, one in which a continuous absorber such as gaseous H_2 is used in a Helical Cooling Channel (HCC) [1]. In the HCC higher momentum corresponds to a longer path length. The path length dependence means high momentum particles must pass through more absorber and therefore experience a larger ionization energy loss compared to low momentum particles. The theory of this helical channel has been described elsewhere [2]. The use of high pressure gas not only serves as an ideal absorber, it helps in the suppression of RF breakdown, and if one can design the appropriate thermal barrier between the RF cavity and magnet it will also function as part of the cavity cooling system.

An HCC consisting of a pressurized gas absorber imbedded in a magnetic channel that provides solenoid, helical dipole and helical quadrupole fields has shown considerable promise in providing six-dimensional cooling for muon beams. The energy lost by muons traversing the gas absorber needs to be replaced by inserting RF cavities into the lattice. Replacing the substantial muon energy losses using RF cavities with reasonable gradients will require a significant fraction of the channel length be devoted to RF. However, to provide the maximum phase space cooling and minimal muon losses, the helical channel should have a short period and length.

Demonstrating the technology of such a cooling channel would represent enormous progress toward the next energy frontier machine. The multipurpose 805 MHz cavity described here will facilitate the understanding of how to build a cooling channel. Additionally it is conceptually compatible with another Muons, Inc. proposal that aims to design and build a 10 T, 805 MHz segment of a helical cooling channel which builds on previous work by Muons, Inc. [3].

The cavity can also serve as a test resonator, [4], for a large- acceptance high-gradient linac for acceleration of low energy muons and pions in a strong solenoidal magnetic field. Such a linac was proposed at LANL. The acceleration starts immediately after collection of pions from a target by solenoidal magnets and brings muons to a kinetic energy of about 200 MeV over a distance of the order of 10 m. At this energy, both an ionization cooling of the muon beam and its further acceleration in a superconducting linac become feasible. The required large longitudinal and transverse acceptances can be achieved in a normal-conducting linac consisting of independently fed TM_{010} mode RF cavities with wide apertures closed with thin Be metal windows or grids.

*Work supported under U.S. DOE Grant DE-FG-08ER86352.
grigory@muonsinc.com; gkazakevitch@yahoo.com

ISBN 978-3-95450-115-1

The guiding magnetic field is provided by external superconducting solenoids. Due to the low energy of the initial pions and muons, vacuum cavities are preferred, at least in the beginning of the normal-conducting linac to minimize particle energy losses.

FEATURES OF THE CAVITY MODEL INTENDED FOR COOLING MUONS

The work is an attempt to create a universal design of an accelerating cavity model capable of working with 100 atm of compressed hydrogen or with vacuum. To simplify technology and design, the cavity model has been made from thick elements of copper plated stainless steel SS-316 clamped with bolts, Figure 1, [4]. The sealing identical for the vacuum and for compressed gas is provided by flat pure aluminum gasket rings.

We have developed a technology for manufacturing of the flat aluminum gasket rings and machining of the respective sealing surfaces of the cavity parts required for vacuum sealing. Details of the technology and the cavity preparation can be found in [4].

The pillbox cavity operating in the TM_{010} mode consists of two lids, a cylindrical body and two test plate holders, which allow using test plates as insets to check various materials for operation within a high-gradient RF field. All the elements are plated with 25-37 μm thick copper.

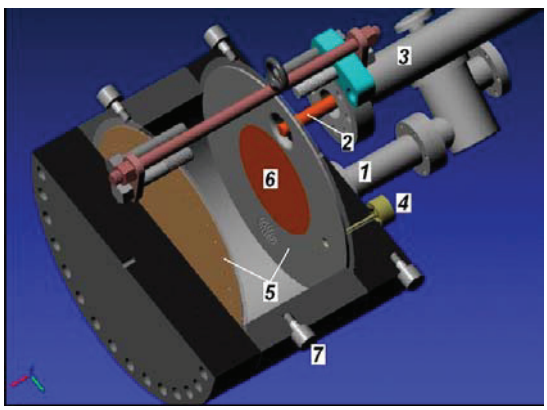

Figure 1: The model of the cavity for cooling of muons, 1-vacuum port, 2-antenna, 3-RF coax feeder, 4- probe, 5-test plateholder, 6-test plate to study materials at high gradients, 7- roller.

Results of the cavity model vacuum test and some parameters of the cavity model are presented in [4].

CONDITIONING PERFORMANCE

The cavity was conditioned in a few runs in the MTA at the Fermilab. The initial runs were performed without an external magnetic field. The cavity was fed by a 805 MHz klystron pulsed transmitter. The cavity was coupled with the klystron waveguide by matched waveguide-coaxial and coaxial-coaxial adapters having commercial vacuum windows for sealing the cavity vacuum system. Outside the vacuum the adapter was pressurized to ~14 psi of SF_6 to avoid breakdowns in the windows. The cavity on the RF bench is shown in Figure 2.

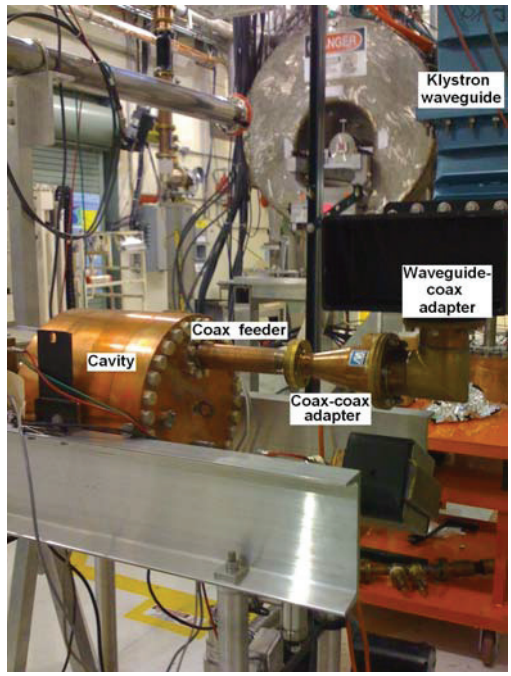

Figure 2: The RF cavity model on the RF bench in the MTA at the Fermilab.

Conditioning without an external magnetic field was initially performed at the RF pulse duration of 20 μs and repetition rate of 15 Hz. In this regime the cavity was conditioned to electric field gradient of 16.4 MV/m. Further conditioning was performed at repetition rate of 2 Hz with the same pulse duration. The field gradient value was measured using calibrated directional couplers in the klystron waveguide system.

Recently the cavity was moved into the MTA superconducting solenoid bore, Figure 3. The cavity axis was aligned parallel to the solenoid axis. A comparison of the operation of the cavity in a magnetic field of 3 T and without the field was done.

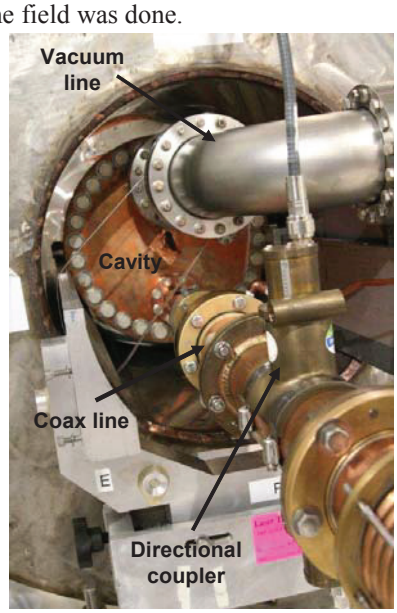

Figure 3: Front view of the cavity model located in bore of the superconducting solenoid in MTA.

In both cases we have reached gradient of electric field of 25 MV/m with or without the magnetic field of 3 T being on. This was studied for several long runs and the same results were achieved. Trying to operate slightly above 25 MV/m caused the reflected power signal to increase by about of 25 to 30 % and have oscillating pattern similar to what is seen in multipactor (MP) or dark current loading of the cavity. The effect went away a soon as we lowered the gradient back to 25 MV/m. The effect occurred immediately with not soft turn on and it turned off with no soft turn off.

This result differs from those achieved for the LBNL cavity, an 805 MHz pillbox. Here a peak electric field of 34 MV/m was obtained without external magnetic field, yet the gradient was limited to 16 MV/m in a 3 T external magnetic field. There are significant geometrical differences between the two cavities that may explain the differing performance limitations observed. The LBNL cavity is 8.1 cm long and utilizes a waveguide input coupler, whereas the Muons, Inc. cavity is ~15 cm long and uses a coaxial capacitive coupling.

Understanding the differences in performance between the LBNL and Muons, Inc. cavities has become a very important step to defining/refining directions for muon acceleration cavity R&D. Now we are using simulation tools to understand the performance differences. The next steps toward understanding the differences are described below.

FUTURE WORK TOWARD UNDERSTANDING PERFORMANCE LIMITATIONS IN A MAGNETIC FIELD

Simulation work has begun to understand the performance limitations of the Muons, Inc. cavity using 2D FishPact [6] and 3D ACE3P/Track3P [7]. The focus of these studies was to reveal potential multipacting (MP) sites and barriers within the cavity. Sustained secondary electron trajectories (surviving at least 20 RF cycles) have been found with impact energies peaking around 23.6 MV/m, which end on the outer cylinder of the cavity wall (1-point MP, 1st order). The impact energies however are very low (< 20 eV, SEC <1 for copper), i.e. to not induce a sustained MP, Figure 4.

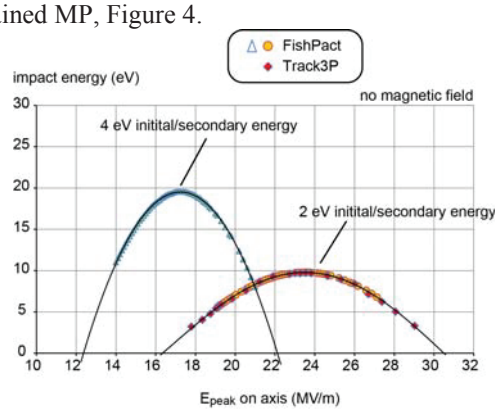

Figure 4: Impact energy vs. electric field for stable 1-point (1st order) resonant trajectories ending on the cavity cylindrical wall without solenoidal field. Once a 3T is applied however, these resonances disappear.

Hereby the impact energy depends also on the initial/secondary energy assumed. We have taken into account 2eV and 4eV, respectively. Moreover, the resonant trajectories completely ceased once a 3T solenoidal field was applied.

A 2-point MP (1st to few higher orders) between the cavity end lids as theoretically possible between parallel plates can exist only at much lower fields that cannot explain the experimental limitations seen at 25 MV/m. Our focus is therefore on field emission loading as a possible operational limitation. A high magnetic solenoidal field can strongly focus electron trajectories on the path between the end lids as verified with both codes mentioned above. Corresponding simulations are still in progress including estimates of field emission induced heating of the end plates. We intend to compare the findings with those obtained in the LBNL cavity. Understanding the differences in performance between the LBNL and Muons, Inc. cavities has become a very important step to defining/refining directions for muon acceleration cavity R&D.

SUMMARY

A test model of the RF cavity for the HCC tasks has been developed, built and tested with an 805 MHz klystron. Conditioning without external magnetic field demonstrated operation of the cavity with a maximum electric field gradient of 25 MV/m. Conditioning the cavity in the external 3 T solenoidal magnetic field a maximum gradient of electric field of 25 MV/m was reached. Simulations including estimates of field emission induced heating of the end plates are still in progress.

REFERENCES

[1] G. Flanagan et al., Helical Muon Beam Cooling Channel Engineering Design. These proceedings.
[2] Y. Derbenev and R. P. Johnson, PRSTAB *, 041002 (2005).
[3] S. A. Kahn et al., "Incorporating RF into a Muon Helical Cooling Channel." Proceedings of EPAC08, Genoa, Italy.
[4] G. M. Kazakevich, et al., "Multi-purpose 805 MHz Pillbox RF Cavity for Muon Acceleration Studies", Proceedings of PAC11, New York, USA.
[5] K. Ko et al, "Advances in Parallel Electromagnetic Codes for Accelerator Science and Development", LINAC2010, Tsukuba, Japan.
[6] http://code.google.com/p/fishpact/.
[7] D. Li, et al., 805 MHz and 201 MHz RF Cavity Development for MUCOOL.

KINETIC MODELING OF RF BREAKDOWN IN HIGH-PRESSURE GAS-FILLED CAVITIES *

D. V. Rose†, C. H. Thoma, Voss Scientific, Albuquerque, NM 87108, USA
A. V. Tollestrup, K. Yonehara, Fermilab, Batavia, IL 60510, USA
J. Byrd, D. Li, LBNL, Berkeley, CA 94720, USA
R. P. Johnson, M. Neubauer, R. Sah, Muons Inc., Batavia, IL 60510, USA

Abstract

Recent studies have shown that high field gradients can be achieved quickly in high-pressure gas-filled cavities without the need for long conditioning times, because the dense gas can dramatically reduce dark currents and multipacting. In this project we use this high pressure technique to suppress effects of residual vacuum and geometry found in evacuated cavities to isolate and study the role of the metallic surfaces in RF cavity breakdown as a function of operating frequency and surface preparation. A series of experiments at 805 MHz using hydrogen fill pressures up to 0.01 g/cm^3 of H_2 have demonstrated high electric field gradients and scaling with the DC Paschen law limit, up to ∼30 MV/m, depending on the choice of electrode material. At higher pressures, the breakdown characteristics deviate from the Paschen law scaling. Fully-kinetic 0D collisional particle-in-cell (PIC) simulations give breakdown characteristics in H_2 and H_2/SF_6 mixtures in good agreement with the 805 MHz experimental results below this field stress threshold. At higher pressures the formation of streamers at operating parameters below the Paschen limit are examined using 2D simulations.

INTRODUCTION

Breakdown data obtained from the Muons Inc. test cell (TC), a high pressure RF cavity developed to support ionization cooling experiments for muon colliders [1, 2], is analyzed. These experiments exhibit Paschen-like breakdown characteristics for field gradients below a threshold value. At higher field gradients and gas pressures, deviations from the Paschen limit are found, and a nearly constant field gradient operating limit is established, dependent on the choice of electrode material. Fully-kinetic particle-in-cell (PIC) simulations are used to examine the initial breakdown phase in both the Paschen limit and the high-pressure, field-gradient threshold limit.

For the analysis of Paschen law characteristics, 0D simulations are carried out to establish the applied field required to initiate an electron avalanche for a given gas pressure. The results of these simulations are described in the next section. To analyze the breakdown characteristics above the threshold for deviations from the Paschen limit, 2D simulations are used. The conjecture explored in this limit is that at field gradients above the vacuum space-charge-limit (SCL) emission threshold for various materials, the formation of high-density localized plasmas at the electrode surface can lead to the formation of streamers. The local net fields at the tips of these streamers can exceed the average fields in the electrode gap and propagate into the gap. In the third section, we describe initial 2D simulations of streamer formation at different applied field levels. The results of these simulations are found to be in rough agreement with experimental measurements.

* Work supported in part by USDOE STTR Grant DE-FG02-08ER86352
† david.rose@vosssci.com

0D KINETIC MODEL ANALYSIS

A significant amount of data for high pressure H_2 has been collected on the Muons TC for a variety of electrodes materials. A subset of this data is shown in Fig. 1. The main features of the data are a nearly linear region at lower gas pressures where the maximum electric field gradient increases with pressure, transitioning to a region where the peak electric field gradient either increases slowly or is essentially constant. This behavior is characteristic of, and consistent with, other high pressure Paschen law deviations [3] reported in the literature (see, for example, Ref. [4]). This latter region is sometimes referred to as the electrode-dominated regime and is discussed further in the later sections.

Simulation Model and H_2 Analysis

The LSP PIC code [5] is used throughout for time-dependent 0D simulations. A Monte Carlo collision (MCC) package is used to treat the elastic and inelastic particle interactions within a computational cell. This model has been benchmarked against experimental data for RF breakdown in He [6], and steady-state breakdown of H_2 and SF_6 [7].

The 0D simulations apply a sinusoidally oscillating electric field as a function of time,

$$E(t) = E_0 \sin(2\pi f t), \quad (1)$$

where E_0 is amplitude of the RF field and f is the frequency. For all cases presented here, $f = 805$ MHz. The simulations are initialized with a low density "seed" population of electrons and ions (H_2^+), typically with initial number densities between 10^{10} and 10^{12} cm^{-3}. After 10-100 RF cycles, the presence of an electrode density growth (avalanche) indicates breakdown for a given value of E_0.

ISBN 978-3-95450-115-1

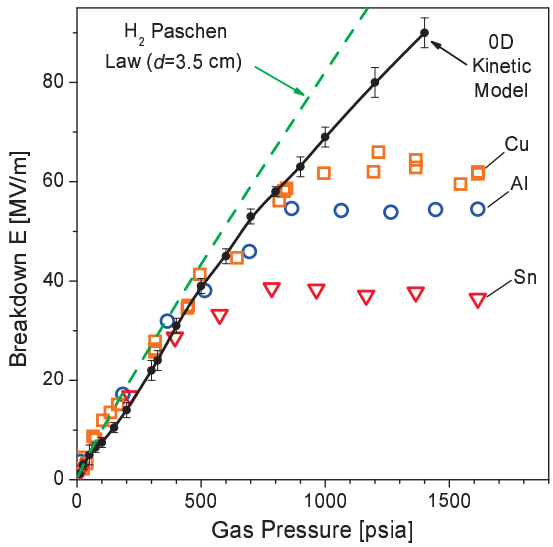

Figure 1: Breakdown curves as a function of H_2 gas pressure. The individual open points are different electrode materials from the 805 MHz RF test cell [1]. The solid black line is the result of 0D kinetic simulations that estimate the breakdown independent of electrode materials. For comparison, the dashed green line is the Paschen curve for H_2 for an electrode spacing of 3.5 cm.

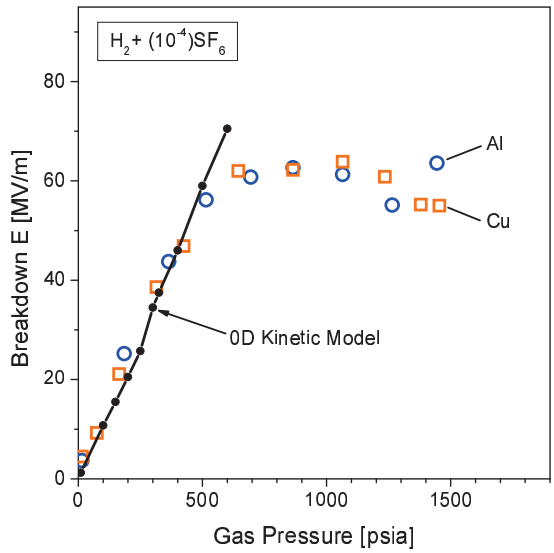

Figure 2: Breakdown curves for H_2 with 10^{-4} admixture of SF_6. The individual open points are different electrode materials from the 805 MHz RF test cell [1]. The solid black line is the result of 0D kinetic simulations that estimate the breakdown (independent of electrode materials).

The solid black lines joining the black circles in Fig. 1 represent the results of the 0D simulations identifying approximately the Paschen breakdown limit for H_2. The error bars shown with the individual data points indicate the approximate level of refinement in E_0 that was used to find the breakdown field value for a given gas pressure. As a check, several gas pressures were evaluated with a DC applied electric field. No significant difference in the breakdown value was found between the DC and RF simulations. This is due to the electron-neutral collision frequency ν_{en} being much larger than f for the parameters examined here, and assuming that no significant recombination takes place on the RF cycle timescale. Finally we note that the 0D simulations give an effective E/P for breakdown of roughly 40 Td for pressures above 100 psia.

Also shown in Fig. 1 is the Paschen Law for H_2, expressed as

$$V_B(\mathrm{V}) = V_{\min}\frac{\delta}{1+\ln(\delta)}, \qquad (2)$$

where $\delta = pd/(pd)_{\min}$, with d the electrode separation (cm), and p the pressure (Torr). For H_2, $V_{\min} \simeq 273$ V and $(pd)_{\min} \simeq 1.15$ Torr-cm. The value of $d = 3.5$ cm is larger than the 2.5-3 cm gap spacing in the experiment, but is used in the figure to illustrate the near linear scaling of Eq. (2) at these relatively high pressures.

H_2/SF_6 Mixture

In an effort to improve the breakdown characteristics of the high pressure RF cavity, small admixtures of electronegative gas have been explored [1]. Figure 2 plots the results of experiments with a 10^{-4} level addition of SF_6. A significant increase in the effective field gradient was achieved at lower total H_2 pressures.

The 0D simulation results (solid black circles connected by black line segments in Fig. 2) show an essentially linear rise with total gas pressure, as expected. The experimental data is in good agreement with the simulations, for both Cu and Al electrodes, for gas pressures up to about 500 psia. The 0D simulations give an effective E/P for breakdown of roughly 60 Td for pressures above 100 psia, a 50% increase over the case of pure H_2.

2D KINETIC SIMULATIONS OF STREAMER PROPAGATION

Typical metallic electrode surfaces are covered by microscopic whiskers, with scale sizes typically of a few micrometers and whisker densities between 1 and 10^4 cm^{-2} [8, 9]. Under high voltage, electric field enhancement at the whisker tips leads resistive heating of the whisker, and eventually these whiskers explosively vaporize, forming a high density, localized plasma. In vacuum these plasma flares merge, eventually covering the electrode surface. In a high pressure gas, it is postulated that the expansion velocities of the flares are moderated, potentially leading to the formation of individual streamers that propagate away from the electrode surface. As the streamers propagate, the will expand and merge, eventually crossing the entire electrode gap [10]. As the streamer body is comprised of a relatively dense plasma, the impact of field reversal under RF operating conditions is mitigated since the streamer can resume propagation once the RF cycle completes.

ISBN 978-3-95450-115-1

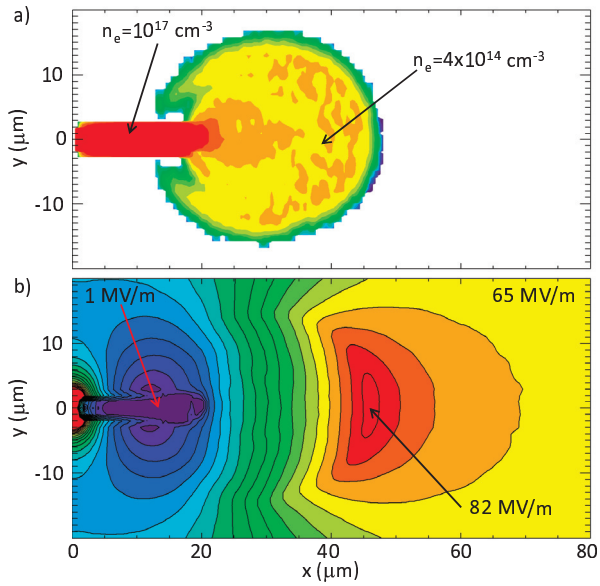

Figure 3: Electron number density (a) and electric field magnitude (b) from a 2D kinetic simulation at 65 MV/m and 1000 psia after 0.5 ns. The simulation is seeded with a 10^{17} cm^{-3} neutral plasma whisker 18 μm long and 2 μm thick.

To explore this possible breakdown mode, a series of 2D (x,y) simulations have been carried out. A constant value DC electric field $\vec{E} = -E_0\hat{x}$ is imposed on a gas-filled region. A relatively high-density plasma region, representing the exploded whisker, is placed in the neutral gas, on or near a conducting electrode surface. The simulated region is roughly 0.01 cm by 0.008 cm (x,y). The grid sizes are roughly 0.5 μm. A typical result is shown in Fig. 3. A 10^{17} cm^{-3} number density plasma whisker is initialized in contact with a conducting wall at $x = 0$. The whisker extends 18 μm from the electrode surface and is 2 μm wide. For this example the neutral gas is at 1000 psia and the applied electric field is 65 MV/m. After 0.5 ns, electric field enhancement at the whisker tip leads to the formation of a plasma density avalanche that in turn initiates streamer propagation. In this case, electric field enhancements at the whisker tip exceed 80 MV/m, well in excess of the Paschen limit ($\simeq$ 70 MV/m) at this pressure.

For an non-electronegative gas, diffusion modifies or limits the transition from an avalanche phase to streamer formation [11]. In the high pressure H_2 simulations carried out to date, streamer formation generally requires a relatively high field enhancement (or E/P value) in the vicinity of the streamer head, roughly 20% greater than the Paschen limit value, due in part to electron diffusion. For example in H_2, the transverse diffusion value is roughly a factor of 3 times the longitudinal value for E/P values greater than 20 Td [12].

DISCUSSION

The basic breakdown characteristics of the 805 MHz RF cavity are well-explained by the 0D kinetic simulation model in the Paschen limit. Examples for H_2 and H_2+SF_6 cases have been presented here. At higher field gradients, experimental measurements show deviations from the Paschen limit, suggesting a high-field-limit transition in behavior of the electrode materials. Previously, the different material melting temperatures has been examined as a signature of the high-field transition[13]. Here we have begun to explore the possibility that explosive electron emission is creating high-density plasma seeds leading to the formation of self-propagating streamers. The limited data available for explosive electron emission thresholds for different materials scales roughly with the maximum field gradients obtained in the RF cavity experiments. However, further modeling work is required to demonstrate that micrometer-scale streamers can efficiently propagating under these high-pressure RF conditions.

ACKNOWLEDGMENT

We thank R. E. Clark, D. R. Welch, C. Mostrom, W. Zimmerman and D. Voss at Voss Scientific for assistance and valuable discussions regarding the numerical simulations.

REFERENCES

[1] K. Yonehara, *et al.*, PAC'09, Vancouver, BC, 2009, TU5PFP020, p. 855, http://www.JACoW.org.

[2] R. Sah, *et al.*, PAC'11, New York, NY, 2011, MOP046, p. 184, http://www.JACoW.org.

[3] W. S. Boyle and P. Kisliuk, Phys. Rev. **97**, 255 (1955).

[4] Yu. D. Korolev and G. A. Mesyats, *Physics of Pulsed Breakdown in Gases* (URO-Press, Ekaterinburg, 1998).

[5] LSP is a software product developed by ATK Mission Research, with initial support from the Department of Energy SBIR Program.

[6] C. Thoma, *et al.*, IEEE Trans. Plasma Sci. **34**, 910 (2006).

[7] D. V. Rose, *et al.*, Proc. 2007 IEEE Pulsed Power and Plasma Sci. Conf. p. 1205.

[8] R. B. Miller, *An Introduction to the Physics of Intense Charged Particle Beams* (Plenum, NY, 1982).

[9] G. A. Mesyats, *Explosive Electron Emission* (URO-Press, Ekaterinburg, 1998).

[10] D. V. Rose, *et al.*, Phys. Plasmas **18**, 093501 (2011).

[11] C. Montijn and U. Ebert, J. Phys. D: Appl. Phys. **39**, 2979 (2006).

[12] L. G. Christophorou, *Atomic and Molecular Radiation Physics* (Wiley, NY, 1971), p. 266.

[13] R. Sah, *et al.*, LINAC'08, Victoria, BC, 2008, THP066, p. 945, http://www.JACoW.org.

INFLUENCE OF INTENSE BEAM IN HIGH PRESSURE HYDROGEN GAS FILLED RF CAVITIES*

K. Yonehara#, M. Chung, M.G. Collura, M.R. Jana, M. Leonova, A. Moretti, M. Popovic, T. Schwarz, A. Tollestrup, Fermilab, Batavia, IL 60510, USA, R.P. Johnson, G. Flanagan, M. Notani, Muons, Inc., Batavia, IL 60510, USA, B. Freemire, Y. Torun, P. Hanlet, Illinois Institute of Technology, Chicago, IL 60616, USA

Abstract

The influence of an intense beam in a high-pressure gas filled RF cavity has been measured by using a 400 MeV proton beam in the Mucool Test Area at Fermilab. The ionization process generates dense plasma in the cavity and the resultant power loss to the plasma is determined by measuring the cavity voltage on a sampling oscilloscope. The energy loss has been observed with various peak RF field gradients (E), gas pressures (p), and beam intensities in nitrogen and hydrogen gases. Observed RF energy dissipation in single electron (dw) in N_2 and H_2 gases was 2 10^{-17} and 3 10^{-17} Joules/RF cycle at E/p = 8 V/cm/Torr, respectively. More detailed dw measurement have been done in H_2 gas at three different gas pressures. There is a clear discrepancy between the observed dw and analytical one. The discrepancy may be due to the gas density effect that has already been observed in various experiments.

INTRODUCTION

Operating a high accelerating gradient RF cavity in a magnetic field is an essential requirement for muon a muon cooling channel to confine a large beam phase space in the muon cooling structure. However, the available RF accelerating field gradient in a pillbox vacuum RF cavity is limited because the field strongly concentrates the dark current in the cavity. Consequently, the probability of RF breakdown that is ignited by the dark current is higher in stronger magnet. By putting a dense buffer gas in a RF cavity, the current flow can be diffused by a Coulomb scattering. Molecular hydrogen is the ideal buffer gas since it produces the lowest multiple scattering for the muon beam and beam phase space growth.

A high pressure hydrogen gas filled RF (HPRF) cavity has been made to experimentally validate the gas-filled cavity breakdown model under various conditions [1, 2]. From experimental results, a model for energy loss by beam-induced plasma in a HPRF cavity has been successfully generated [3]. The plasma is shaken by the RF field, and takes energy from the field and loses it by collision of its ions and electrons with the gas molecule. Consequently, the cavity Q factor is degraded as a function of the amount of density of beam-induced plasma. We call this process as the beam-plasma loading effect. It is worth noting that the plasma is very dilute being only 10^{-6} or less than the ambient hydrogen molecular density which is of the order of 10^{21} molecule/cm^3. The degradation can be an issue since the beam in the later part of bunch train will see less electric acceleration than that in the earlier part of bunch train. In case of a muon collider design, 3.5 10^{12} muons per bunch train with 12 bunches separated by 5 nsec at kinetic energy 100 ~ 400 MeV passes through a 180 atm HPRF cavity at E = 15 ~ 25 MV/m during 60 ns with a 15 Hz repetition rate. The muon beam will generate 5.6 10^{15} cm^{-3} electron-ion pairs per muon beam bunch in the cavity.

A HPRF cavity beam test has been carried by using a 400 MeV proton beam in the MTA (Mucool Test Area) at Fermilab in Summer 2011 and Spring 2012. We mainly report the former experimental result and analysis in this document. RF energy consumptions of single electron (dw) in pure hydrogen and nitrogen gases were investigated with various peak RF field gradients (E) and gas pressures (p). The observed dw is well agreed with the beam-plasma loading effect. It means that we have a way to estimate the RF Q factor reduction at different E/p, beam intensity, and time structure by the theory. The theory also suggests that a small amount of electronegative gas doping can remove the ionized electron in the cavity. The dopant gas test has been done and reported in Ref. [4]

EXPERIMENT

Details of the experiment are depicted in Refs. 5, 6 and 7. Here, we describe the experimental parameters that are needed for data analysis. A 400 MeV H^- beam was delivered from an extended Fermilab Linac beam line to a high pressure gas filled RF cavity in the MTA. The beam intensity in the cavity was tuned by changing the beam spot size at the input to a collimator with a 4 mm diameter hole located upstream of the cavity. Beam current in the cavity was measured by using a toroid beam current monitor. The total number of beam bunches was 1500 spaced by 5 ns and a total length of 7.5 μs.

An 800 MHz high pressure RF cavity was used for this test. The shunt impedance of the cavity (R) was 2.0 MΩ at 1 atm. The cavity was powered by a 13 MW Klystron. Since the time constant of beam-plasma loading effects were longer than the 200 MHz beam bunch spacing the phase of 800 MHz cavity was not locked to that of the beam. There was a pickup loop in the cavity to monitor RF field strength.

*Supported in part by DOE STTR grant DE-SC0006266 and FRA under DOE cotract DE-AC02-07CH11359
* yonehara@fnal.gov

Table 1 shows the variables for H_2 run in this experiment. The cavity shunt impedance changed at different gas pressure for unknown reasons. It was measured separately by taking data without beam.

Table 1: Variables in this Experiment

	Unit			
Beam intensity	10^8 p/bunch	2	0.4	0.2
Gas pressure	psi	500	800	950
RF amplitude	MV/m	10	20	30

Figure 1 shows a typical RF pickup signal and a toroid signal. It should be emphasized that the cavity did not breakdown under an intense beam although the beam-plasma loading effect was seen, i.e. a rapid RF amplitude drop when the beam was on. After the beam was turned off, the RF power was restored.

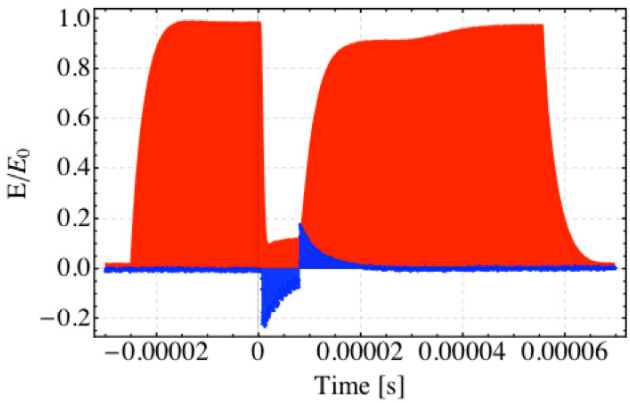

Figure 1: Observed RF pickup signal (red) and toroid current monitor signal (blue).

ANALYZE DATA

Solve Equivalent Resonant Electric Circuit Model

An RF system can be represented as an *LCR* resonant circuit diagram as shown in Figure 2. Thevenin's Theorem has been used to combine the cavity load and the generator resistance, i.e. $V_0 = V_g/2$ and if the cavity is matched $Z = R$ without beam loading. When a beam appears in the cavity, a new resistance, R_p is added in the equivalent circuit. It represents the conductance of beam-induced hydrogen plasma in the cavity.

The power balance equation is given by:

$$p_{plasma} = \frac{1}{2}\frac{(V_0 - V)V}{R/2} - \frac{d}{dt}\left(\frac{CV^2}{2}\right) \qquad (1)$$

where p_{plasma} is the RF dissipated power in a plasma and V_0 is the peak initial field potential in the cavity without beam and V is the measured RF amplitude. The first term in the right hand side equation is the RF power gain from the Klystron and the second one power lost or gained from the cavity when its peak voltage changes.

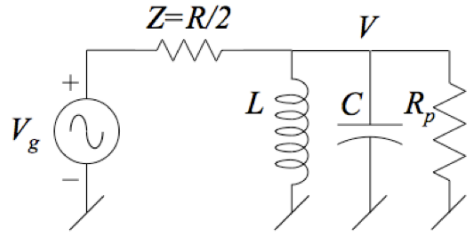

Figure 2: RF resonance circuit diagram with beam-plasma loading.

The ionization energy loss of a proton in a matter is well reproduced by the Bethe-Bloch formula. Since the ion-electron pair production energy (W) in hydrogen and nitrogen are known 35 and 35.5 eV, respectively [7], the number of electrons in the cavity produced by single proton can be estimated by

$$n_e = \langle \frac{dE}{dx} \rangle \frac{\rho}{W}, \qquad (2)$$

where $\langle dE/dx \rangle$ is the Bethe-Bloch formula, ρ is the density of gaseous hydrogen.

The time-domain rate equation of the number of electrons in a pure hydrogen gas is

$$\frac{dn_e}{dt} = \dot{N} - \beta n_e n_{ion}, \qquad (3)$$

where $\dot{N}$ is a production rate of electrons due to the ionization process, β is the hydrogen recombination rate. The electron diffusion rate is small and is omitted from Eq. (3). Because the hydrogen recombination process goes as n^2 it is zero at the beginning of beam-on, hence the dn_e/dt is simply represented as the electron production rate $\dot{N}$. Then, the RF dissipation energy of single electron, dw can be estimated from Eqs. (1) and (2),

$$dw = \frac{p_{plasma}}{dn_e/dt} \qquad (4)$$

The dw is extracted in N_2 and H_2 gases, which are 2 10^{-17} and 3 10^{-17} Joules/RF cycle at E/p = 8 V/cm/Torr, respectively (shown in Figure 3). The dw in H_2 was taken with wider variables range. Figure 4 shows the dw as a function E in p = 500, 800, 950 psi. There is a strong correlation between dw and E. A line in each plot shows the best chi-square fit of the data by using an equation aE^b. We found that the fitting also depends on the gas pressure. On the other hand, we do not see any beam intensity dependence on the dw. In fact, a point at the same E in the plot is taken with different beam intensity.

ISBN 978-3-95450-115-1

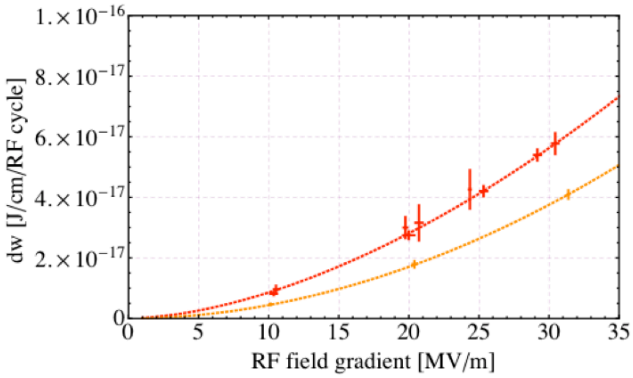

Figure 3: *dw* in N_2 and H_2 at 500 psi as a function of *E*. Error bars show the statistic error.

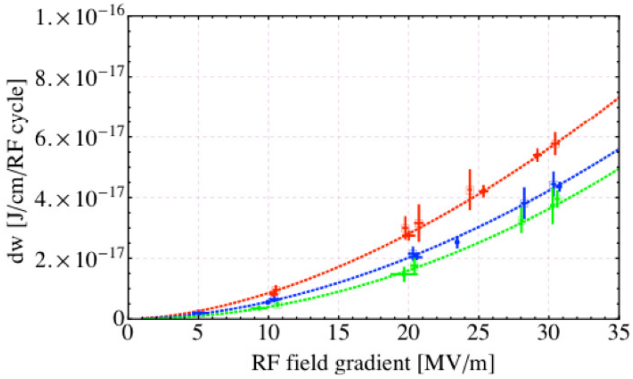

Figure 4: Observed *dw* as a function of *E*. Red, blue, and green marks are *dw* in 500, 800, 950 psi, respectively. Error bars show the statistic error.

Table 2: Fitting Parameter of *dw* in 500, 800, and 950 psi Pure H_2 and 500 psi Pure N_2. Fitting Factor is aE^b where *E* is MV/m.

	a	*b*
500 psi pure H_2	1.67 10^{-19}	1.71
800 psi pure H_2	8.67 10^{-20}	1.82
950 psi pure H_2	3.89 10^{-20}	2.01
500 psi pure N_2	5.00 10^{-20}	1.95

Estimate RF Energy Dissipation Per Single Electron

The RF energy dissipation per single electron, *dw* can be estimated by using a simple electron transport analysis. Since the electron drift velocity in H2 gas is known [8], the total RF power dissipation can be given by

$$p_{model} = jE = qn_e u_e E \tag{5}$$

where *j* and *E* are a current and an electric field gradient, respectively, and u_e is the drift velocity of electron in a matter. u_e is a function of *E/p*. Therefore, in order to estimate *dw*, eq. (5) must be integrated as a function of time,

$$dw = 2\int_{T/2} qn_e u_e(E_0 \sin(2\pi\nu t), p) E_0 \sin(2\pi\nu t) \tag{6}$$

where E_0 is a peak RF gradient, ν is an RF resonant frequency, *T* is an RF period, and *p* is a gas pressure.

The observed *dw* in this experiment is smaller than the estimated *dw* that is given from eq. (6). Figure 5 shows the correction factor of *dw*. The correction factor becomes larger in higher gas pressure. It indicates that the correction factor has gas density dependence. Table 3 shows the fitting parameter of correction factor where we use a linear fitting, $aE + b$. Interestingly, correction factor is met at the same electric field gradient, i.e. it is 40 MV/m in three different gas pressures.

Table 3: Fitting Parameter of Correction Factor. Fitting factor is $aE + b$ where *E* is MV/m

	a	*b*
500 psi pure H_2	5.89 10^{-3}	0.516
800 psi pure H_2	7.50 10^{-3}	0.449
950 psi pure H_2	11.2 10^{-3}	0.302

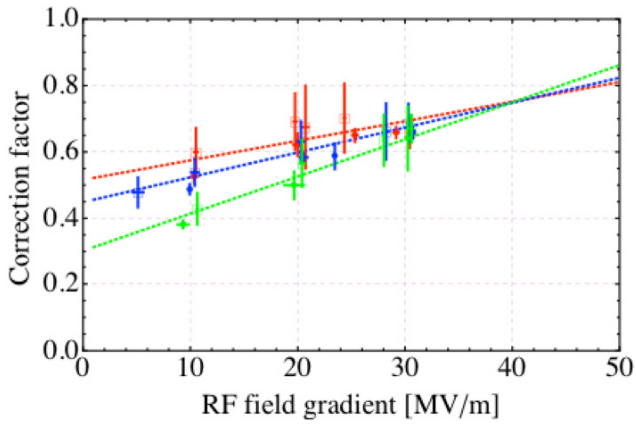

Figure 5: Correction factor of *dw*. Red, blue, and green marks are 500, 800, and 950 psi pure H_2 gases, respectively. Error bars show the statistic error.

ACKNOWLEDGEMENT

We thank to Vladimir Shiltsev and Mark Palmer for supporting this program. We also great thank to the Fermilab Accelerator Division, the safety group, and the beam operator for helping this experiment.

REFERENCES

[1] K. Yonehara et al., PAC09, TU5PFP020.
[2] P. Hanlet et al., EPAC06, TUPCH147.
[3] A. Tollestrup et al., FERMILAB-TM-2430-APC.
[4] M. Leonova et al., Proceedings of IPAC'12, MOPPC040.
[5] T. Schwarz et al., Proceedings of IPAC'12, WEOBA03.
[6] M.R. Jana et al., Proceedings of IPAC'12, MOPPR070.
[7] F. Ben et al., Proceedings of PAC'11, MOP032.
[8] J.J. Lowke, Aust. J. Phys., 1962, 16, 1, 15.

HIGH PRESSURE GAS-FILLED RF CAVITIES FOR USE IN A MUON COOLING CHANNEL

B. Freemire*, P.M. Hanlet, Y. Torun, IIT, Chicago, IL 60616, USA
M. Chung, M.R. Jana, M. Leonova, A. Moretti, T. Schwarz, A.V. Tollestrup, K. Yonehara, FNAL, Batavia, IL 60510, USA
R.P. Johnson, Muons, Inc., Batavia, IL 60510, USA
M.G. Collura, Politecnico di Torino, Torino, Italy

Abstract

A high pressure hydrogen gas-filled RF (HPRF) cavity can operate in the multi-Tesla magnetic fields required for a muon accelerator cooling channel. A beam test was performed at the Fermilab MuCool Test Area by sending a 400 MeV proton beam through an 805 MHz cavity and quantifying the effects of the resulting plasma within the cavity. The resulting energy loss per electron-ion pair produced has been measured at 10^{-18} to 10^{-16} J every RF cycle. Doping the hydrogen gas with oxygen greatly decreases the lifetime of an electron, thereby improving the performance of the HPRF cavity. Electron lifetimes as short as 1 ns have been measured, and electron-ion recombination rates are on the order of 10^{-6} cm^3/s. The recombination rate of positive and negative ions in the cavity has been measured on the order of 10^{-8} cm^3/s. Extrapolation in both gas pressure and beam intensity are required to obtain Muon Collider parameters, however the results indicate HPRF cavities can be used in a muon accelerator cooling channel.

INTRODUCTION

A recent White Paper submitted to the 2013 U.S. Community Summer Study of the Division of Particles and Fields by the U.S. Muon Accelerator Program (MAP) outlines a staged Muon Accelerator facility based at Fermilab [1]. The report outlines two main programs; a Neutrino Factory (NF), and a Muon Collider (MC). For the case of a MC, a Higgs Factory and multi-TeV collider are described. Because muons are created with a large initial phase space, the colliders requires significant (roughly six orders of magnitude) cooling.

The only cooling method that can work within the muon's lifetime is ionization cooling, and a so-called Helical Cooling Channel (HCC) has been proposed to do so [2]. The HCC is composed of normal conducting RF cavities arranged in a helix within a solenoidal magnetic field (see Fig. 1 & 2). The RF cavities are filled with a high pressure gas to allow operation in multi-Tesla magnetic fields. A series of six HCC cells, approximately 230 m long, reduces the 6D emittance by a factor of 175,000 [3].

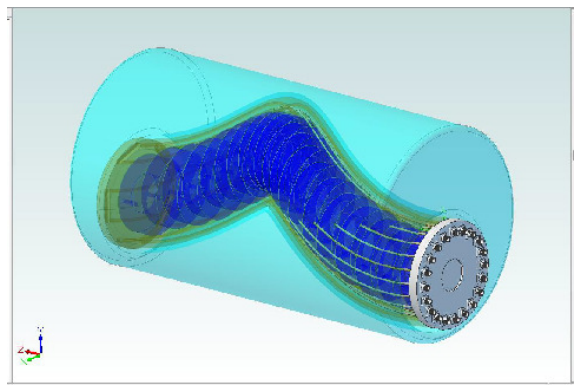

Figure 1: The 2D side view of one cell of the HCC, with components labeled. RF power is fed through the end. The solenoid coils are thermally isolated from the RF cavities [4].

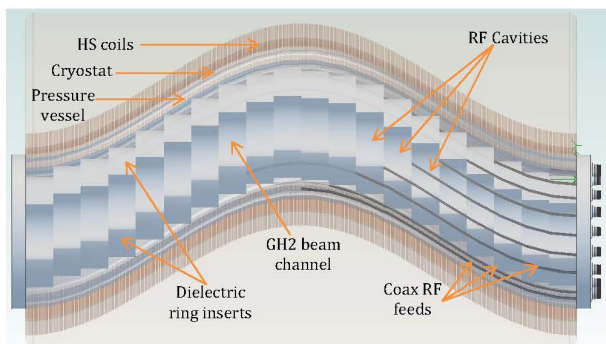

Figure 2: The 3D view of one cell of the HCC [4].

VALIDATION OF HIGH PRESSURE CAVITIES

A high pressure gas-filled RF (HPRF) cavity has been demonstrated to work in an external 3 T magnetic field without an ionizing beam [5, 6]. To validate its use in a HCC, a beam test using the 400 MeV Fermilab linac proton beam was performed at the MuCool Test Area (MTA). The cavity's performance using various beam intensities, gas pressures, dopant concentrations, and electric fields were studied with and without a 3 T magnetic field. Figure 3 shows a schematic of the experimental setup.

As the beam passes through the cavity, it ionizes the gas.

* freeben@iit.edu

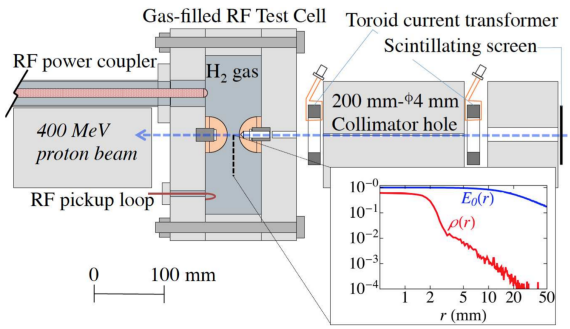

Figure 3: Schematic of the HPRF beam test setup. The beam enters from the right, passing through two collimators before impinging on the test cell. The inset plot shows the normalized electric field amplitude and simulated plasma density distribution as functions of radius.

The number of electron-ion pairs can be calculated:

$$N_{pairs} = \frac{\frac{dE}{dx}\,\rho\,L}{W_i} \tag{1}$$

where dE/dx is the stopping power, ρ is the gas density, L is the path length, and W_i is the average energy required to ionize a molecule.

Due to the high gas density, ionization electrons quickly come into equilibrium with the plasma, and drift with the cavity electric field. The electrons collide with gas molecules and transfer energy from the cavity to the plasma. The amount of energy transfered per charged particle can be evaluated by:

$$dw = q \int v\,E_0\,\sin(\omega\,t)\,dt \;=\; q \int \mu\,E_0^2\,\sin(\omega\,t)\,dt \tag{2}$$

where q is the charge of the particle, v is its drift velocity, E_0 is the amplitude of the electric field, and μ is the particle's mobility. The effect of the entire plasma is called plasma loading. To minimize the loading caused by electrons, an electronegative dopant gas can be used.

The results of the beam test are illustrated in Fig. 4 [7]. It can be seen that the addition of oxygen, present in dry air (DA), greatly decreases plasma loading. Additionally, there is very little difference between data taken with and without an external magnetic field.

The electric and magnetic fields inside the cavity as well as the ionization electrons' kinetic energy that would be present in a HCC were producible. However the maximum gas pressure was 100 atm while in a HCC it would be 180 atm. Additionally, the plasma density peaked at roughly 7×10^{11} cm^{-3} while in a real channel, due to the higher gas pressure and beam intensity, would be roughly 10^{16} cm^{-3}. Because of this, the results obtained in this beam test must be extrapolated to these higher densities.

The energy loss per particle, electron-ion and ion-ion recombination rates, and electron capture (by oxygen) time were measured as functions of electric field, gas pressure, and dopant concentration in order to extrapolate to the HCC parameters listed in Table 1.

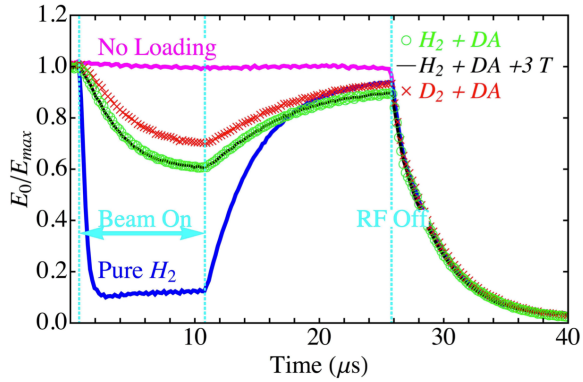

Figure 4: Typical RF envelopes recorded during the beam test. The beam is sent through the cavity once the flat top (E_{max}) has been reached. The magenta curve represents an RF pulse without beam.

Table 1: RF Parameters

Parameter	Unit	MTA Beam Test	HCC
RF frequency	MHz	801-808	325, 650
Gas pressure	atm	20-100	180
Oxygen conc.	%	2×10^{-4}-1	0.2
Peak E field	MV/m	5-50	20
External B field	T	0-3	4-14

Figure 5 shows the results of the electron attachment time, τ as a function of gas pressure. A fit to the data was used to extrapolate the time constant to 180 atm, which corresponds to 0.14 ns, indicated by the black lines on the plot.

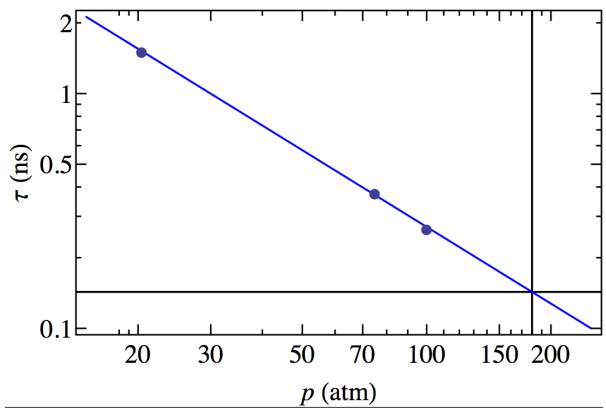

Figure 5: Electron attachment time as a function of gas pressure. The data (points) are taken from hydrogen gas doped with 1% DA (0.2% oxygen), and a fit was used to extrapolate the value of τ to 180 atm. The electron kinetic energy was kept constant at 0.4 eV.

PLASMA LOADING CALCULATION

A calculation of the plasma loading using muon accelerator beam and HCC RF parameters has been done. The beam parameters are given in Table 2. The beam bunches were assumed to be delta functions. The HPRF cavity's

length was 10 cm and the stored energy was 19 J at 325 MHz and 4.7 J at 650 MHz.

The electron attachment time, electron-ion recombination rate, ion-ion recombination rate, and electron energy loss used in the calculation were based on extrapolations of measurements made at the MTA. The ion energy loss was based on classical values for the mobility.

Table 2: Beam Parameters

Parameter	Unit	Value
# of bunches	-	21
Bunch intensity	μ/bunch	10^{11}, 10^{12}
Bunch frequency	MHz	325
Injection phase	degrees	160

The results of the calculations are given in Table 3 & 4, for the two bunch intensities considered. Luminosity requirements dictate the bunch intensity before the final acceleration. To account for losses, the bunch intensity in the cooling channel will be between 10^{11} and 10^{12}.

Table 3: Plasma Loading Results for 10^{11} Muons per Bunch. The percent the accelerating voltage has dropped by the final bunch is given.

Parameter	Unit	325 MHz	650 MHz
Energy dissipated	J	0.292	0.317
% of total energy	-	1.5	6.7
% V_{accel} drop	-	0.8	3.4

Table 4: Plasma Loading Results for 10^{12} Muons per Bunch. The percent the accelerating voltage has dropped by the final bunch is given.

Parameter	Unit	325 MHz	650 MHz
Energy dissipated	J	1.84	1.98
% of total energy	-	9.7	42
% V_{accel} drops	-	5.0	24

It can be seen that, due to the larger stored energy, the 325 MHz cavity is only minimally loaded by the plasma, for either bunch intensity. The 650 MHz cavity experiences considerable plasma loading at the larger bunch intensity. This is due primarily to the buildup of ions over the course of the beam pulse. This is illustrated in Fig. 6. However, results obtained at the MTA indicate that the mobility of ions is smaller than the classical mobility, which was used here. This would have the effect of decreasing the loading due to ions.

CONCLUSIONS

The initial evidence suggests high pressure gas-filled cavities will work in a helical cooling channel for a muon accelerator. Extrapolation of parameters obtained at the MTA suggest that in the highest bunch intensity case, the accelerating gradient the final 10^{12} muon bunch would see would be degraded by 24%. The plasma dynamics inputs into this calculation were all taken to be conservative, and in reality the plasma loading should be less.

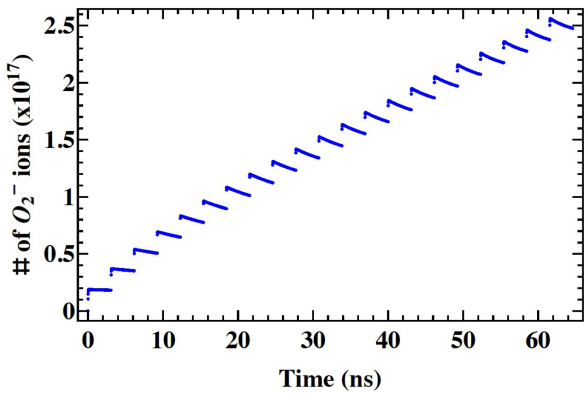

Figure 6: Number of O_2^- ions present in the cavity over the beam pulse.

The effects of higher gas and plasma density must be considered, and simulations [8] are underway to address this. Evidence suggests that higher densities have a positive effect on the cavity's performance.

Additionally, wakefields and beam loading have not yet been considered. These are not issues unique to gas-filled cavities, and may be a serious consideration for $10^{11}-10^{12}$ muons per bunch. The impact and mitigation are being investigated.

REFERENCES

[1] J-P. Delahaye et al., "Enabling Intensity and Energy Frontier Science with a Muon Accelerator Facility in the U.S.: A White Paper Submitted to the 2013 U.S. Community Summer Study of the Division of Particles and Fields of the American Physical Society," arXiv:1308.0494, August 2013.

[2] Y. Derbenev and R. P. Johnson, "Six-dimensional muon beam cooling using a homogeneous absorber: Concepts, beam dynamics, cooling decrements, and equilibrium emittances in a helical dipole channel," Phys. Rev. ST Accel. Beams, 8, 2005, 041002.

[3] R.P. Johnson et al., "Helical Muon Beam Cooling Channel Engineering Design," Proc. of NA-PAC'13, THPBA22.

[4] R.P. Johnson, private communication.

[5] K. Yonehara et al., "A Helical Cooling Channel System for Muon Colliders," IPAC 2010, Kyoto, May 2010, TU5PFP020, p. 870.

[6] P. Hanlet et al., "High Pressure RF Cavities in Magnetic Fields," EPAC 2006, Edinburgh, June 2006, TUPCH147, p. 1364-1366.

[7] M. Chung, et al., "Pressurized H_2 RF Cavities in Ionizing Beams and Magnetic Fields," accepted by Phys. Rev. Lett., October, 2013.

[8] R. Samulyak, et al., "Algorithms and Self-consistent Simulations of Beam-induced Plasma in Muon Cooling Devices," Proc. of NA-PAC'13, MOPBA06.

ISBN 978-3-95450-138-0

SUMMARY OF DENSE HYDROGEN GAS FILLED RF CAVITY TESTS FOR MUON ACCELERATION *

K. Yonehara#, M. Chung, M.R. Jana, M. Leonova, A. Moretti, A. Tollestrup, Fermilab, Batavia, IL 60510, USA
R.P. Johnson, Muons, Inc., Batavia, IL 60510, USA
B. Freemire, Y. Torun, P. Hanlet, Illinois Institute of Technology, Chicago, IL 60616, USA

Abstract

We show the recent analysis of a dense gas-filled RF cavity test by using a 400 MeV proton beam from Fermilab Linac. A large amount of RF power loading was observed in a gas-filled RF test cell when protons pass through the test cell. It can be explained that an ionized electron-ion plasma consumes RF power and transfers its kinetic energy to neutral gas molecules via the Coulomb interaction. We used several correction factors based on certain assumptions to evaluate the RF power consumption. The validity of these corrections and assumptions is discussed in this report.

PROTON INTERACTION WITH EXPERIMENTAL APPARATUS

Figure 1 shows the experimental apparatus. A 400 MeV proton beam passes through a collimator system and dense gas-filled RF test cell (TC). It is damped in a beam absorber. The TC is made of copper coated stainless steel. There is a pair of hemisphere copper electrodes to concentrate the RF field near the beam path. A 200 mm-4 mm$^{\phi}$ collimator hole is located in front of the TC to confine the beam in the TC. The beam current and profile are measured by using a toroid current transformer and a scintillating screen. The observed beam profile and simulated beam emittance from a beam lattice calculation are used to simulate the gas plasma distribution in the TC that will be discussed later. An induced RF field in the TC is measured by an RF pickup loop [1-3].

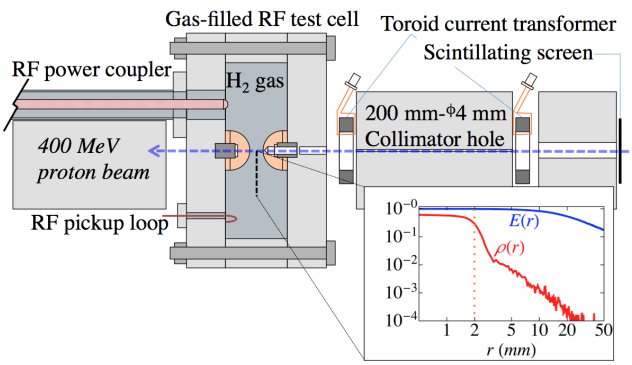

Figure 1: Whole layout of experimental apparatus and simulated radial distribution of electron-ion gas plasma in the TC and the normalized radial electric field distribution.

*Work supported by Fermilab Research Alliance, LLC under Contract No. DE-AC02-07CH11359 with the United States Department of Energy.
#yonehara@fnal.gov

Protons lose some of their kinetic energy before entering the RF field. Table 1 shows the average energy loss of protons in the various materials in which the protons pass through. Secondary particles are produced in the apparatus and air via the interaction between protons and materials.

The stopping range of electrons in air has been reported [4]. Low energy electrons (K < 1 keV) in air are eliminated from this analysis because their stopping range is very short (<< 1 mm). On the other hand, a large number of delta rays (K > 1 keV) that are produced upstream of the collimator are eliminated by the collimator. A very small number of delta rays (< 2 10^{-4} e/p) can be produced in air and go through the beam monitor system. The yield of surface emission electrons [5,6] in the collimator hole is calculated. Although there are some uncertainties due to the details of geometric correlation between the beam angle and the material surface, the spectrum of surface emission electrons per proton is given $P(\varepsilon) = c \times \varepsilon(\varepsilon + U_0)^{-(a+2)}$, where c is a constant, U_0 (~ 10 eV) is the work function of material, and a is the power of stopping power (a ~ 4). $P(\varepsilon)$ is maximum at ε ~ 2 eV and it is ~ 10^{-9} at ε > 1 keV. The overall effect of secondary electrons on the toroid current transformer and the scintillating screen is less than 1 %, which is negligible in the rest of analysis.

Table 1: Material, Thickness, Energy Loss and Initial and Final Kinetic Energies of a Proton Beam, Respectively

Element	Thickness	dK	K
Unit	mm	MeV	MeV
Initial			401.5
Ti-vacuum window	0.05	0.051	
Air	880	0.283	
Scintillating screen	1.00	0.814	
Air	400	0.129	
SS-beam window	3.18	5.56	
Cu electrode	3.18	5.99	
Final			388.2

Estimating the yield of gamma rays and its contribution in the TC is more complicated because high energy photons have long attenuation lengths in a material. We use *G4beamline* [7] to estimate the yield of gamma rays in our exact geometry. Table 2 shows the abundance of secondary particles in the TC. A large amount of high-energy gamma rays (> 10 keV) are produced in the

ISBN 978-3-95450-122-9

upstream apparatus from the TC via nuclear interactions. The cross-section of electron-production interactions of high-energy gamma rays with hydrogen is negligible (10^{-21} cm^2 or less). Photons in the middle energy range (100 eV to 10 keV) could also be produced via the Bremsstrahlung and K-shell electron capture processes. However, the production rates of such photons are negligible (See Table 2). Overall contributions of the photo-ionization process should be less than 1 %. It is reasonable to ignore all secondary particles except for secondary protons in the analysis.

Table 2: Simulated Yield of Secondary Particles in the TC: Values are Normalized by the Yield of Protons

Species	Yield
Proton (With the primary)	1.0
Gamma (All K)	0.73
Gamma (K < 10 keV)	$4.2\ 10^{-5}$
Pion (+/-)	$8.0\ 10^{-4}/1.6\ 10^{-4}$
Electron-Positron	$6.3\ 10^{-4}$

The electron-ion pair production rate is estimated by using a formula,

$$\dot{N} = \dot{N}_b \times h \sum_k w_k \left(\frac{\rho_m \, dE/dx}{W_i} \right)_k . \qquad (1)$$

where h is the propagation distance, and w_k, ρ_m, dE/dx, and W_i are the abundance, mass density, stopping power, and effective average energy to produce single ion-pair [8] of the k-th gas molecule ($\sum_k w_k = 1$), respectively. The mass density of hydrogen is calibrated by using the Van der Waals equation. The correction factor is 7.5 % in 100 atm H_2.

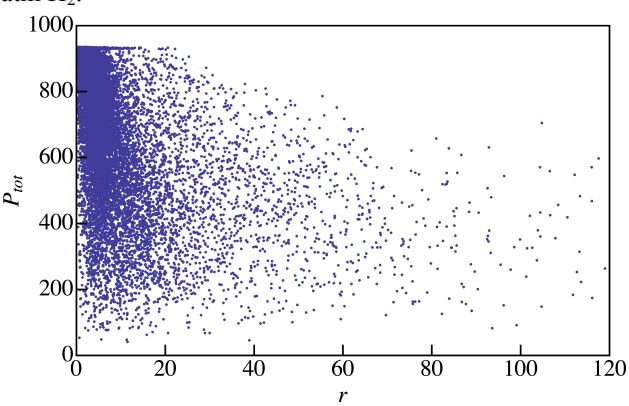

Figure 2: Total momentum (MeV/c) of protons in the TC as a function of radius (mm).

An accurate W_i is found in ref. 8. $\dot{N}_b$ has a wide momentum distribution. It is determined from the beam current measurement and simulation. Figure 2 shows the simulated momentum distribution of protons in the TC as a function of radius. By using Eq. (1), we estimate the radial and longitudinal distribution of electron-ion plasma per incident primary proton, $\rho(r,z)$ as shown in Fig. 1 (mid-plane of the TC).

ESTIMATED GEOMETRIC CORRECTION FACTOR

We represented the measured RF power consumption due to beam-induced plasma, *dw* at the peak RF electric field [1,2]. Actually, *dw* takes into account the gas plasma and electric field distributions. In this section, we show the geometric correction factor used to evaluate the measured *dw*.

The *dw* is analytically given by the following formula,

$$dw = \iiint 2\pi r \rho(r,z)(\mu_e + \mu_+) E(r,z)^2 \sin^2(\varpi t)\, dt\, dr\, dz , \qquad (2)$$

where μ_e and μ_+ are the mobility of the electrons and positive ion in hydrogen gas, respectively. $E(r,z)$ is estimated using *SuperFish* [9]. There are measurements of μ_e and μ_+ as functions of gas pressure and electric field. Then, we can estimate the geometry correction factor for *dw* as

$$c_{geometry} = \frac{dw}{\mu_{e,\pm} E_{peak}^2} , \qquad (3)$$

where E_{peak} is the peak RF electric field. $c_{geometry}$ is 0.66 for the electron swarm and 0.58 for the positive ion plasma.

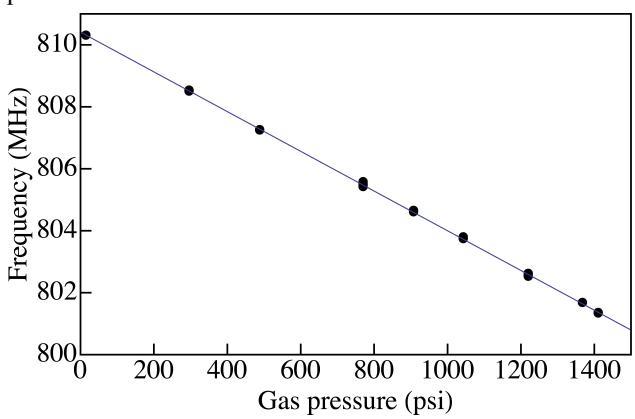

Figure 3: Observed resonant frequency as a function of gas pressure. Gas pressure is calibrated by the Van deer Waals equation. The fit is -0.0064 x + 810.409, where x is gas pressure.

In order to estimate the RF stored energy in the TC, we calculate the capacitance of the TC, C_{TC}. *SuperFish* provides the RF stored energy, $\varepsilon = 2.4\ 10^{-4}$ Joules at $E = 1$ MV/m in 100 atm H_2 gas (frequency = 801.4 MHz). The gap between the two electrodes is 17.7 mm. Thus, C_{TC} is 1.53 pF ($C_{TC} = 2\varepsilon/V^2$). C_{TC} is a function of resonant frequency, hence it is a function of gas pressure. It is worth noting that the capacitance correction also takes into account the possible deformation of the TC due to high gas pressure because we use the measured resonant frequency to estimate C_{TC}. Figure 3 shows the measured resonant frequency as a function of gas pressure in pure H_2 gas.

POSSIBLE SYSTEMATIC ERROR IN BEAM INTENSITY DEPENDENCE ON RF POWER LOADING MEASUREMENT

Figure 4 shows the measured *dw* in 20 atm H_2 gas at various electric fields (E_{peak} = 5, 10, 18 MV/m) as a function of beam intensity. First, the fluctuation of RF peak gradient is calibrated by using a power curve fit to *dw* as a function of X_0 where X_0 is the ratio between E_{peak} and the gas pressure. The residual of fit is within a few %. Then, the *dw* is averaged. That is the corrected *dw*.

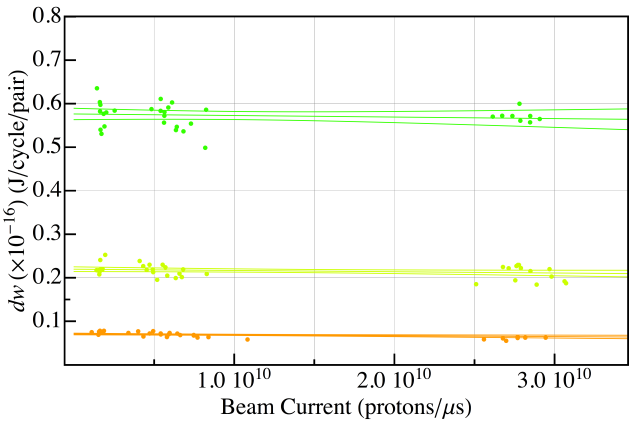

Figure 4: Measured *dw* vs Beam current. Gas pressure is 20 atm. The middle line in the set of lines is the best fit and other two correspond to a range of error with 3σ confidence level.

Figure 5 shows the deviation of measured *dw* at the lowest and highest beam intensities for various gas pressures. The measured *dw* tends to be low at high beam intensity in low gas pressure (negative deviation) and vise versa in high gas pressure (positive deviation). We define this deviation as a systematic error, which is 5~10 %.

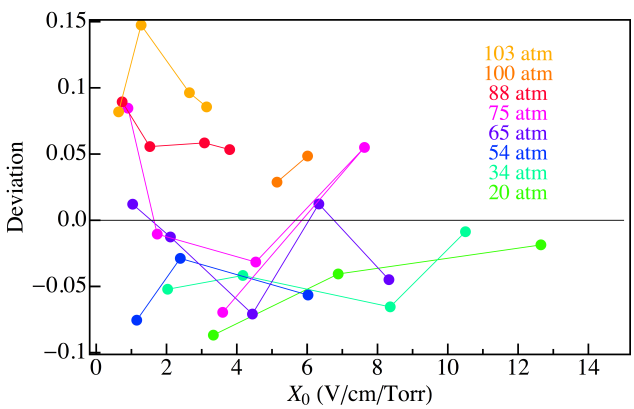

Figure 5: Plot shows the systematic error due to the beam intensity dependence.

Figure 6 is the corrected *dw* as a function of X_0 for various gas pressures. Each *dw* has an analysis error which involves the statistic and fit errors. It is typically a few %. The solid lines are the analytical *dw* that is estimated by using Eq. (2). The analytical *dw* is in good agreement with the measured *dw* at low gas pressure. However, the measured *dw* has larger discrepancy at higher gas pressure and lower X_0. It can be a gas pressure effect. We discuss the gas pressure effect in refs. [1,10,11].

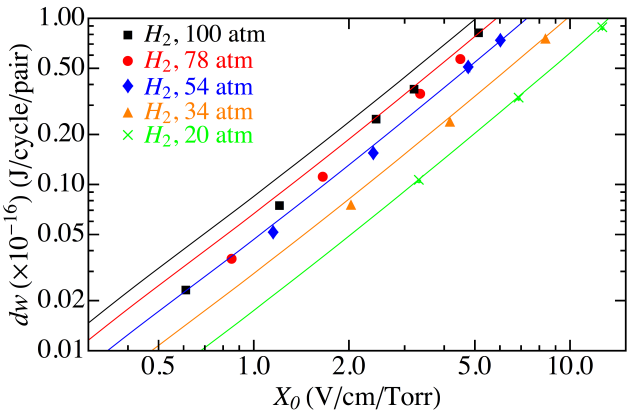

Figure 6: Corrected *dw* as a function of X_0. The solid lines are a prediction from gas-plasma dynamics in RF fields [1, 2].

SUMMARY

We investigated the measured *dw* and evaluated its systematic error. The large systematic error was found in the beam intensity dependence. It is 10 %. On the other hand, the statistic error is very small, i.e. it is typically 2 ~ 3 %. The deviation of measured *dw* from the prediction is larger than any systematic and statistic errors. It means that the pressure dependence is real.

ACKNOWLEDGMENT

We thank to Vladimir Shiltsev and Mark Palmer for supporting this program. We also great thank to the Fermilab Accelerator Division, the safety group, and the beam operator for helping this experiment.

REFERENCES

[1] B. Freemire, Doctoral Thesis at IIT, 2013.
[2] K. Yonehara et al., IPAC12, MOPPC036, pp. 208.
[3] M.R. Jana et al., IPAC12, MOPPR070, pp. 948.
[4] A. Cole, Radiation Research 38, 7-33, 1969.
[5] A.L. Hanson et al., J. Vac. Sci. Tech. A 19 (5) 2001.
[6] P.H. Stoltz et al., Phys. Plasmas 13 056702, 2006.
[7] T. J. Roberts, *G4beamline* (Muons, Inc. 2013), http://www.muonsinc.com/muons3/G4beamline.
[8] C. J. Bakker and E. Segre, Phys. Rev. 81 489 (1951).
[9] R.F. Holsinger and K. Hlbach, *SuperFish* (LANL), http://laacg1.lanl.gov/laacg/services/download_sf.phtml#ps1.
[10] K. Yonehara et al., Proceedings of IPAC13, TUPFI058.
[11] B. Freemire et al., Proceedings of IPAC13, TUPFI064.

ISBN 978-3-95450-122-9

RF CAVITY DESIGN ASPECTS FOR A HELICAL MUON BEAM COOLING CHANNEL*

F. Marhauser#, G. Flanagan, R.P. Johnson, S.A. Kahn, Muons, Inc., Batavia, 60510 IL, USA
K. Yonehara, Fermilab, Batavia, 60510 IL, USA

Abstract

A Helical Cooling Channel (HCC) promises efficient six-dimensional ionization cooling of muon beams by utilizing high-pressurized gas as a continuous absorber within a magnetic channel embedding RF cavities. The progress on cavity design, tailored for such a cooling channel, is discussed.

INTRODUCTION

Muon accelerators bear unique potential for the high energy physics community supporting the US Intensity Frontier research program and - when relying on the infrastructure developed - the Energy Frontier using one or more muon colliders as a subsequent stage [1]. Muon beam ionization cooling is deemed the only solution to provide the very high beam intensities required for a neutrino factory or muon collider. Cooling channels generally demand strong magnetic fields enclosing RF cavities that compensate for the energy loss due to ionization. Cooling by at least a factor of ~10^6 - defined as the ratio of initial to final six-dimensional beam emittance - is necessary for a muon collider [2]. E.g., to achieve this reduction for a 250 MeV/c muon beam necessitates about seven times that much energy loss, which means an equivalent accelerator of about 1.75 GeV. This represents a multi-billion dollar expense based on large diameter superconducting magnets, pillbox-like cavities, and present RF power source technology. The HCC is considered a cost-saving solution for muon cooling, though its engineering design remains challenging. After briefly introducing the HCC concept and the benefit of gaseous absorbers, the paper focuses on the development of RF cavity concepts.

HCC CONCEPT

The cooling technique utilized in an HCC has been under study since several years both analytically [3] and numerically (e.g. [4], [5]). The most effective approach to implement the desired magnetic field is a low-temperature (4 K), superconducting helical solenoid (HS) channel composed of short solenoid coils arranged in a helical pattern [6]. In addition, a helical quadrupole field is used to provide beam stability. Solenoidal and transverse helical dipole field components provide a constant dispersion along the cooling channel for emittance exchange to allow longitudinal cooling. Whereas the helical dipole component creates an outward radial force due to the longitudinal momentum, the solenoidal component creates an inward force due to the transverse momentum. This yields a beam motion with helical period ($\lambda = 2\pi/k$) at constant radius (a) as depicted in Fig. 1, i.e. unlike the motion in a pure solenoidal field, where the radius would diminish. The momentum of the equilibrium orbit obeys eq.(1) [3]. Herein B is the solenoidal magnetic field component, b the transverse helical component, and $\kappa = k \cdot a$.

$$p(a) = \sqrt{\frac{1+\kappa^2}{\kappa}} \cdot \left[B - \frac{1+\kappa^2}{\kappa} \cdot b \right] \qquad (1)$$

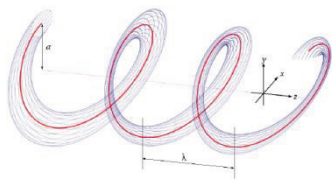

Figure 1: Theoretical helical muon beam motion in an HCC. Red is the equilibrium orbit obeying eq. (1) [3].

The presently conceived HCC concept makes use of a series of six different cooling segments, wherein a and λ decreases as the muon beam is cooled, but not within the same segment [7]. The pitch angle is 45 deg. throughout ($\tan^{-1}(\kappa=p_t/p_z=1)$). Two operating frequencies are envisaged to cover all six segments, i.e. 325 MHz and 650 MHz. The frequencies derive from Project-X (now PIP-II) at Fermilab, which could serve as a proton driver. Within the magnetic channel, high-pressurized, gas-filled normal-conducting RF cavities have to be embedded. The high pressure gas serves as a homogeneous absorber for continuous ionization cooling. The energy lost is replenished by the RF cavities to maintain the total beam momentum (p_μ). A momentum around $p_\mu = 200$ MeV/c ($\beta = v/c_0 = 0.88$) has been found optimal for cooling.

GASEOUS ABSORBER

Hydrogen (H_2) is the most promising gaseous absorber, since it has the largest product of ionization loss and radiation length. Moreover, H_2 has the largest heat capacity and lowest viscosity of all gases making it well suited as a coolant. Thin beryllium (Be) windows are foreseen to close the cavities electrically on each side, which reduces the surface peak fields compared to cavities with open beam tubes. The windows are almost transparent for the muon beam. At $p_\mu = 200$ MeV/c, the ionization losses in H_2 are ~4.4 MeV·cm^2/g and ~1.75 MeV·cm^2/g in Be, respectively. This determines the required accelerating field (E_{acc}) in a cavity. As the helical period decreases along the segments during cooling, the

*Work supported under U.S. DOE Grant Application Number DE-SC0006266
#frank@muonsinc.com

required E_{acc} rises and may exceed 20 MV/m depending on design. (This considers the synchronous phase). The cavities have to operate within multi-Tesla fields generated by the magnets, while avoiding RF breakdown and multipacting. These phenomena have been a prevalent problem in vacuum cavities. Pressurized gas-filled cavities have so far not revealed a significant difference whether or not an external magnetic field was applied [8]. Common to all tests is the characteristic that the RF breakdown threshold field linearly increases with pressure since the mean free path for ions and electrons is reduced with higher gas density. This in turn lowers the achievable collision energy. Thus, higher fields are required to initiate a breakdown shower in the gas (Paschen effect). At sufficiently high pressures however, the onset of RF breakdown is determined by the metal surface, whereas the gas pressure plays a negligible role. Overall, the gas combines multiple functions as a benefit:

- Continuous, homogeneous ionization cooling
- Elevation of RF breakdown limit as compared to vacuum cavities, particularly important in presence of external multi-Tesla magnetic fields
- Mitigation of multipacting and dark current phenomena
- Thermal cooling of cavity walls and Be windows

RF CAVITIES

The engineering design of the RF cavities is challenging since the HS channel limits the usable size. Several cavity candidates were investigated towards a realistic HCC concept. While peak power (P_{peak}) levels per cavity may be in the MW-range depending on the design, the thermal power dissipation is reasonably low (few hundred Watts) thanks to the low duty factor. Yet, the cavities require adequate thermal management since these operate at room temperature in close vicinity of the superconducting magnets. To cope with the envisioned gas pressures beyond 100 bar, pressure-resistant walls (~1/2" stainless steel) have to be employed. More recently it has been proposed to share a common pressure vessel among all cavities within a thermodynamically independent HS cryostat as sketched in Fig. 2 [7]. This does not save space, but simplifies cavity fabrication (only few mm thin copper walls required), thermal management and avoids cryostat penetration by RF feeds.

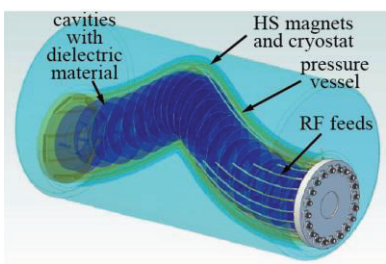

Figure 2: Concept of an HCC module using RF cavities enclosed in a pressure vessel within a HS cryostat [7].

H_2 gas may flow through the interior and exterior of the cavities for cooling. The pressure vessel itself can implement channels for circulating water, LN_2 or gaseous Helium. Each cavity is offset radially with respect to the preceding unit to smoothly follow the helical path. One requires additional space for input coupler and instrumentation feeds to be attached to each individual unit. Pillbox-like cavities will not fit into the cooling lattice. Thus, measures have to be provided to reduce the cavity size and to limit RF losses to acceptable levels.

Dielectric-loaded Cavities

Since the early stage of the HCC design, RF cavities filled with a dielectric material have been conceived to minimize the cavity diameter at a given frequency, whereas magnetic materials are not a viable option [9]. Depending on the material and volume filled, the diameter can be halved, making the cavity sufficiently small to fit into the HCC lattice, but RF power requirements are significantly enhanced at the same time. Note that Ohmic wall losses increase with decreasing diameter for the same cavity shape and same frequency, while dielectric (volumetric) losses are added according to the product of loss tangent (tan δ) and permittivity (ε') of the ceramic. One of the initial concepts consisted of 24 cavity units per helical period (similar to Fig. 2) that implemented ceramics filling the upper volume of a cavity unit along its full length [10]. Despite the small cavity diameter, the input couplers pointed out radially. This claims significant space and complicates the practical usage for an HCC. A large number of cavities implies rather short cavities (few cm). This reduces the stored energy (W_s), hence P_{peak} per unit, but increases the peak power per active length (P_{peak}/L) on the other hand. The latter determines the overall power demands. To reduce P_{peak}/L, 12 instead of 24 cavities are considered for the arrangement depicted in Fig. 3. Short drift tubes are used between the cavities, which is advantageous to not disrupt the HCC. The magnets enclosing the cavities are not shown for clarity. The interior ceramics are depicted on the right hand side. Technical Alumina (Al_2O_3) is the preferred choice since readily available in high purity offering low dielectric losses (tan δ ~ 1e-4, ε'~9-10 at room temperature in the considered frequency regime).

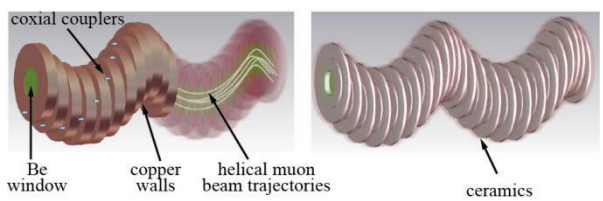

Figure 3: Schematic showing RF copper cavities for one HCC segment (solid color, left). The cavities are filled with low-loss Alumina ceramic rings (right).

A ceramic placed at the outer perimeter of the cavity has the least influence on frequency since the electrical fields decrease with distance from the axis. Therefore, instead of filling the cavity along its full length, a ceramic ring - centered in the cavity - with a bulge at the lower end and a neck at the upper end is utilized. This design

ISBN 978-3-95450-132-8

sacrifices diameter to reduce P_{peak}/L, but space is regained since coaxial antenna couplers can be attached to the cavities' front plates. The couplers do not interfere with the ceramics inside. The RF cables can be fed sideward through the ends of the HS cryostat to yield a practical concept. Moreover, the typical electric field enhancement at the ceramic-metal-gas interface is mitigated as best as practicable. Potential RF breakdown at the ceramics is a separate issue. The breakdown is initiated by electron avalanche at the ceramic surface, which determines its dielectric strength. An experiment with a special 805 MHz cavity holding an Alumina (99.8% purity) rod along its center confirmed that RF breakdown can be prematurely initiated in accordance with the materials' dielectric strength [11]. For the proposed design however, the electrical fields at the ceramic surfaces are comparably small and would allow operation beyond the envisioned field levels before breakdown occurs (e.g. $E_{acc} > 30$ MV/m). A dielectric-loaded cavity prototype based on the present layout will be built and tested at Fermilab to verify this statement. Potential charge build-up at the ceramic surface due to the traversing beam is another concern, which will be addressed.

Re-entrant Cavities

An HCC with dielectric-loaded cavities requires a large amount of ceramics. This adds costs and complicates the engineering design compared to conventional cavities (e.g. how to integrate the ceramics). As an alternative, re-entrant cavities are proposed omitting the ceramics. Re-entrant cavities enhance the shunt impedance by introducing nose cones on each side, which focus the electrical field. Since the capacitance (C) is increased, the frequency is lowered ($f \sim \sqrt{(L \cdot C)}$) at a given cavity diameter. One may also consider that the inductance (L) is enlarged due to a broader dome at a given accelerating gap. In fact, re-entrant cavities as shown in Fig. 4 have been designed to yield the same diameter at the same frequency as the dielectric-loaded cavities above.

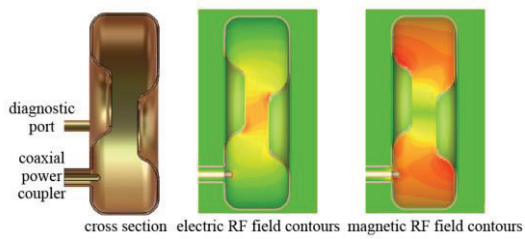

Figure 4: Cross-sectional view of a re-entrant cavity unit. Electric and magnetic RF field contours are shown (a.u.).

The broad dome provides ample space for a coaxial coupler and a diagnostic probe. One crucial feature is that the nose cones (holding the Be windows) are offset from the cavity axis to follow the helical path such that the equilibrium orbit crosses the center of each Be window. This provides the maximum clearance for the beam. The radii of the Be windows can be minimized to merely the size of the beam envelope passing through. This is better visualized in the perspective view of Fig. 5. The front view illustrates the idea how the instrumentation cables can be attached avoiding conflict with neighbouring cavities. As for pillbox-like cavities, the muons will experience longitudinal and transverse fields along the helical path. Yet, reasonable field uniformity is achieved along the orbit.

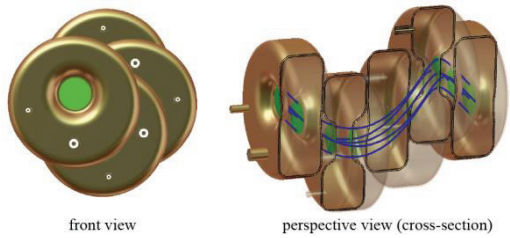

Figure 5: Re-entrant RF cavity design for the HCC.

Note that the number of cavities is only four per helical period (cavity center to center), which is a factor six reduction compared to the design in ref. [9] and a factor three compared to Fig. 3. The peak power requirement per cavity has actually been reduced despite the larger gap due to the re-entrant cell shape. This is crucial to minimize costs for the RF system. E.g., P_{peak} can be limited to a few hundred kW instead of operating in the MW regime (per unit), and P_{peak}/L has been reduced at the same time (several factors). All technical and operational issues associated with the ceramics are eliminated. The disadvantage of the design is that the fill factor of the accelerator (active/passive length) is reduced, which impacts beam dynamics. The effects will be studied numerically. Also, the required E_{acc} is increased (up to ~25 MV/m), however, fields still remain below the RF breakdown limit based on past experimental tests [8].

CONCLUSION

RF cavities concepts have been discussed for usage in an HCC, which imposes strict space constraints given by the surrounding magnets. Cavities filled partially with ceramic as well as exhibiting a re-entrant shape (no ceramics) have been proposed as candidates to be embedded in the channel, while allowing for space of input couplers, pickup probes, and a pressure vessel. The number of cavities employed per helical period is still a matter of trade-off between space and power requirements (cost driver). Alternative designs, e.g. cavities with elliptical cross-section, helical outline, tilted nose cones, or nested cavities have been investigated as well, but not presented here. The work is considered as in progress.

REFERENCES

[1] J-P. Delahaye et al., Fermilab-Conf-13-307-APC, 2013.
[2] A. Ankenbrandt et al., PRST-AB, 2, 081001 (1999).
[3] R.P. Johnson, S. Derbenev, PRST-AB, 8, 041002 (2005).
[4] K. Yonehara et al., Proc. EPAC 2006, WEPLS016.
[5] C. Yoshikawa et al., Proc. IPAC 2013, TUPFI060.
[6] S.A. Kahn et al., Proc. PAC 2013, THPBA26.
[7] R.P. Johnson et al., COOL 2013, MOAM2HA03.
[8] P. Hanlet et al., Proc. EPAC2006, TUPCH147.
[9] M. Popovic et al. "Proc. IPAC2010, THPEA047.
[10] K. Yonehara et al., Proc. IPAC2010, MOPD076.
[11] L.M. Nash et al., Proc. IPAC2013, TUPFI068.

PLASMA CHEMISTRY IN A HIGH PRESSURE GAS FILLED RF TEST CELL FOR USE IN A MUON COOLING CHANNEL

B. Freemire*, Y. Torun, Illinois Institute of Technology, Chicago, IL 60563, USA
M. Chung, M.R. Jana, M. Leonova, A. Moretti, T. Schwarz, A.V. Tollestrup, K. Yonehara
FNAL, Batavia, IL 60510, USA
R.P. Johnson, Muons, Inc., Batavia, IL 60510, USA

INTRODUCTION

Current muon collider schemes call for significant six dimensional (6D) cooling of the muon beam before it is accelerated [1]. One cooling scheme, the Helical Cooling Channel (HCC), employs RF cavities filled with high pressure hydrogen gas [2]. The gas acts both as an energy loss mechanism to allow for ionization cooling [3, 4], and as a buffer in order to prevent RF breakdown [5].

When a beam of particles passes through a HPRF cavity, it will ionize the gas. The amount of plasma generated is dependent on the beam energy, the stopping power of the gas, and the density of the gas. The resulting plasma will gain energy from the RF electric field and transfer it through collisions to the gas. This effect is called plasma loading. An experiment performed at the MuCool Test Area at Fermilab studied the formation of plasma created by a proton beam and its evolution over the course of many 805 MHz RF cycles [6].

PLASMA PROCESSES

In a pure gas, electrons may only recombine with ions. For the range of pressures in this experiment (20 - 100 atm), it is in most cases a three-body reaction in which the third body can be an electron, an ion, or a neutral molecule. Large clusters of positive ions, for example hydrogen, can form through the processes:

$$H_n^+ + 2H_2 \leftrightharpoons H_{n+2}^+ + H_2 \quad (1)$$

An equilibrium in the population of each cluster is reached based on the gas pressure and temperature.

When an electronegative dopant is added, electrons may become captured by the dopant, forming a negative ion. For the case of O_2 this is a ternary process.

Positively and negatively charged ions may "recombine", or become neutral, and this is also a ternary process for the pressure range of this experiment.

It is important to note that for the three-body processes listed above, the identity of the third body plays a significant role. For example, oxygen captures an electron and forms an excited state with a certain lifetime. If the excited oxygen molecule experiences a collision within that lifetime, one of two things can happen: the oxygen ion may become ionized, or the collision may de-excite the oxygen ion, with the third-body carrying off the excess energy. How frequently de-excitation occurs is largely dependent on the identity of the third body.

Rate equations for each of the charged particles can be written:

$$\frac{dn_e}{dt} = \dot{N}_e - \sum_k \beta_k n_e n_{H_k^+} - \frac{n_e}{\tau} \quad (2)$$

$$\frac{dn_{H^+}}{dt} = \dot{N}_{H^+} - \sum_k \beta_k n_e n_{H_k^+} - \sum_{k,l} \eta_{k,l} n_{H_k^+} n_{O_l^-} \quad (3)$$

$$\frac{dn_{O^-}}{dt} = \frac{n_e}{\tau} - \sum_{k,l} \eta_{k,l} n_{H_k^+} n_{O_l^-} \quad (4)$$

where $\dot{N}$ is the production term, β is the electron-ion recombination rate, τ is the electron attachment time, η is the ion-ion recombination rate, and the sums are taken over the existing ion species. For the case of a pure gas, the final terms of the electron and positive ion equations are dropped (and the negative ion equation isn't applicable).

RESULTS

Hydrogen

The results for electron-hydrogen recombination are shown in Figure 1. There was some beam intensity dependence observed over the three beam intensities used during the experiment. This is most likely due to varying cluster populations. It can be seen that the general trends are for the recombination rate to increase with gas pressure and decrease with X_0 (electric field amplitude normalized by the gas pressure).

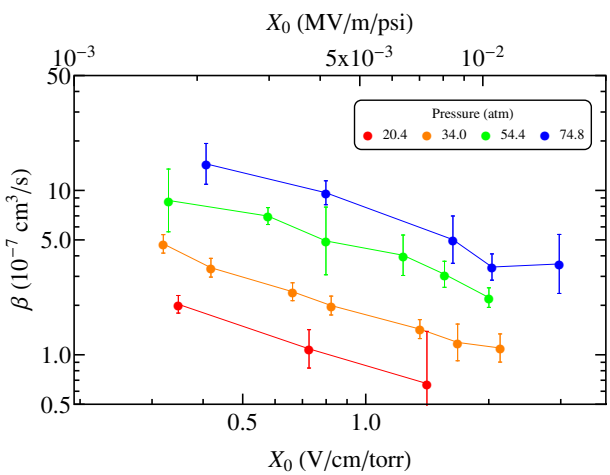

Figure 1: Electron-hydrogen recombination rates at the lowest beam intensity for various gas pressures.

* freeben@iit.edu

ISBN 978-3-95450-132-8

Hydrogen doped with Dry Air

The results dry air doped hydrogen are shown in Figures 2, 3, and 4. The timing resolution of the experiment was such that attachment time measurements below 1 ns could not be made accurately.

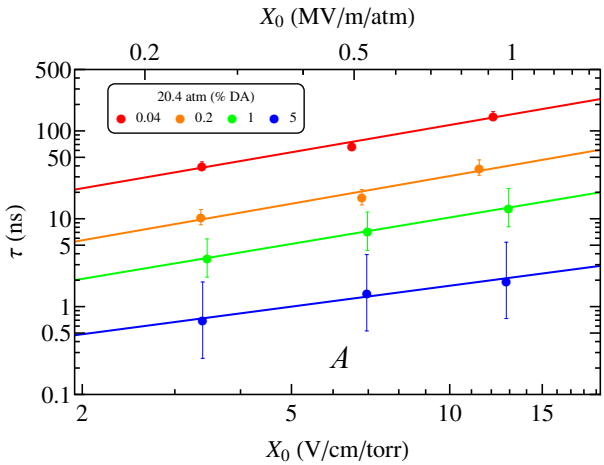

Figure 2: Measurements of electron attachment time to oxygen in hydrogen (points) and fits to the data (lines) at 20.4 atm for various dopant concentrations.

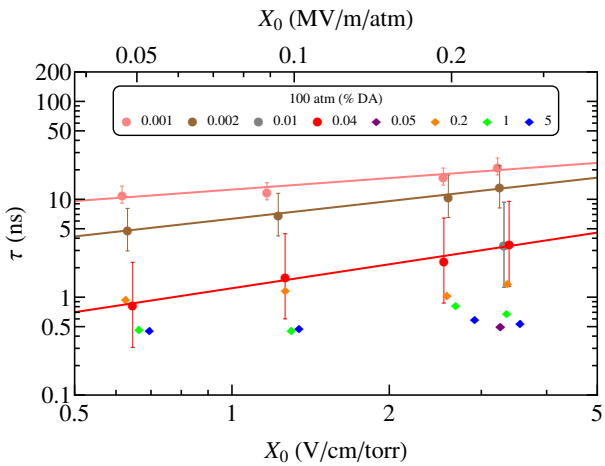

Figure 3: Measurements of electron attachment time to oxygen in hydrogen (points) and fits to the data (lines) at 100 atm for various dopant concentrations.

The attachment time gets smaller with increasing gas pressure and dopant concentration, and larger with increasing X_0

The ion-ion recombination rate is fairly independent of X_0 and tends to decrease with increasing dry air concentration.

Deuterium

Figure 5 shows the results for deuterium. As in the case of hydrogen, the electron-ion recombination rate increases with increasing gas pressure, and the values are roughly equivalent.

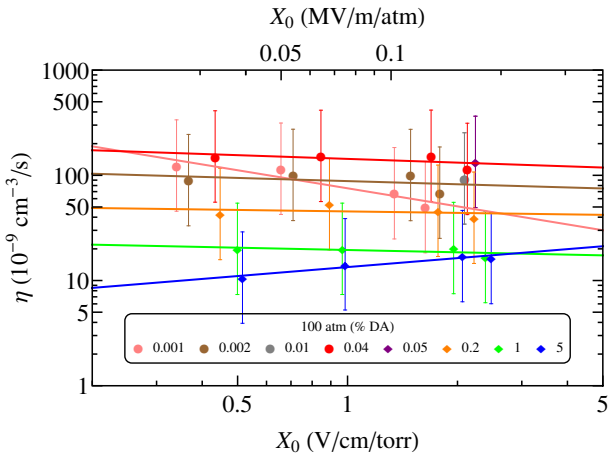

Figure 4: Measurements of ion-ion recombination rates for oxygen in hydrogen (points) and fits to the data (lines) at 100 atm for various dopant concentrations.

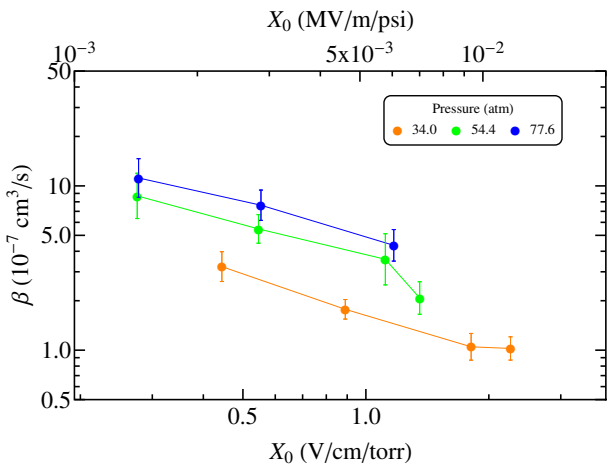

Figure 5: Electron-deuterium recombination rates at the lowest beam intensity for various gas pressures.

Deuterium Doped with Dry Air

Figures 6 and 7 show the results for dry air doped deuterium. As can be seen in the electron attachment time, there are residual electrons only for the smallest gas pressure. The ion-ion recombination rate tends to decrease slightly with gas pressure and is larger than that of hydrogen for 1% dry air at 100 atm.

Nitrogen and Helium

Figure 8 shows the results for nitrogen and helium. The highest beam intensity was used for these data, and only one pressure was recorded for each.

Nitrogen and Helium Doped with Dry Air

Figures 9 and 10 show the results for dry air doped nitrogen and helium. Residual electrons can be observed in the 0.1% and 1% nitrogen and for all cases in helium.

ISBN 978-3-95450-132-8

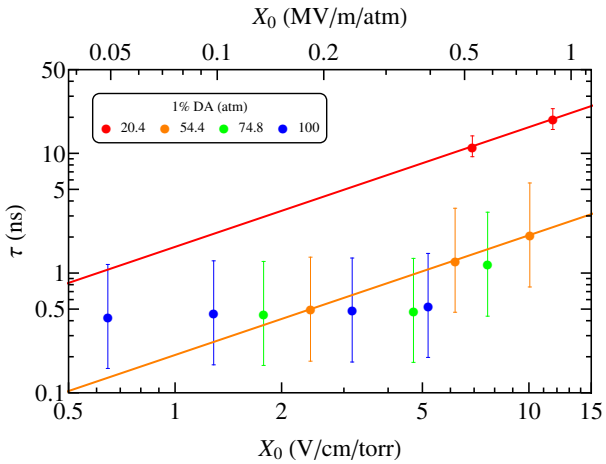

Figure 6: Measurements of electron attachment time to oxygen in deuterium with 1% dry air (points) and fits to the data (lines) for various gas pressures.

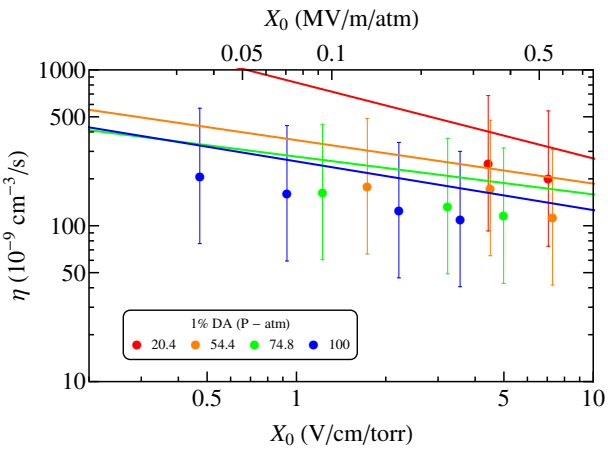

Figure 7: Measurements of ion-ion recombination rates for 1% dry air in deuterium (points) and fits to the data (lines) for various gas pressures.

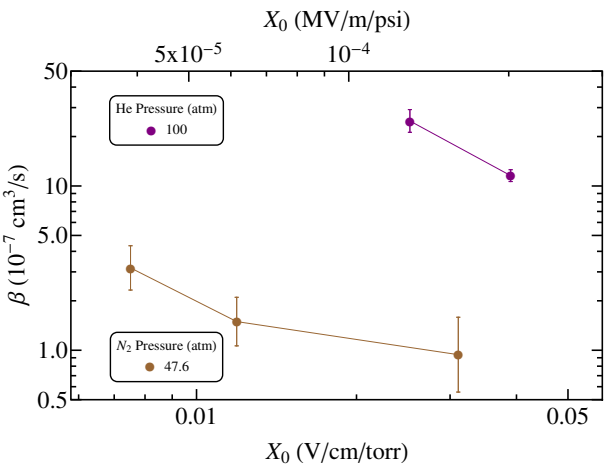

Figure 8: Electron-nitrogen and electron-helium recombination rates at the highest beam intensity.

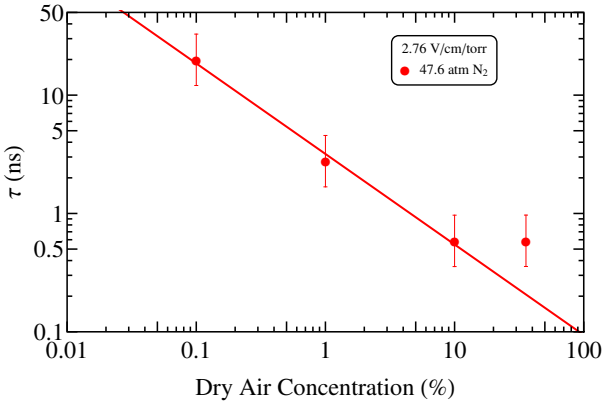

Figure 9: Measurements of electron attachment time to oxygen in nitrogen (points) and a fit to the data (line, excluding the largest concentration) at 10 MV/m.

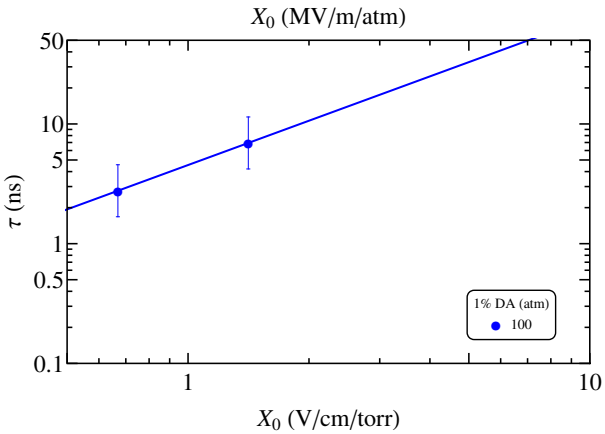

Figure 10: Measurements of electron attachment time to oxygen in helium at 1% dry air (points) and a fit to the data (line).

REMARKS

Measurements of electron-ion recombination rates are difficult to interpret because the exact ion cluster is not known. The general trends of increasing rate with gas pressure and decreasing electric field are consistent with past measurements. The magnitude of values of 10^{-7} to 10^{-6} cm^3/s are reasonable.

Very few results of electron attachment time to oxygen in hydrogen and deuterium have previously been made. Increasing gas pressure and dopant concentration decrease the electron lifetime, and the limit should be dependent on the collision frequency.

Ion-ion recombination results are also difficult to interpret, for the same reason as electron-ion recombination results. Very few measurements of ionic oxygen recombination have been made, however the order of magnitude and trend of decreasing with increasing gas pressure are consistent with previously measured non-oxygen results.

It should be noted that these measurements were taken at room temperature. Decreasing the temperature at which the cavity operates would decrease the plasma loading and electron attachment time, and increase the electron-ion recombination rate.

ISBN 978-3-95450-132-8
3919

REFERENCES

[1] J-P. Delahaye et al., "Enabling Intensity and Energy Frontier Science with a Muon Accelerator Facility in the U.S.", FERMILAB-CONF-13-307-APC, (2013).

[2] Y. Derbenev and R.P. Johnson, Phys. Rev. ST Accel. Beams 8, 041002 (2005).

[3] D. Neuffer, Part. Accel. 14, 75 (1983).

[4] M.M. Alsharo'a et al., Phys. Rev. ST Accel. Beams 6, 081001 (2003).

[5] P.M. Hanlet et al., "High Pressure RF Cavities in Magnetic Fields", EPAC'06, Edinburgh, June 2006, TUPCH147 (2006).

[6] M. Chung et al., Phys. Rev. Lett. 111, 184802 (2013).

(DRAFT) Electrical Breakdown in the All Seasons Cavity

Abstract: The All Seasons Cavity (ASC) was tested at the MTA in December 2013. The maximum RF surface gradient was measured as a function of solenoid magnetic field. The ASC interior was inspected after the test, where many pits were found on the surface of the RF windows (called end plates in this note). The end plate has a contour structure to tune the resonant frequency. The pit pattern on both plates seems to be mirror symmetric. It suggests that a pit pair is simultaneously generated by electric conduction, i.e. an electric breakdown. Interestingly, the pits are distributed uniformly on the plate, even though the field enhancement on the iris is higher than that on the cavity center. Probably, the cavity was conditioned well. In this note, the electron dynamics in the ASC is described first to show how the uniform pit distribution seems to be unexpected. We also show that the pit pattern has two specific orientations in this note.

1. Electron dynamics in ASC

1.1 ASC geometry

Figure 1 shows the cross section of the ASC. It was originally designed to operate as a real 805 MHz pillbox cavity in a multi-Tesla solenoid field under vacuum or with high-pressure hydrogen gas in the cavity. The cavity was only operated under vacuum pressure in the tests described here. The end plate has a step structure to tune the resonant frequency by adjusting the inductance and capacitance. There are mainly two gaps in the cavity. We refer them as the RF gap (gap length = 149 mm) and the iris gap (129 mm) for convenience. The plate is made of stainless steel and plated with 20 μm thick copper. There are three holes on one end plate for instrumentation; RF pickup antenna, RF power port, and vacuum port. We call the instrumentation plate the upstream plate.

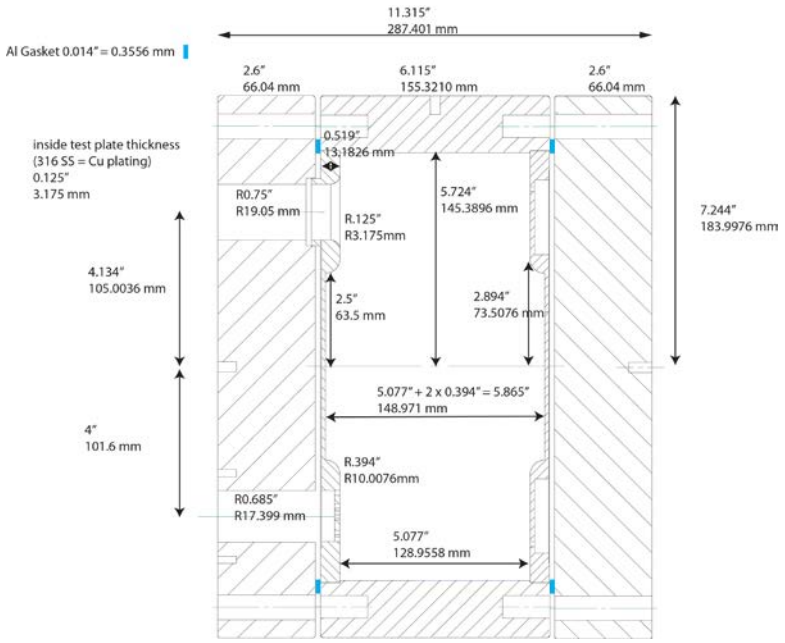

Figure 1: Drawing of the ASC.

Figure 2 shows the simulated field map in the ASC. Since the ASC is a re-entrant structure there are two places to generate a very high surface electric field. One is at the center of end plate and other is on the iris. The highest surface gradient is on the iris, which is 10 % higher than the center of end plate. The maximum RF gradient is refers the measured electric field on the iris. It is also worth to note that the excited field is slightly shifted toward the RF power coupler.

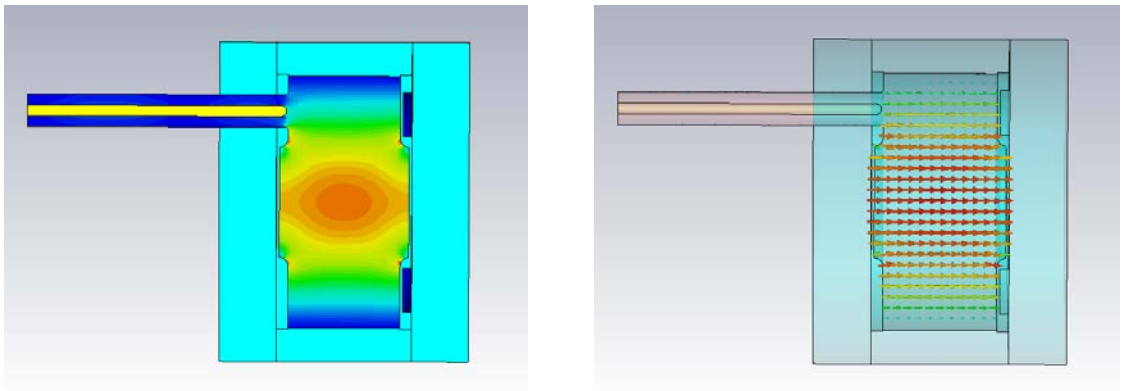

Figure 2: ASC field maps

1.2 Observed peak surface gradient in ASC as a function of magnetic field

Figure 3 shows the observed maximum RF surface gradient in the ASC as a function of external solenoid magnetic field [1]. The observed maximum surface gradient was ~22 MV/m when the solenoid magnet was turned on. It seemed to be constant when the magnetic field strength is > 0.25 T. The cyclotron wavelength [2] is calculated as a function of magnetic field,

$$\lambda_{cyclotron} = 2\pi \frac{p\cos\theta}{B}. \quad (1)$$

Figure 4 shows the calculated cyclotron wavelength as a function of the external solenoid field. The kinetic energy is 2 MeV and the tilt angle is 31 mr in this calculation. These values are chosen for convenience. The plot shows that the longest cyclotron wavelength is ~20 mm at B = 0.25 T. The RF gap is 150 mm. Consequently, free electrons revolve 7~8 turns in the gap. It means that the electron motion follows the magnet flux when the field is above 0.25 Tesla.

[1] "R&D Overview", H. Kirk, https://indico.fnal.gov/conferenceOtherViews.py?view=standard&confId=8013

[2] $\varpi_{Larmor} = \frac{eB}{m}$, $f = \frac{\varpi_{Larmor}}{2\pi}$, $\lambda_{cyclotron} = \frac{2\pi v}{\varpi_{Larmor}} = \frac{2\pi p_z}{eB}$.

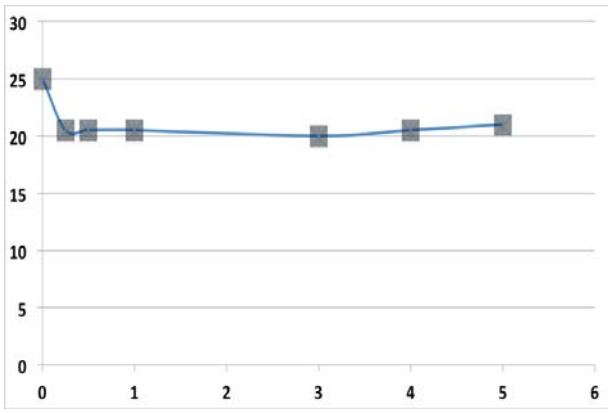

Figure 3: The observed maximum RF surface gradient (MV/m) in the ASC as a function of external solenoid magnetic field (Tesla).

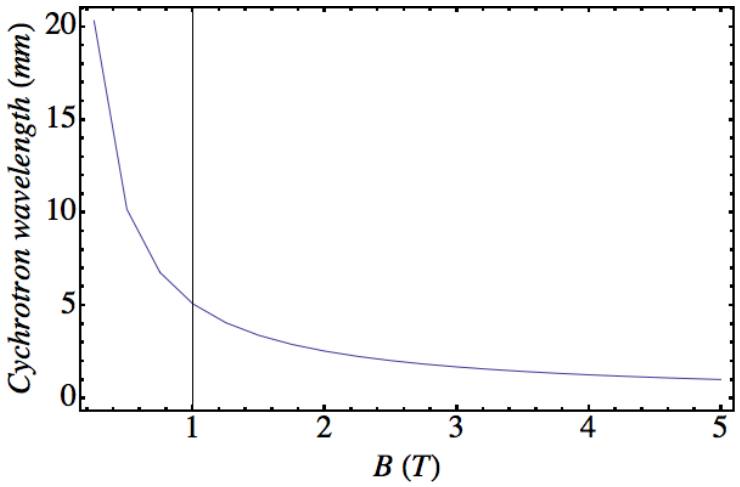

Figure 4: Calculated cyclotron wavelength by using eq. (1).

1.2 Electron impact energy

The relativistic equation of motion [3] of an electron in an RF field is given,

$$\beta'(t) = \frac{cE_0 \sin(2\pi ft + \phi_0)}{m_e}\left(1-\beta^2(t)\right)^{3/2}. \quad (2)$$

Thus, the kinetic energy is given,

$$K = \gamma m_e. \quad (3)$$

In order to evaluate the impact energy of accelerated electrons when they arrive at the end plate, the current density of surface emission (SE) electrons is calculated by using the Fowler-Nordheim formula,

[3] Note: Acceleration in stationary state is given $A^{\mu} = \gamma^2\left(\gamma^2 a\mathbf{v}\mathbf{v}_m + a_m\right)$. We consider one direction, i.e. $\mathbf{v}_m = \mathbf{v}$, $a_m = a$, thus $A^m = \gamma^4 a$. From particle frame, the acceleration is $A^{\mu'} = (0, \alpha, 0, 0)$. Transform the particle frame into the stationary one, $A^1 = \gamma\left(vA^{0'} + A^{1'}\right) = \gamma\alpha$. Finally, the relativistic equation of motion is given, $\gamma\alpha = \gamma^4 a$, thus $\gamma^3 a = \frac{dv}{dt}$, where a is the Newtonian acceleration, thus $a = \frac{F}{m}$.

$$i(\beta E) = \frac{A_{fn}(\beta E)^2}{\phi} Exp\left[-\frac{B_{fn}\phi^{3/2}}{\beta E}\right], \quad (4)$$

where $A_{fn} = 1.54\ 10^6\ eV\ A/(MV)^2$, $B_{fn} = 6830\ MV/m/(eV)^{3/2}$, $\beta = 100$, and $\varphi = 5$ eV, respectively. The impact energy of the SE electrons on the plate per unit area is defined,

$$p(E) = K(E) \times i(\beta E). \quad (5)$$

The kinetic energy of SE electrons in the ASC is estimated. Figure 5 shows the electric field profile along with the RF and the iris gaps simulated in SuperFish. The peak surface gradient at the RF and the iris gaps are 1.25 and 1.42, respectively. For example, the surface gradient on the iris of 22 MV/m corresponds to 19.4 MV/m on the RF gap. The field profile is used to estimate the kinetic energy of electrons.

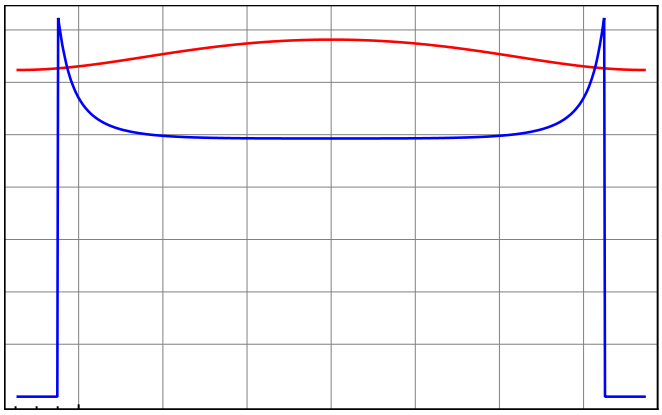

Position

Figure 5: RF gradient profile (Blue) on the iris and (Red) on the accelerating gradient.

Figure 6 shows the estimated kinetic energy of electrons on the RF and the iris gaps as a function of time by using eqs. (2) and (3). The RF frequency is 800 MHz and the initial RF phase is $\pi/2$ in this simulation. The energy gain of electrons at the RF gap is ~15 % higher than at the iris.

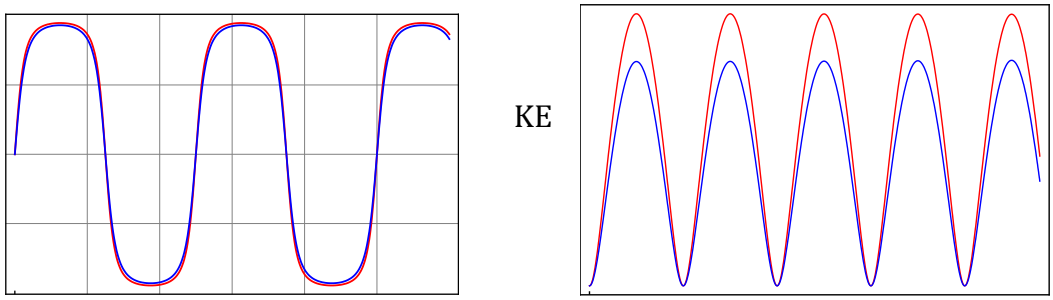

Figure 6: (Left) calculated β and (Right) kinetic energy in the ASC. The red line is the value at the RF gap and a blue one is for the iris gap.

Figure 7 shows the estimated kinetic energy of electrons at one end plate with various maximum RF surface gradients, 22, 21, 20 and 19 MV/m as a function of the initial RF

phase. Since the RF gap in the ASC is so long that the transit time near the initial RF phase $\pi/2$ is small or zero. On the other hand, the final kinetic energy of electrons at zero initial RF phase is drastically changed. However, it is not important to estimate the electron impact energy because the probability of surface electron emission is near zero at low RF surface gradient.

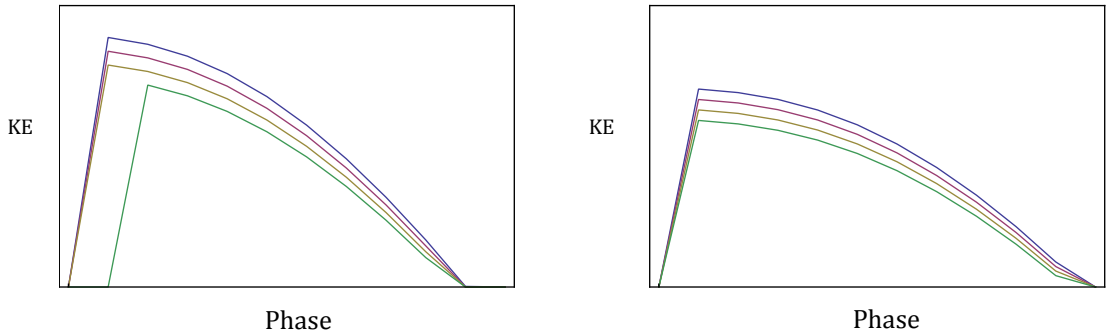

Figure 7: Simulated final kinetic energy of electrons in the ASC with various maximum surface gradients as a function of the initial RF phase. (Left) is at the RF gap and (Right) is at the iris gap.

The current density as a function of the RF phase is calculated by using eq. (4) and the result for the instantaneous impact energy as a function of RF phase is shown in Figure 7. Because the transit time at the crest (the initial RF phase = $\pi/2$) is zero, the highest impact energy appears at the initial RF phase $\pi/4$. Besides, the impact energy at the iris gap is two orders of magnitude bigger than that at the RF gap. The reason is because the current density is very sensitive to βE. Figure 8 shows the deviation of $i(\beta E)$ with respect to βE to show the sensitivity of $i(\beta E)$. The current density is changed by two orders of magnitude when βE is changed by 10 % (which is the difference of surface gradient at the RF and iris gaps).

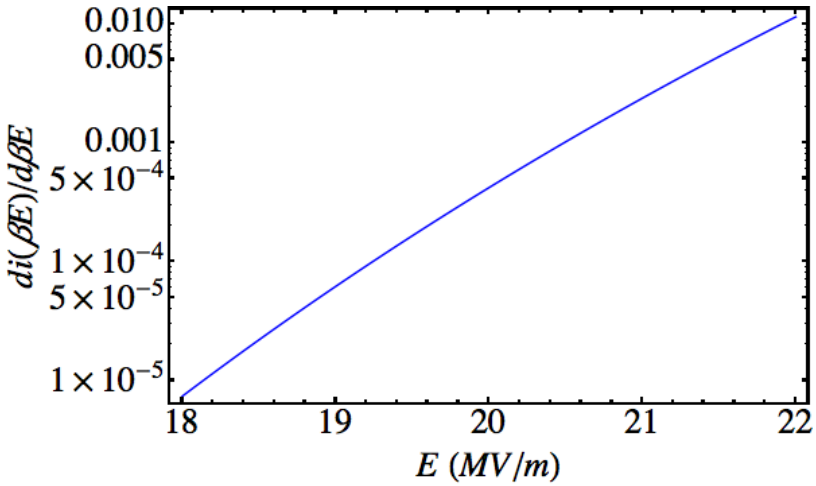

Figure 8: The plot shows the sensitivity of βE on the dark current.

1.3 Conditioning

If the conventional breakdown model is correct, the impact energy analysis shows that the breakdown damage should be more severe on the iris than the RF center since the impact energy is two orders of magnitude larger than that at the RF gap. However, as we will discuss later in the pit image analysis, the pits are distributed uniformly over the end plate.

One hypothesis is that the RF is conditioned well. The breakdown probability at the iris gap becomes equal to that at the RF one. If the cavity ran for a long time and the breakdown was induced enough the pit might be generated on the RF gap as well as the iris. We need to investigate the field enhancement of the surface before and after the conditioning.

2. Pit image analysis

The last ASC test was operated with special attention. Because the cooling system of the cavity was very poor the cavity ran with very low repetition rate, 1 Hz. The number of breakdowns was also limited to avoid any critical damage to the cavity. As the result, the total number of breakdowns was ~500 including those during conditioning. This gives us a special opportunity that we could distinguish the pit pattern on the end plates.

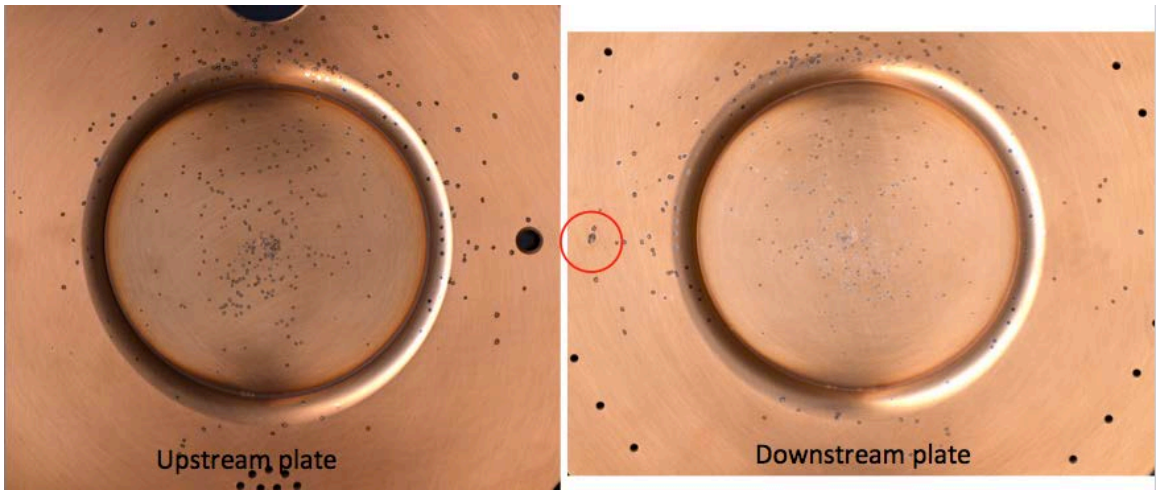

Figure 9: (Left) the upstream and (Right) the downstream end plates.

Figure 9 shows pictures of upstream and downstream end plates after the breakdown test. A tiny black spot shows a possible breakdown pit. There is a big breakdown pit at the left-hand-side on the downstream plate (a red circle). First, we realized that the big spot should be caused with the RF pickup antenna that is located in a big hole at the right-hand-side on the upstream plate. It was the clue that we noticed the pit patterns to be mirror images.

The picture of upstream plate was flipped and found that there are more identical pit patterns on both plates. Figure 10 shows pictures of both end plates where the upstream plate is flipped. A red oval shows the typical identical pit pattern on both plates. A square box, a circle, and lines are for an eye guide. We found that almost all pits have a pair.

2.1 Identifying pit pairs

We made an image processing code written in Mathematica and made a pit map as shown in Figure 11. A red oval shows the identified pit pattern shown in Figure 10. The plot shows that there is a small position offset between red and blue circles. Figures 12 and 13 show the orientation and position offset of identical pit pairs, respectively. Interestingly, there are

two orientations, one is around 60 degrees and other is 150 degrees. The position offset is, on the other hand, distributed around 4 mm. Since the RF gap is ~140 mm the azimuth angle of electric conduction is ~30 mr.

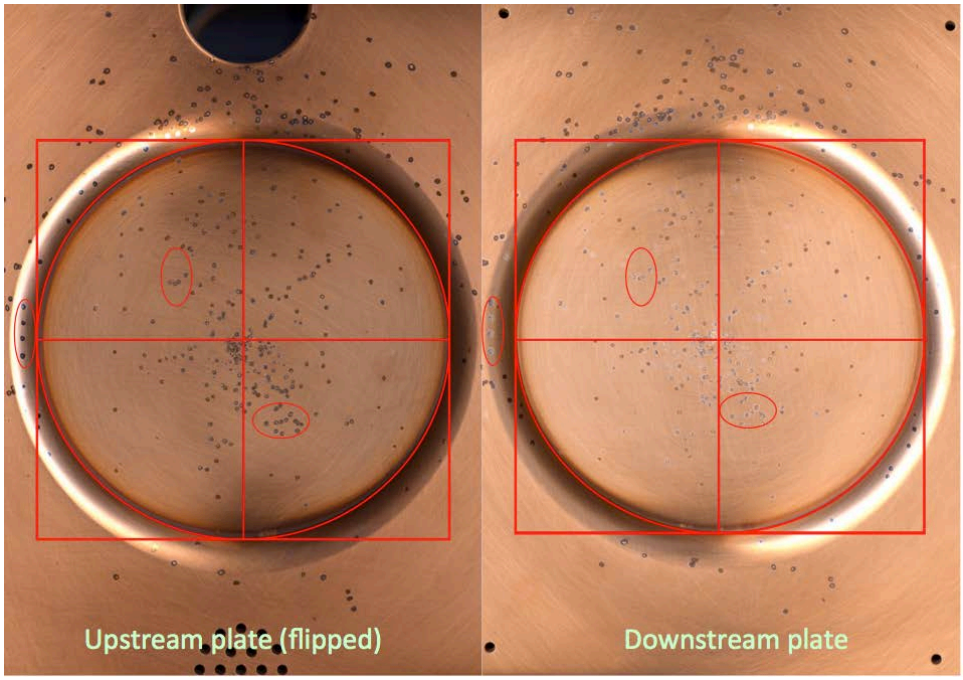

Figure 10: (Left) the flipped upstream plate and (Right) the downstream plate.

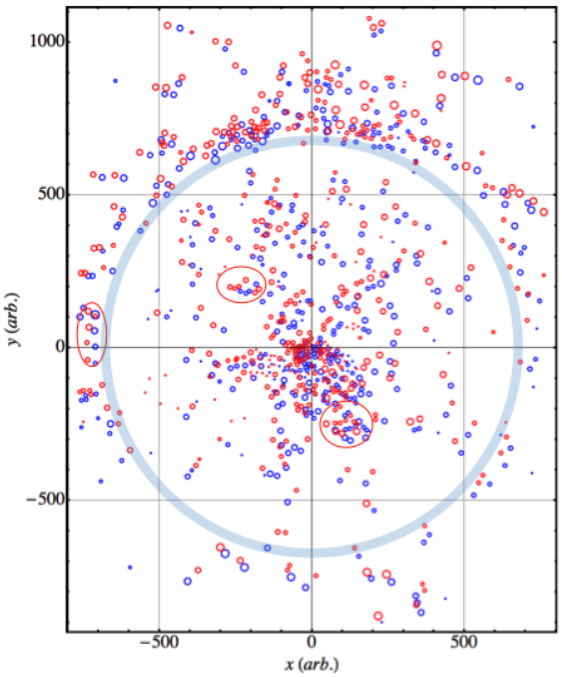

Figure 11: The breakdown pit map. Blue and red circles are the pit on the upstream and downstream plates, respectively.

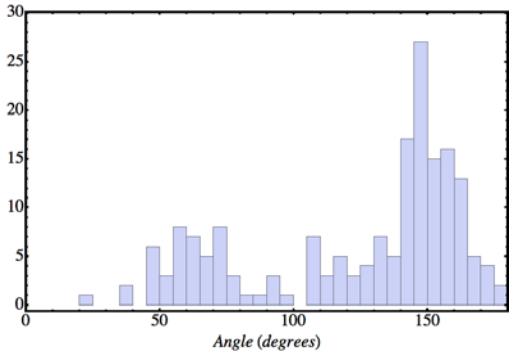

Figure 12: The orientation of pit pair.

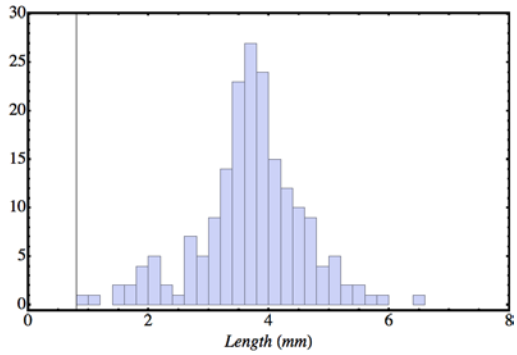

Figure 13: The position offset of pit pair.

Figure 14 shows the vector line between a red and blue circles and enlarged plot near the cavity center. Although we do not have any solid algorithm to identify the pit pair we notice that the orientation near the cavity center is distributed around 150 degrees while that around the iris is distributed around 60 and 150 degrees. This may be a clue as to what is going on in the cavity during the breakdown process.

3. Future analysis

It is still a big mystery why the breakdown conduction has two orientations. In order to solve it, we have started simulating the electron motion in the cavity by using the ACE3P simulation code. The two orientations were shown in the simulation although only one specific orientation appears when the magnet is turned on in the simulation. It strongly suggests that one of orientations would be produced when the magnet is turned on. This is indirect evidence that the RF breakdown is taken place. More measurements are needed to figure out the breakdown mechanism.

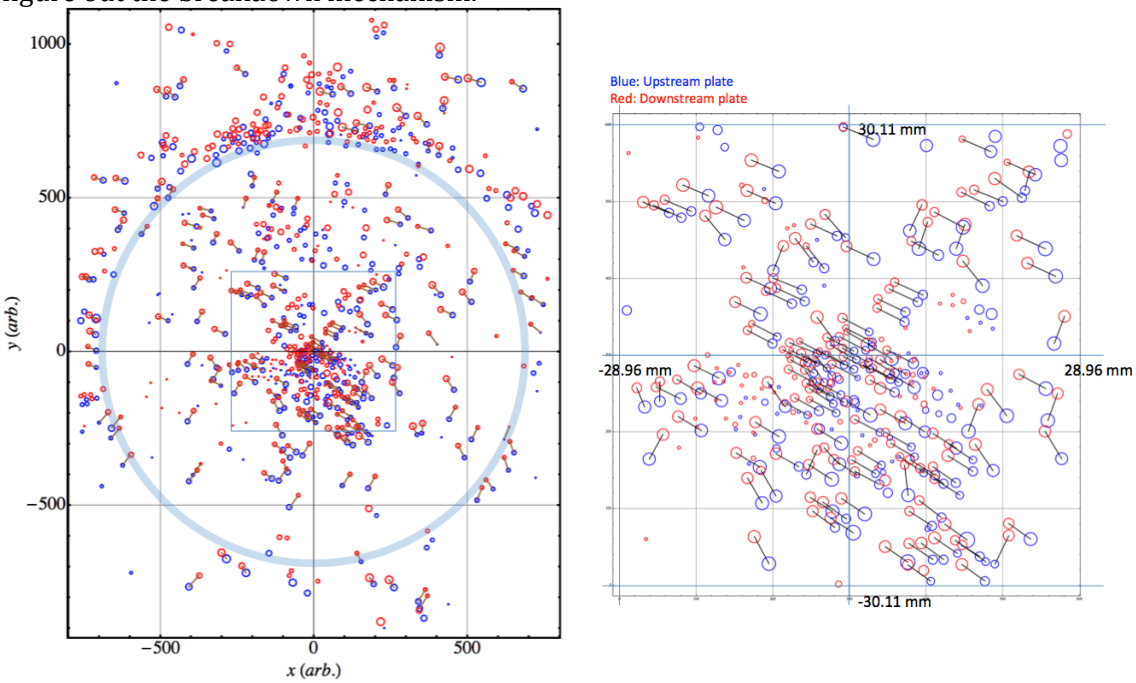

Figure 14: Result of pit image analysis. (Left) shows large view and (Right) shows the detail pit image around the cavity center.